R+D
Nuclear Waste
Disposal

Seismic in situ Methods
for the Characterisation of
Excavation Damaged Zones

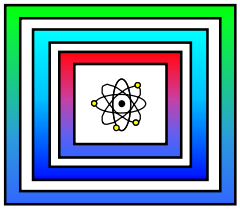

Final Report

Hannover, July 2002

The work was supported by "Projektträger des BMBF und BMWi für Wassertechnologie und Entsorgung" under the identification number: 02 E 9098.

The work at the Mont Terri Rock Laboratory was partly founded by the EC within the 5th Framework Program under Contract No. **FIKW-CT-2000-00017** („Engineered Barrier Emplacement Experiment in Opalinus Clay“).

Responsibility for the contents of this publication lies solely with the authors.

Keywords: excavation damaged zone, borehole seismic, refraction seismic, seismic anisotropy

BUNDESANSTALT FÜR GEOWISSENSCHAFTEN
UND ROHSTOFFE
HANNOVER

Seismic in situ Methods for the Characterisation of Excavation Damaged Zones

Final Report

1. Author:	Schuster, Dr. Kristof
2. Client:	Projektträger des BMBF und BMWi für Wassertechnologie und Entsorgung
3. Contract No.:	02E9098
4. Date:	11. July 2002
5. Tagebuch-No.:	11970 / 02

Table of Contents

Total No. of Pages: 155

Summary

Author: Dr. Kristof Schuster

Title: Seismic in situ Methods for the Characterisation of Excavation Damaged Zones

Keywords: excavation damaged zone, borehole seismic, refraction seismic, seismic anisotropy

The petrophysical properties in the vicinities of underground openings are influenced by several factors e.g. stress field, method of excavation, geometry and age of the opening. A characterisation of the properties and the extent of the damage is essential for safety assessment modelling.

The application of different seismic techniques and the methodology used for the characterisation of the excavation damaged zone (EDZ) with the help of seismic parameters are described by means of results from the Mont Terri Rock Laboratory (Opalinus Clay) exemplary in full detail. The most important derived parameters for the characterisation of the EDZ are seismic P- and S-wave velocity, amplitude damping and Poisson's ratio. Seismic borehole methods as for instance interval velocity and cross hole measurements (incl. seismic tomography) as well as the seismic refraction method as a non-destructive technique were applied. All methods are discussed including a description of the uncertainty of results. Furthermore, results from seismic and comparative geophysical measurements performed at several international rock laboratories are presented.

The detection and characterisation of the EDZ was very successful in different potential host rock formations: Opalinus Clay, Boom Clay, granite and salt rock. The applied seismic in situ methods proved to be reliable and robust tools for the determination and characterisation of the EDZ.

1 Introduction

Excavation of underground openings generally damages the rock in the vicinity of the opening. The level of damage depends, among other factors, on the method of excavation, the rock properties, the stress field, the geometry of the opening and its age. Knowledge of the extent and the property of the excavation damaged zone (EDZ) is important in the design and construction of seals and plugs for nuclear waste repositories (Fairhurst and Damjanac 1996, Emsley et al. 1997).
It is well known that seismic velocities in rock change significantly with progressive failure. Thus seismic methods can help to analyse changes in elastic rock properties in the EDZ around underground openings.

Aim of the research work was the development and the test of non-destructive seismic in situ methods for the assessment of geomechanical and hydraulic rock properties in the vicinity of repository underground cavities.[1]
The project started 1st of July 1998 and ended 30th of June 2001. It was prolonged until 31st of December 2001 neutral in coast for the principle. The prolongation gave the opportunity to perform investigations in June and October 2001 with different seismic methods within a short time window at the Mont Terri Rock Laboratory. Furthermore geoelectric measurements were performed at the same location. This allows to compare and ultimately to control results from different seismic methods as well as the comparison with results derived from geoelectric measurements at the same site (Kruschwitz 2002).

In the final stage of the preceding project[2] priority was given to the development and application of small scale investigations of rock properties in the vicinity of underground excavations with seismic borehole methods. Within the starting phase of the actual project this work was continued in order to improve the knowledge of seismic parameters derived from measurements within the EDZ.

[1] Entwicklung und Erprobung von zerstörungsfreien seismischen in situ-Methoden zur Beurteilung der geomechanischen und hydraulischen Gebirgseigenschaften in der Umgebung untertägiger Hohlräume in Endlagerformationen. Förderkennzeichen: 02E9098, Projektträger des BMBF und BMWi für Wassertechnologie und Entsorgung.

[2] Entwicklung von Methoden zur Erkundung der dynamischen Gebirgseigenschaften in der Umgebung von untertägigen Hohlräumen. Förderkennzeichen: 02E 8391.

For the evaluation more S-wave data were analysed. In addition elastic parameters like Poisson's ratio, dynamic Young's modulus and modulus of rigidity were derived. The application of high resolution cross hole measurements revealed seismic anisotropy. The repetition of measurements gave the opportunity to observe changes of seismic parameters with time. Data processing methods were further improved.

In order to give a comprehensive view of the potential of the applied seismic in situ methods and to demonstrate the complexity of the characterisation of the EDZ with the help of seismic methods, results from two measurement campaigns performed in the Mont Terri Rock Laboratory (Switzerland, Opalinus Clay) (Schuster and Alheid 2002) will be presented exemplary in full detail in chapter 2.1.

Comparable measurements were performed within the last three years during several measurement campaigns in the following national and international rock laboratories:

- Hard Rock Laboratory Äspö (Sweden), granite
- Rock Laboratory Grimsel (Switzerland), granite
- Asse Research Mine (Germany), rock salt
- Underground Research Facility HADES Mol (Belgium), Boom Clay
- Mont Terri Rock Laboratory (Switzerland), Opalinus Clay
- Laboratoire de Recherche Souterrain de Meuse / Haute Marne (France), laboratory is under construction, Kimmeridgien Marls

Results are published in several reports. An appropriate list can be found in chap. 6.

Because results achieved at the Mont Terri Rock Laboratory can be regarded as exemplary in terms of explaining the borehole methods only those results from other sites are discussed in the following, where comparison with results derived from different methods was possible:

- At the Underground Research Facility Mol (Belgium) the predictions over the extent and stage of damage of the EDZ made on the basis of seismic interval velocity and cross hole measurements were confirmed after the excavation of the investigated rock mass (chap. 2.2).

- The comparison of results from seismic interval velocity measurements and fracture mappings done with borehole scanning tools at the Hard Rock Laboratory Äspö (Sweden) can be assessed as good (chap. 2.3). At the Rock Laboratory Grimsel (Switzerland) fracturers were detected successfully with the same methods (chap. 2.4).
- Results from seismic interval velocity measurements which were performed at the Asse Research Mine are very good in line with results from permeability measurements which were performed in the same boreholes a few days before (chap. 2.5).

The development and application of seismic refraction methods will be described in the third chapter. In spring 1999 a feasibility test for the application of high resolution seismic refraction methods was performed in the Rock Laboratory Grimsel (chap. 3.1). At that time only a four channel digital storage oscilloscope was available, thus the classical refraction method was modified. Instead of using many receivers and few shotpoints, three receivers and many shot positions for the excitation of seismic waves were used. This type of measurement is time consuming and an evaluation of seismic amplitudes is difficult. The EDZ could be resolved with this attempt.

In parallel the procurement of an appropriate high resolution, multi-channel seismic apparatus was pressed ahead. In January 2000 three 16 channel digital storage oscilloscopes and 48 piezoelectric transducers were available. First tests were performed at surface in the laboratory (chap. 3.2). The control software had to be modified and adjusted. In a further step the instruments were protected with a special casing against the rough conditions during measurements in the underground rock laboratories. In August 2000 a first in situ test with 48 channels at the Asse Research Mine could be performed (chap. 3.3). The data quality was good and the extent of the EDZ could be estimated. For this test several seismic sources were applied.

In June and October 2001 the refraction seismic equipment was used in the Mont Terri Rock Laboratory (Switzerland) in Opalinus Clay (chap. 3.4). The evaluation of these high resolution data resolved the extent of the EDZ and gave additionally strong indications for the existence of fractures (Schuster and Alheid 2002).

2 Seismic Borehole Methods - Results from Selected Sites

In the following five examples of seismic borehole investigations at selected sites are discussed. In chapter 2.1 the borehole methods are explained in full detail by means of results from the Mont Terri Rock Laboratory. In the framework of special scientific research programs seismic borehole measurements were performed at several other international rock laboratories. Results are presented from those sites where seismic investigations could be combined with other geophysical or geotechnical measurements for comparison. This concerns measurements in Boom Clay (chap. 2.2), in granites (chap. 2.3 and 2.4), and in rock salt (chap. 2.5).

Within the framework of the investigations at the Mont Terri Rock Laboratory six boreholes were drilled and used for the application of different seismic borehole methods. The principles are briefly listed in the following.

Video Scan

Immediately after drilling boreholes are scanned with a BGR video camera. The analyses of these inspections provide information about the condition of the boreholes which is useful for the planning of the following seismic measurements and the later interpretation of data.

Interval Velocity Measurements

The seismic interval velocities are measured successively in steps between 2 and 20 cm along the boreholes. The step width depends on the desired lateral resolution. The BGR mini-sonic probe with one source and three receivers is used. For the source signals frequencies between 50 and 150 kHz are used. Measurements start at the tunnel wall. The probe is moved progressively towards the end of the borehole in steps of 10 cm for example. This method reveals the seismic velocity as a function of distance from the tunnel wall. The advantage of this method is that the length of the ray path is independent from the measuring depth.

Cross Hole Measurements

Cross hole measurements are carried out between two boreholes. In this case a piezoelectric transducer with an emitting frequency of about 7 kHz as a source is located in one borehole whereas the receivers are located in a second one. Both, source and receivers are positioned at the same depth in both boreholes. In steps of 10 cm both, source and receivers were moved towards the end of the borehole. In this case the assumed ray paths are more or less parallel to the wall of the drift. According to the theory, the ray paths not compelling run geometrically the shortest way. Instead they "find" the shortest way in time (Kertz 1969). In practice the results yield at least a rough model of the velocity distribution. An advantage of course is the fact, that a bigger rock volume is scanned with this method.

Seismic Tomography

In order to increase the ray coverage of the rock volume under investigation the above mentioned cross hole measurements have to be modified. Measurements start with the first source position in the first borehole and all possible receiver positions in the second borehole (steps of 10 cm are used in general). Afterwards the source is moved 10 cm and the measurements are repeated. This goes on until the source reaches the end of the borehole. Then the source and receivers are changed and the measurement continues in the same way. This type of measurement is more time consuming than the "normal" cross hole or interval velocity measurement. But the advantage is, that anomalies and seismic anisotropy effects can be detected.

2.1 Mont Terri Rock Laboratory - Opalinus Clay - Detailed Seismic Investigations

2.1.1 Introduction

Seismic measurements were performed by the Federal Institute for Geosciences and Natural Resources, Hannover, Germany (BGR) during two field campaigns in June and October 2001 in the EB niche of the Rock Laboratory Mont Terri (Schuster and Alheid 2002). The Mont Terri Rock Laboratory will be introduced in chapter 2.1.1.2. The location of the EB niche in the laboratory is marked in Fig. 2.1-1b, whereas Fig. 2.1-2 shows a photograph of the EB niche. Aim of the investigation is the petrophysical characterisation of the EDZ. Different seismic methods were applied in order to investigate the vicinity of the EB-niche in more detail and to get a very high spatial resolution of seismic parameters. As could be shown in the past, not only in the New Gallery of the Mont Terri Rock Laboratory, parameters like seismic P- and S-wave velocity, amplitude damping and anisotropy of seismic velocities yield an important contribution for the characterisation of the EDZ and the undisturbed rock around a drift (Alheid and Knecht 1996, Schuster et al. 2001a). In addition elastic parameters like Poisson's ratio, Young's modulus and modulus of rigidity can be estimated from these in situ measurements. These parameters are of interest for later numerical dynamic modelling. Repetition of measurements after a certain period of time moreover offer the possibility of a comparison of data and results and allows the assessment of changes in elastic parameters with time.

The work at the Mont Terri Rock Laboratory was partly founded by the EC within the 5th Framework Program under Contract No. **FIKW-CT-2000-00017** („Engineered Barrier Emplacement Experiment in Opalinus Clay“).

2.1.1.1 Objectives

Six new 3 m long boreholes with diameters of 87 mm were drilled in two planes in the NE wall of the EB niche by Heinz Steiger (staff of the Rock Laboratory) with a "hand held" drilling machine. Both planes are 1 m apart. Boreholes are drilled subhorizontal (10° up), 45° upwards and vertical in the roof. In Fig. 2.1-2 the mouths

of the boreholes are marked by coloured dots. Fig. 2.1-3 shows a sketch of the boreholes with their relative locations. All boreholes were used for interval velocity measurements and the two subhorizontal ones for cross hole and tomography measurements.

In June 2001 the following seismic borehole measurements were carried out:

- Interval velocity measurements in six boreholes (BEB-B09, BEB-B10, BEB-B11, BEB-B19, BEB-B20, BEB-B21).
- Cross hole measurements between boreholes BEB-B09 and BEB-B19.
- High resolution tomography between boreholes BEB-B09 and BEB-B19.

Four months later, in October 2001, a second campaign was performed in the EB niche, mainly to repeat measurements which were carried out in June.

- Repetition of interval velocity measurements in six boreholes (BEB-B09, BEB-B10, BEB-B11, BEB-B19, BEB-B20, BEB-B21)

The seismic refraction measurements will be discussed in chap. 3.4. The Technical University of Berlin performed as a subcontractor of BGR supplementary geoelectrical measurements along two circular and one horizontal profile in the EB niche (Kruschwitz 2002).

2.1.1.2 The Mont Terri Rock Laboratory

The Mont Terri Rock Laboratory will be described briefly because the majority of data and results presented in this report originates from this rock laboratory, located in north-western Switzerland. In the Rock Laboratory an international research project is carried out by ten organisations from six countries. BGR is one of the ten partners and started their work in 1996. The aim of the research programme is to investigate the hydrogeological, geomechanical and rock mechanical properties of a clay formation, known as the Opalinus Clay.

The Mont Terri Rock Laboratory is located in and beside the Reconnaissance Gallery of the Mont Terri motorway tunnel, in north-western Switzerland (see Fig. 2.1-1a). The 3962 m long tunnel crosses the northernmost anticline of the Jura

mountains, the Mont Terri anticline, which was folded during the Late Miocene to Pliocene period, about 10 to 2 Million years ago (Thury and Bossart 1999). The Mont Terri Rock Laboratory is located in the Opalinus Clay (Lower Aalenian), a shale formation. The present overburden is 250 m to 320 m. The estimated overburden in the past was at least 1000 m. The Reconnaissance Gallery intersects a 243 m long section of the Opalinus Clay.

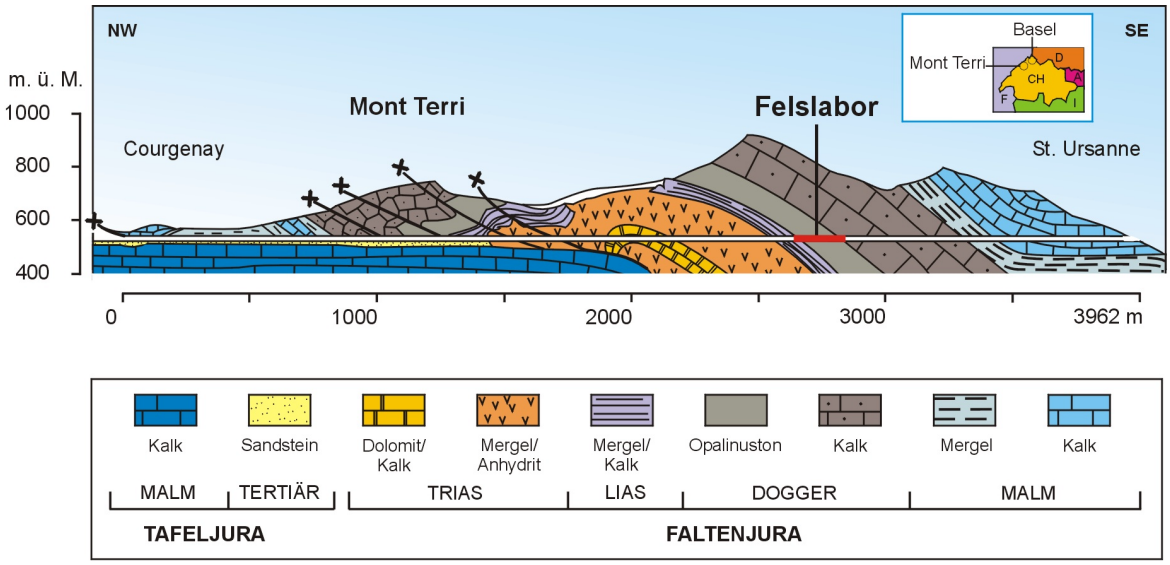

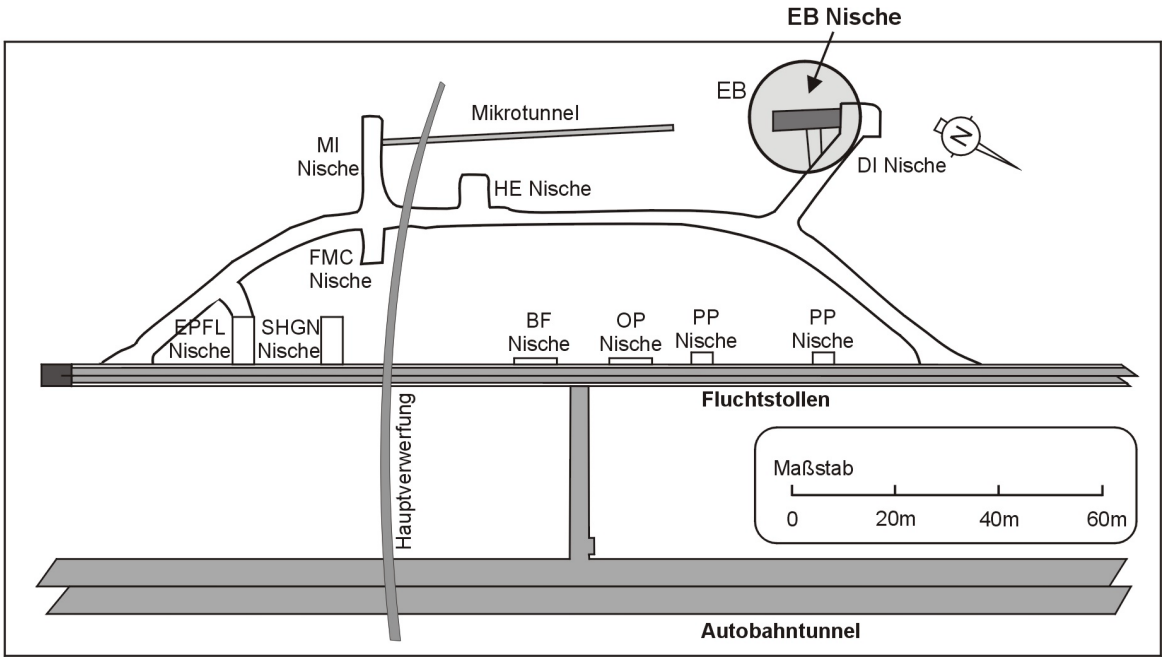

Fig. 2.1-1: Mont Terri Rock Laboratory, Switzerland. Top (a): Location and geology, after Thury and Bossart, 1999. Below (b): Test site of seismic measurements in the EB niche (arrow).

In the EB niche an "Engineered Barrier Experiment" will be carried out. The location of the EB niche is marked in Fig. 2.1-1b. In Fig. 2.1-2 a photograph of the EB niche is shown. The EB Experiment aims mainly to demonstrate a new concept for a backfill emplacement technique in horizontal drifts, in competent clay formations, such as the Opalinus Clay.

Fig. 2.1-2: Photograph of the EB niche. On the NE wall (left side) the six investigated boreholes are marked by blue dots. Blue lines indicate the location of the seismic refraction profiles. On the left hand side the seismic refraction equipment can be seen.

The EB niche was excavated during April and May 2001. It is 15 m long and 2.5 m high. Two techniques were used for the excavation. For tunnel meters 0 - 9 m a pneumatic hammer was used whereas a road header was used at the end of the niche (tunnel meters 9 - 15 m). The tolerances in diameter are ± 10 cm in the front of the niche (tunnel meters 0 - 9 m) and ± 5 cm for the final six meters, where the geophysical measurements took place.

The EB niche was excavated through three SSE dipping minor thrust planes. These fault planes show slicken-sides and shear fibres on polished surfaces, with a sense of shear that consistently indicates overthrusting (Nussbaum et al. 2002).
A mapping of artificial fractures was performed by Nussbaum et al. (2002). Basically, there are three main types of damage structures related to excavations in the Opalinus Clay: 1) extensile brittle fracturing due to stress re-distributions, 2) brittle reactivation of bedding planes (e.g. bedding parallel slip) due to low compressive strength of such planes, and 3) stress and gravity induced borehole breakouts. The locations of the boreholes used for the investigation can be seen in Fig. 2.1-3.

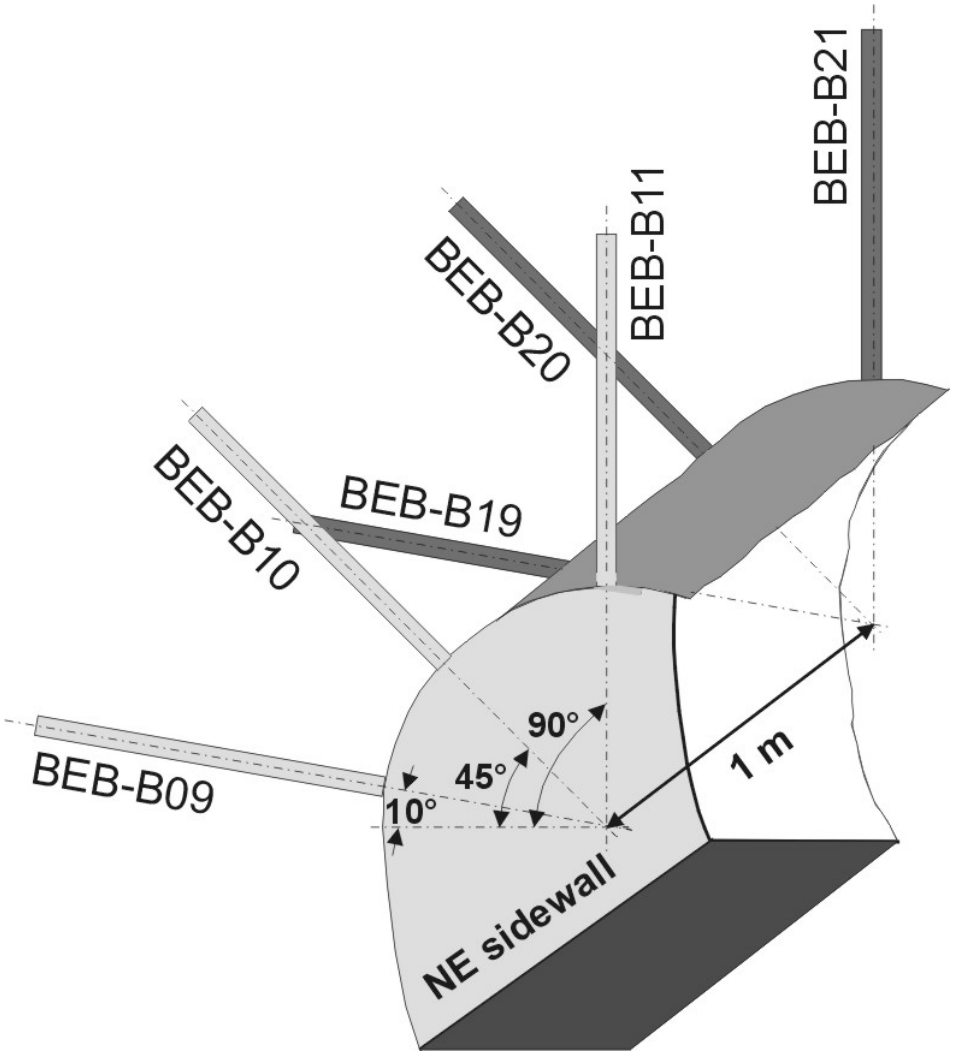

Fig. 2.1-3: Locations of six boreholes in the EB niche of the Mont Terri Rock Laboratory. The boreholes with diameters of 87 were used for seismic borehole measurements.

2.1.2 Results of Borehole Camera Inspections

About one week after the drilling of the boreholes were finished an inspection of the boreholes with a BGR borehole video camera was performed. The quality and stability of the borehole walls could be valued that way.

In general the borehole walls were in very good conditions. Only in both subhorizontal boreholes noticeable breakouts could be observed. The state of the borehole wall was classified according to the following five criteria:

1. intact
2. thin shells
3. shells
4. thick shells
5. jagged deep bursts

Twelve circular viewpoints in steps of 30° were considered. In Fig. 2.1-4 the results are summarised.

Even though in the upright orientation (0° - 30°) breakouts are exist an upward orientation of the mini-sonic probe for the interval velocity measurements was chosen. This orientation facilitates best handling of the probe and the measured data are best comparable with results from previous measurements in other boreholes. After these inspections the seismic measurements started immediately.

BEB-B09, June 2001

Depth [cm]/Angle	[°]-30°	30°-60°	60°-90°	90°-120°	120°-150°	150°-180°	180°-210°	210°-240°	240°-270°	270°-300°	300°-330°	330°-360°
0	1	1	1	1	1	1	1	1	1	1	1	1
10	1	1	1	1	1	1	1	1	1	1	1	1
20	1	1	1	1	1	1	1	1	1	1	1	1
30	1	1	1	1	1	1	1	1	1	1	1	1
40	1	1	1	1	1	1	1	1	1	1	1	1
50	1	1	1	1	1	1	1	1	1	1	1	1
60	1	2	1	1	1	1	1	1	1	1	1	1
70	1	2	1	1	1	1	1	1	1	1	1	1
80	2	2	1	1	1	1	1	1	1	1	1	1
90	1	2	1	1	1	1	1	1	1	1	1	1
100	2	2	1	1	1	1	1	2	1	1	1	1
110	1	2	1	1	1	1	1	2	1	1	1	1
120	2	2	1	1	1	1	1	2	1	1	1	1
130	1	1	1	1	1	1	1	1	1	1	1	1
140	2	2	1	1	1	1	1	2	1	1	1	1
150	4	4	1	1	1	1	2	1	1	1	1	1
160	1	1	1	1	1	1	1	1	1	1	1	1
170	4	4	1	1	1	1	3	1	1	1	1	1
180	3	3	1	1	1	1	4	4	1	1	1	1
190	4	4	1	1	1	1	4	1	1	1	1	1
200	4	4	1	1	1	1	4	1	1	1	1	1
210	4	3	1	1	1	1	4	3	1	1	1	1
220	4	3	1	1	1	1	4	3	1	1	1	1
230	4	3	1	1	1	1	4	3	1	1	1	1
240	4	1	3	1	1	1	4	4	1	1	1	1
250	1	1	1	1	1	1	1	1	3	1	1	1
260	4	3	3	1	4	4	4	4	1	1	1	1
270	1	4	3	1	4	4	4	4	3	1	1	1
280	3	3	3	1	4	4	4	4	3	1	1	1
290	3	3	3	1	4	4	4	3	1	1	1	1

max. depth at 295 cm

BEB-B19, June 2001

Depth [cm]/Angle	[°]-30°	30°-60°	60°-90°	90°-120°	120°-150°	150°-180°	180°-210°	210°-240°	240°-270°	270°-300°	300°-330°	330°-360°
0	1	1	1	1	1	1	1	1	1	1	1	1
10	1	1	1	1	1	1	1	1	1	1	1	1
20	1	1	1	1	1	1	1	1	1	1	1	1
30	1	1	1	1	1	1	1	1	1	1	1	1
40	1	4	1	1	1	1	1	4	1	1	1	1
50	1	1	1	1	1	1	1	1	1	1	1	1
60	1	1	1	1	1	1	1	1	1	1	1	1
70	1	3	1	1	1	1	1	4	1	1	1	1
80	3	3	1	1	1	1	1	4	1	1	1	1
90	4	4	1	1	1	1	4	4	1	1	1	1
100	4	4	1	1	1	1	4	4	1	1	1	1
110	4	4	1	1	1	1	4	4	1	1	1	1
120	4	4	1	1	1	1	4	4	1	1	1	1
130	3	3	3	1	1	1	4	4	1	1	1	1
140	3	3	1	1	1	1	4	4	1	1	1	1
150	4	4	3	1	1	1	4	4	1	1	1	1
160	4	4	3	1	1	1	4	4	1	1	1	1
170	4	4	3	1	1	1	4	4	1	1	1	1
180	3	3	3	1	1	1	4	4	1	1	1	1
190	4	4	3	1	1	1	4	4	1	1	1	1
200	4	4	3	1	1	1	4	4	1	1	1	1
210	4	4	3	1	1	1	4	4	1	1	1	1
220	3	4	3	1	1	1	4	4	1	1	1	1
230	3	3	3	1	1	1	4	4	1	1	1	1
240	3	3	1	1	1	1	1	4	1	1	1	1
250	3	3	3	3	1	1	3	3	1	1	1	1
260	1	1	3	1	1	1	3	1	1	1	1	1
270	4	3	3	1	1	1	3	3	1	1	1	1
280	1	3	3	1	1	1	3	3	1	1	1	1
290	1	3	3	1	1	1	3	3	1	1	1	1

max. depth at 292 cm

1	intact
2	thin shell
3	shell
4	thick shell
5	jagged deep burst

Fig. 2.1-4: Results of inspections of borehole walls with the BGR borehole video camera in June 2001. Top: borehole BEB-B09. Below: borehole BEB-B19. Both boreholes are subhorizontal.

2.1.3 Seismic Interval Velocity Measurements

According to the requested high spatial resolution for the determination of seismic and petrophysical rock properties a BGR high frequency mini-sonic borehole probe was used to perform interval velocity measurements in single boreholes.

2.1.3.1 Data Acquisition

The principle of the seismic interval velocity measurements and the main components of the data acquisition system which are used for the measurements are shown in Fig. 2.1-5. Displayed is also an example of a raw data set for a single excitation point with the source signal (S) and three received signals (1,2,3) at distances of 10, 20 and 30 cm from the source.

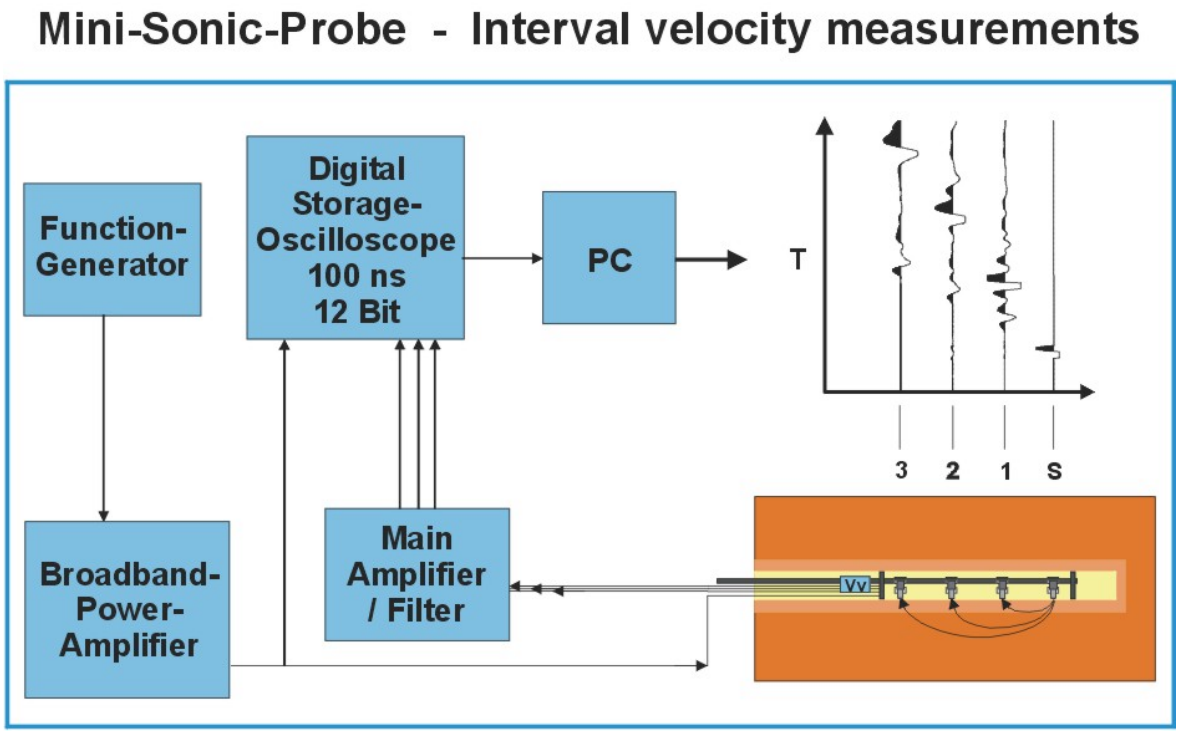

Fig. 2.1-5: Principle of seismic interval velocity measurements. The raw data set (top, right) was measured at a single excitation point (S: source signal, 1-3: received signals for channel 1 - channel 3).

The BGR mini-sonic borehole probe uses a piezoelectric transducer as a seismic source. Three piezoelectric transducers at distances of 10 cm, 20 cm and 30 cm from the source are used as receivers. The transducers were coupled to the bore-

hole wall by pneumatic cylinders. This method allows strong and reproducible force coupling without using any coupling paste. Pressures between 4 and 10 bar for the force coupling of the source and receivers were tested. In general a pressures of 9 bar is used.
The source signal and the three received signals were passed through a signal conditioning unit to a four channel digital storage oscilloscope (Nicolet 440) with a dynamic range of 12 bit. The maximum sampling frequency is 10 MHz. In order to increase the signal to noise ratio, 200 single measurements are averaged (stacked).

Analyses of the video scans gave information about the stability of the boreholes and furthermore the orientation of the mini-sonic probe could be adjusted accordingly. In the vertical boreholes the sensors were orientated towards NE (BEB-B11 and BEB-B21). In the other boreholes the mini-sonic probe was orientated upwards which corresponds 0° when looking into the borehole.

2.1.3.2 Data Analyses

Data are processed and analysed with the seismic software Reflex for Windows (Sandmeier Software). Travel times are measured between the source and the three receivers. Velocities as well as amplitudes were derived from first arrival phases (compressional waves, P-waves) and S-wave onsets (transverse waves, shear waves). In some cases the recognition of the onsets of shear waves is difficult due to a superimposition with other wave trains. Only in some parts of the data the identification and reliable determination of S-wave onsets was very difficult or even impossible.
For all of the following figures it has to be mentioned, that they are sorted for each channel separately along the borehole depth. The sort of seismic traces according to channels corresponds to a COF-section (common offset). Furthermore the derived seismic parameters such as velocities and amplitudes are associated with distances (borehole depths, z) which are assigned to the common mid point between source and receiver (CMP). The depths are given from the wall of the niche.

Two examples are used next to illustrate the high quality of the received seismograms and to demonstrate the possibilities for interpretation. On the basis of derived seismic parameters as

- P- and S-wave velocity distributions,
- amplitude distributions of P- and S-waves and
- seismogram characteristics

criteria were defined and used for the determination of the extent of the EDZ.

2.1.3.2.1 Raw Data and Qualitative Interpretation

In the following we describe in more detail exemplary data and results which were measured in June 2001 in the **first measurement plane** (plane 1 consists of boreholes BEB-B09, -B10 and -B11). Corresponding data acquired along the second plane do not differ very much from the first ones. Only the raw data and the up to now processed P-wave data are presented. This holds also for data measured in the second campaign in October 2001. The differences in the P-wave velocity distributions between the results of both campaigns will be emphasised and discussed later (cf. chap. 2.1.3.3.2).

The source signals were tuned in for each borehole at the beginning of the measurement and stayed constant for the period of the measurement. This is illustrated in Fig. 2.1-6 where the source signal of the interval velocity measurements in borehole BEB-B09 are displayed. The sine wave like signal has a main frequency of 50 kHz. An example of a raw data set for a single excitation point is presented in Fig. 2.1-5 (top, right).

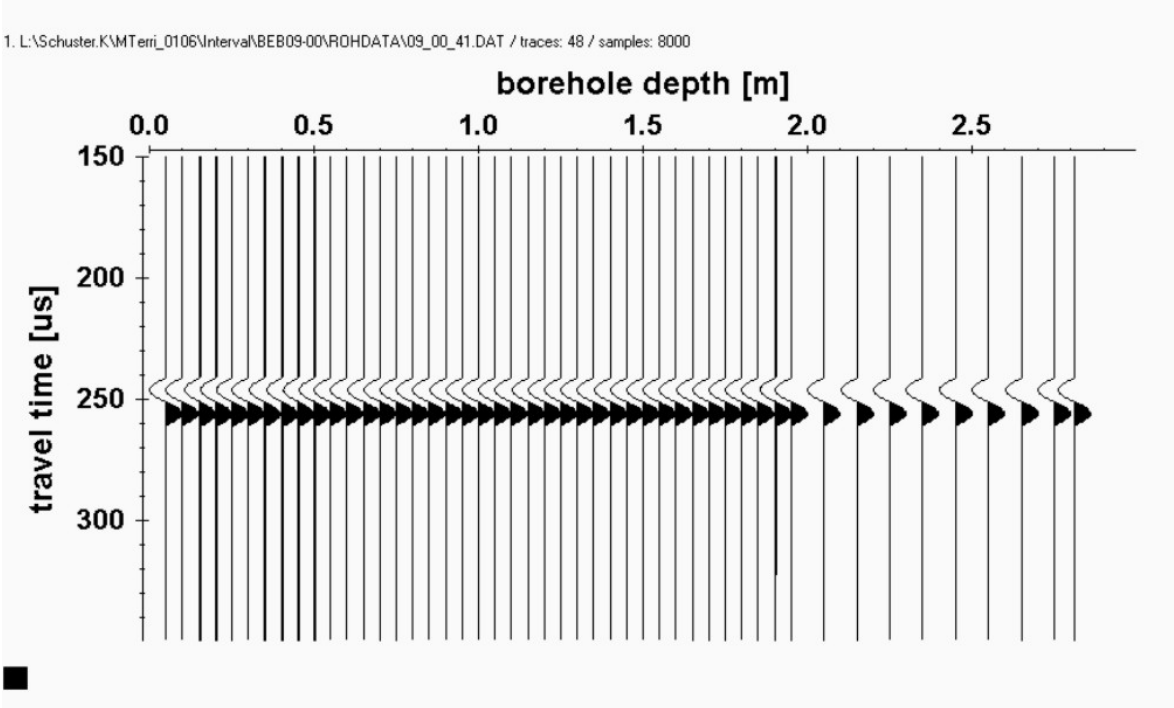

Fig. 2.1-6: Source signal from interval velocity measurements in borehole BEB-B09 (June 2001).

Fig. 2.1-7a and Fig. 2.1-8a show the raw data sets for boreholes BEB-B10 and BEB-B09 which were measured in June 2001. The seismograms for a source-receiver distance of 20 cm are selected, sorted and presented in the wiggle mode display. The displays of the seismograms are trace normalised (normalised to the maximum amplitude of each trace) in order to guarantee an optimum display of any single trace. From a borehole depth of 0.1 m to 1.5 m (BEB-B10) and 2.0 m (BEB-B09) the measurements were carried out in steps of 0.05 m, otherwise a 0.10 m step was used. The data for channel 1 and channel 3 are very similar to channel 2 data and show the same features. In general the quality of all signals are high, especially the signal to noise ratio. Only a moderate data improvement (bandpass filter) was applied. The signal quality (SQ) of first arrival phases (compressional waves, P-waves) and S-wave onsets (transverse waves, shear waves) was subdivided into three groups:

- SQ = 2: nearly all onsets are excellent, the rest is good,
- SQ = 1: majority of the onsets is good, the rest is excellent,
- SQ = 0: a few onsets not reliable identifiable, the rest is good or even excellent. The not reliable identifiable onsets were omitted or in some cases interpolated.

For the final analyses of P-waves, only signals with a very high signal to noise ratio were taken into account (indicated as signal quality SQ=2).

The certain recognition of S-wave onsets is more difficult due to a superimposition with other wave trains. Therefore we put more emphasis on the evaluation of P-waves.

In some cases, where the signal to noise ratios of the S-wave onsets are very low, the onset times had to be interpolated between neighbouring S-wave onsets of good quality. For this interpolation also a visual phase correlation was applied, because the second half of the S-wave phases in general allows a good phase correlation over the whole data set. The S-wave signal quality was set to zero (SQ = 0) in these cases. Mainly channel 3 data (distance between source and receiver is 30 cm) were taken into account for the further S-wave data analyses because at this distance the superimposition of reverberating P-wave phases and S-wave onsets is less disturbing than for shorter distances. An exception was made for BEB-B09 data where also channel 1 and channel 2 S-wave data were analysed, in order to demonstrate that main features can be observed in all three data sets.

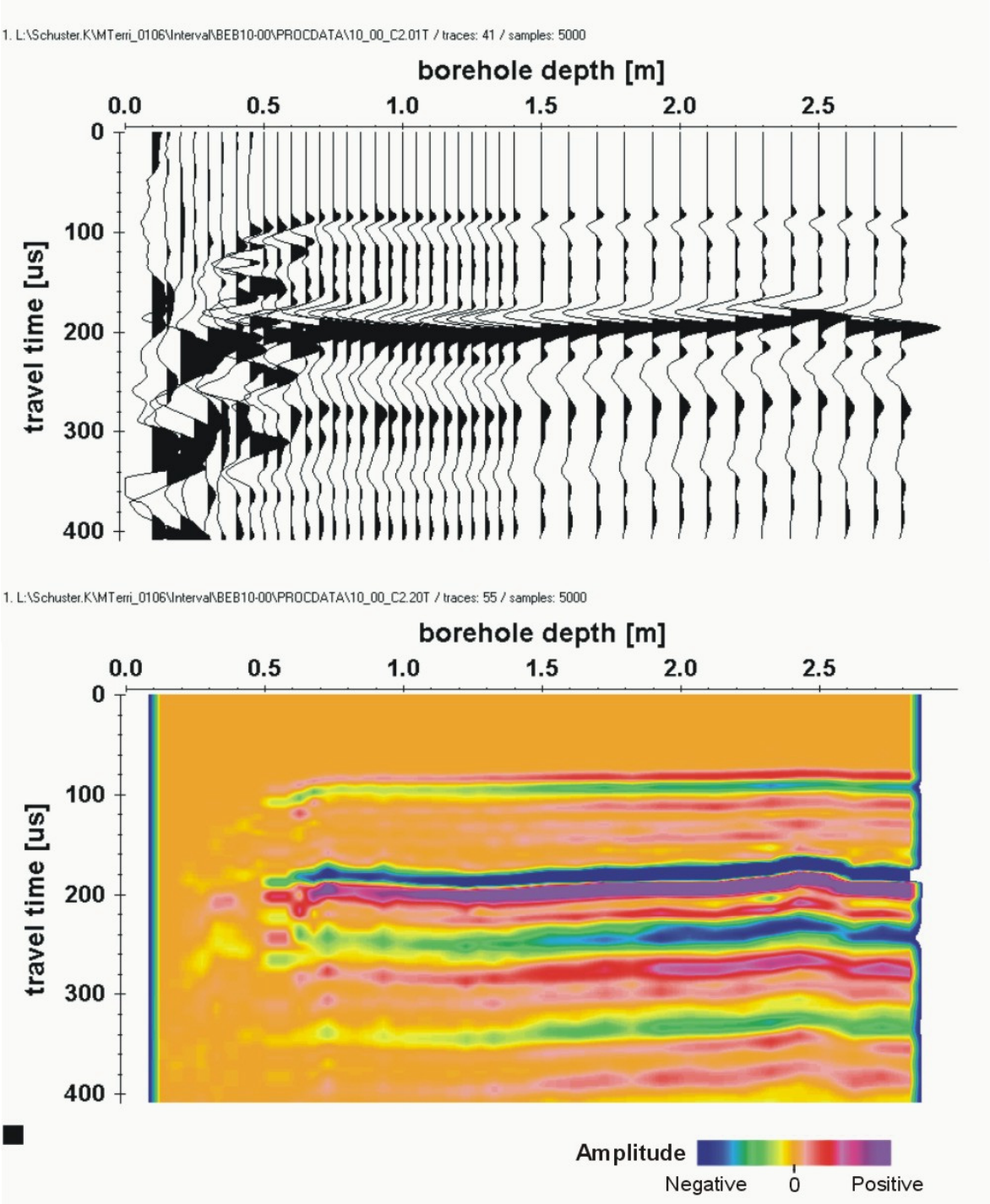

Fig. 2.1-7: Data set for borehole BEB-B10. Borehole 45° inclined. Channel 2 data (source receiver distance = 20 cm) are sorted along the borehole depth, bandpass filtered 5 - 100 kHz. Top (a): wiggle mode display, trace normalised, below (b): point mode display, amplitudes colour coded, ensemble normalised.

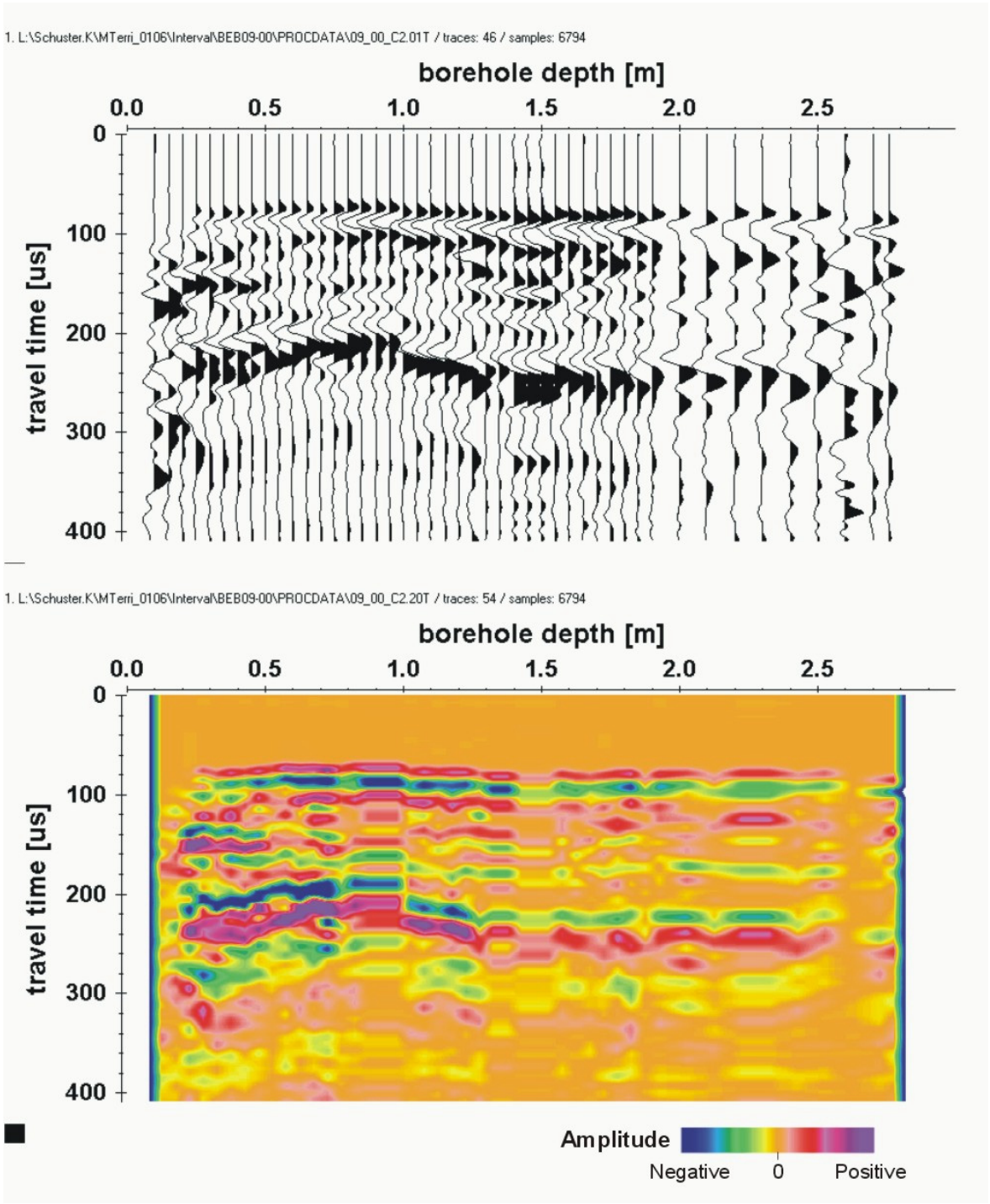

Fig. 2.1-8: Data set for borehole BEB-B09. Borehole 10° inclined. Channel 2 data (source receiver distance = 20 cm) are sorted along the borehole depth, bandpass filtered 5 - 100 kHz. Top (a): wiggle mode display, trace normalised, below (b): point mode display, amplitudes colour coded, ensemble normalised.

In Fig. 2.1-7a a strong decrease of the arrival times of the first arrival phases up to approx. 0.7 m is visible. Towards greater depth arrival times are still increase, but now very slightly. Coherent phases around 160 μs show the onsets of shear waves (S-waves). Up to 0.3 m no first arrival phases can be identified. The signal quality up to 0.5 m is very bad. For depth greater 0.7 m the seismogram looks relatively homogeneous.

In Fig. 2.1-8a also a decrease of the arrival times of the first arrival phases up to approx. 0.8 m is visible, but not as strong as in Fig. 2.1-7a. Towards greater depth arrival times are increase again and then they stay constant. Onsets between 165 μs and 195 μs are related to S-waves. Minor anomalies can be identified. The general appearance of the seismogram is rather inhomogeneous.
A simple visual comparison of both data sets reflects differences for depth greater 0.5 m. In contrast to the BEB-B09 data, which show an irregular appearance, borehole BEB-B10 data are much less disturbed. According to the seismogram characteristic up to 0.4 m the borehole BEB-B10 seems to be more damaged than the borehole BEB-B09.
The above described observations will be quantified and described later in terms of velocity and amplitude distributions along the borehole depth in more detail in Fig. 2.1-9a-d to Fig. 2.1-14a-d.

For a closer qualitative examination, data from both boreholes can be normalised over the complete ensemble of traces and displayed as in Fig. 2.1-7b and Fig. 2.1-8b. Seismic traces are displayed in this case in a point mode, where the amplitudes of the traces of the complete data set are colour coded (violet/red: positive amplitudes, blue/green: negative amplitudes, amber: zero level) and interpolated between adjacent traces. The strong variability in the amplitude distribution as well as in the travel times between the two boreholes are remarkable. For borehole BEB-B10 (Fig. 2.1-7b) the displayed first arrival phases (red band at 80 μs) and the S-waves (blue band at 180 μs) stay almost constant in time for depths greater 0.6 m. Amplitudes are increase gradually. Up to 0.5 m the seismogram is extremely disturbed. Amplitudes nearly disappear totally. Fig. 2.1-8b shows a differ-

ent picture. Only up to a depth of 0.25 m the first arrival phases disappear. The seismogram looks inhomogeneous.

The variability in the amplitude distribution as well as in the travel times are remarkable. Not all features can be seen in the up to now discussed displays due to the limited dynamic resolution of the hardcopies. According to the chosen dynamic range of the display later phases of the onsets are more emphasised.
The onsets of the source signals (Fig. 2.1-6) as well as the first arrival times of P- and S-waves and the maxima of these phases (for P-waves: first positive maximum, for S-waves: first negative minimum) were picked manually and used for further calculations.

2.1.3.2.2 Quantitative Evaluation and Interpretation

In the following figures the results for these two boreholes are presented in a more quantitative form. Fig. 2.1-9 to 2.1-11 (borehole BEB-B10) and Fig. 2.1-12 to 2.1-14 (borehole BEB-B09) present seismic and elastic parameters which were derived from the data. For a better comparison the same axis scaling was chosen for corresponding parameters.
P-wave velocities, amplitudes as well as apparent frequencies were derived from first arrival phases, whereas the S-wave velocities, amplitudes and apparent frequencies were derived from the corresponding S-wave onsets. The results are quantified in terms of velocity, apparent frequency and amplitude distributions along the borehole depth. As mentioned before only signals with a high signal to noise ratio were considered (SQ=2) for the P-wave analyses. For the S-wave analyses also some interpolated time values were considered. This is indicated with SQ = 0.

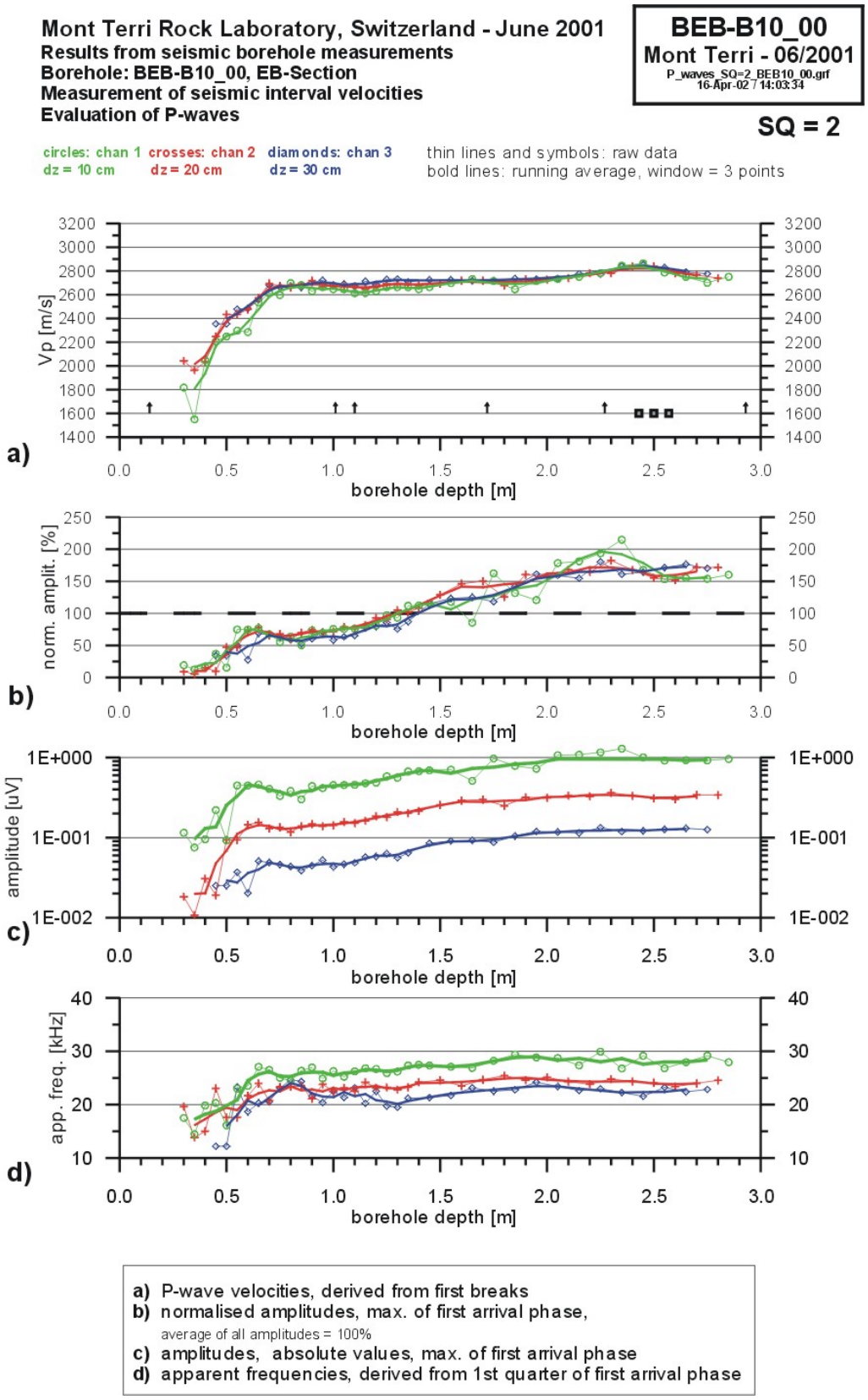

Fig. 2.1-9: Borehole BEB-B10, June 2001: Seismic parameters derived from analyses of P-waves from interval velocity measurements. In addition structural features from drillcore mapping plotted in the Vp-graph (rectangle: sandy layer, arrow: artificial discontinuity).

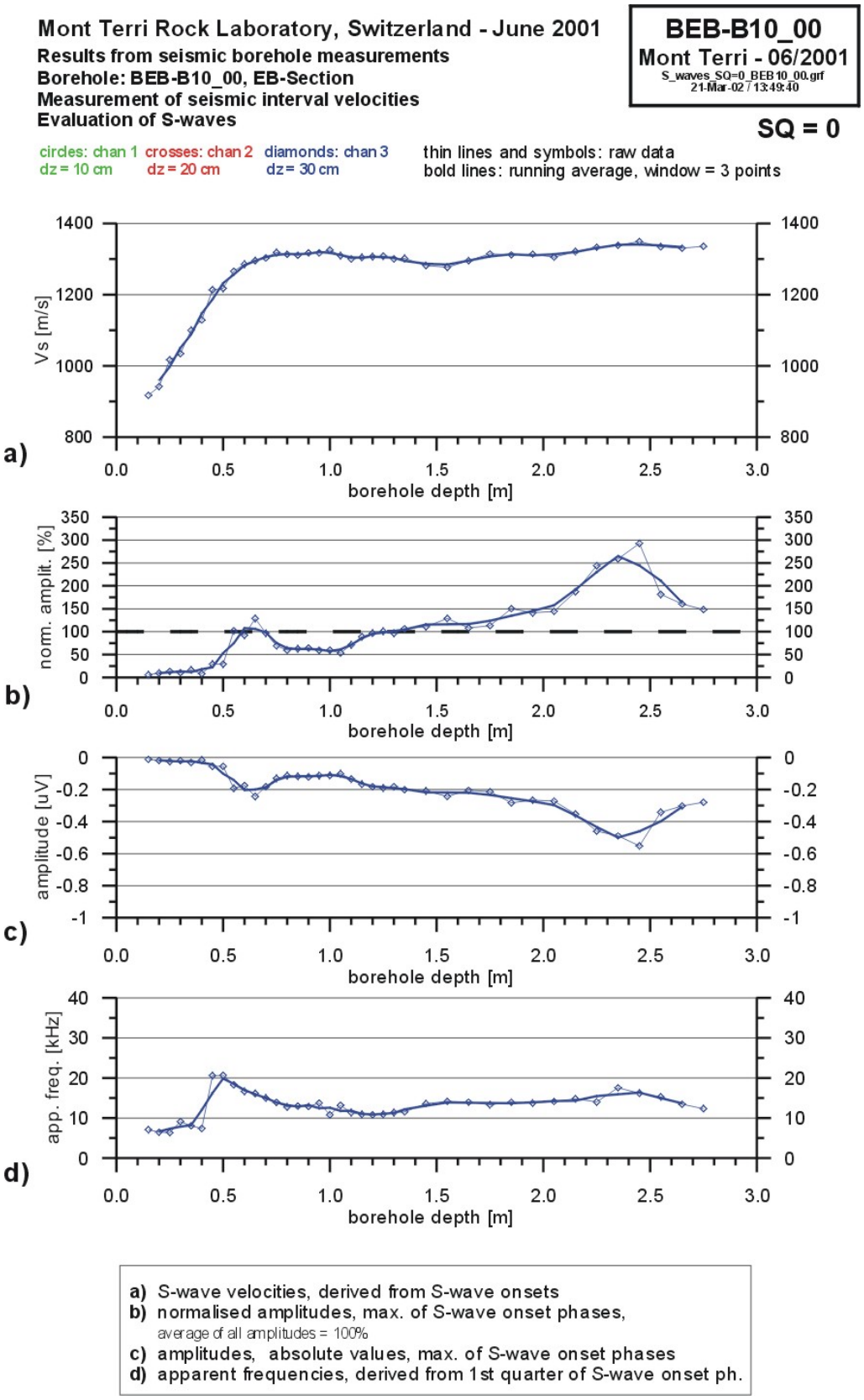

Fig. 2.1-10: Borehole BEB-B10, June 2001: Seismic parameters derived from analyses of S-waves from interval velocity measurements.

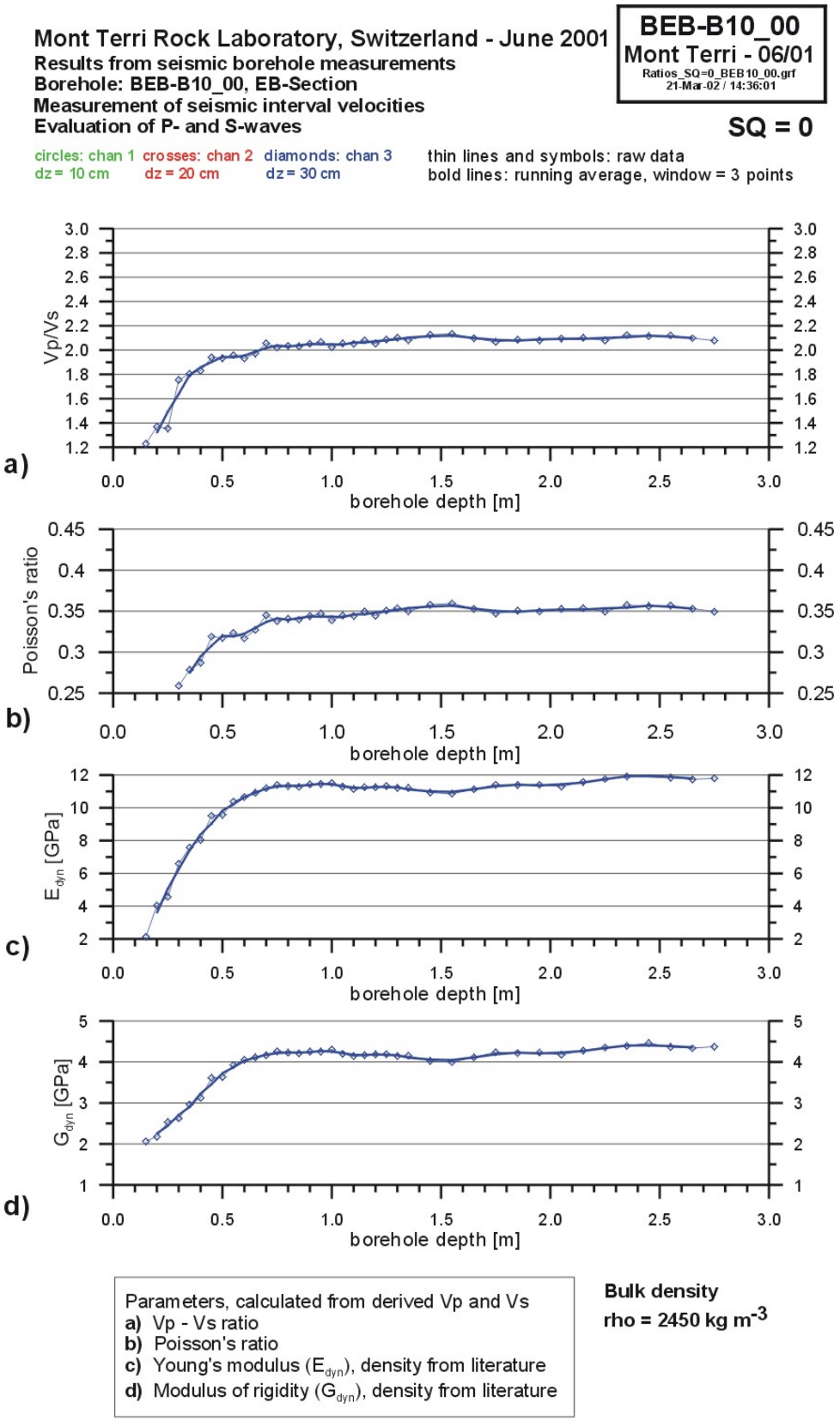

Fig. 2.1-11: Borehole BEB-B10, June 2001: Seismic and elastic parameters derived from analyses of P- and S-waves from interval velocity measurements.

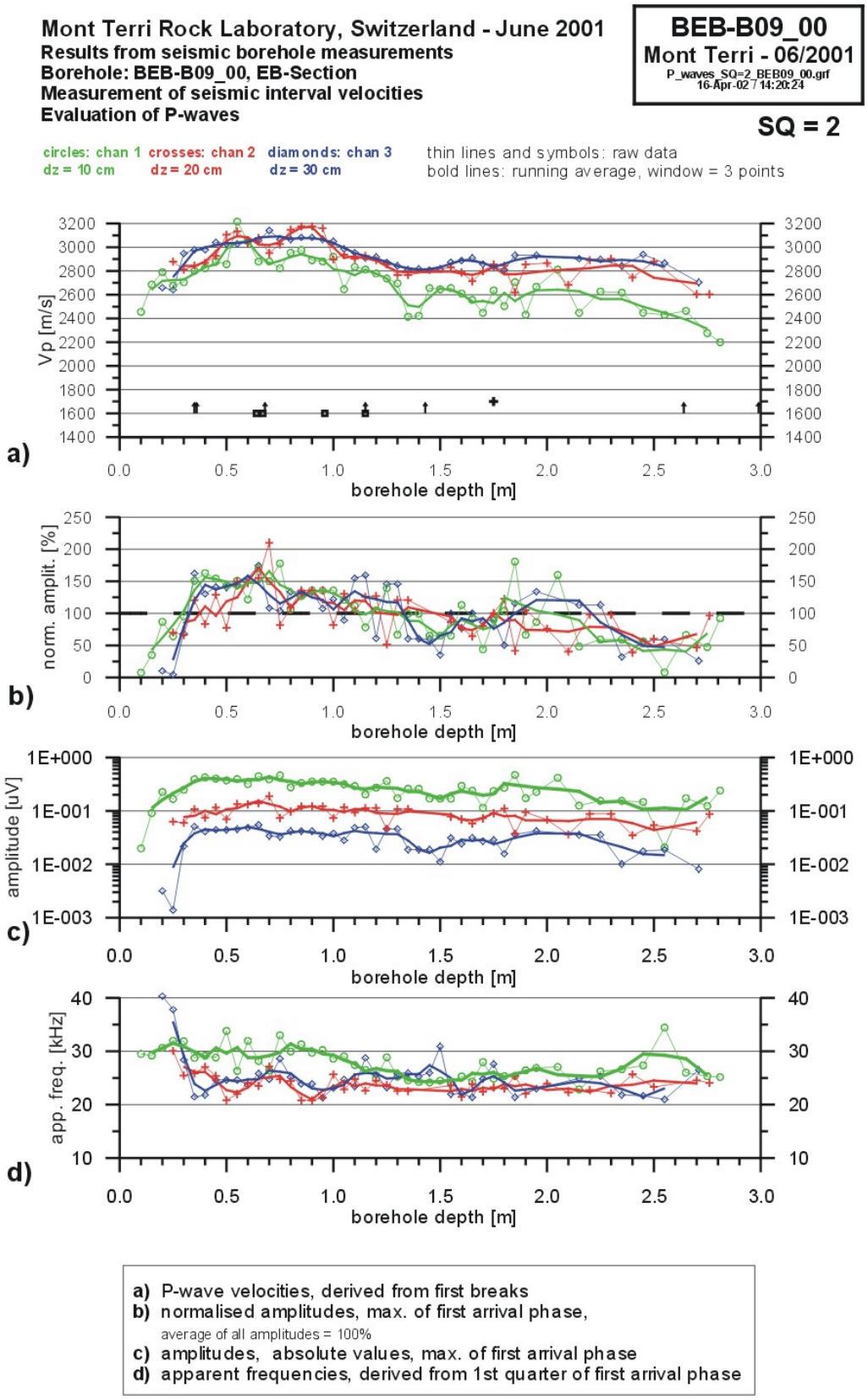

Fig. 2.1-12: Borehole BEB-B09, June 2001: Seismic parameters derived from analyses of P-waves from interval velocity measurements. In addition structural features from drillcore mapping plotted in the Vp-graph (rectangle: sandy layer, arrow: artificial discontinuity, cross: slickenside).

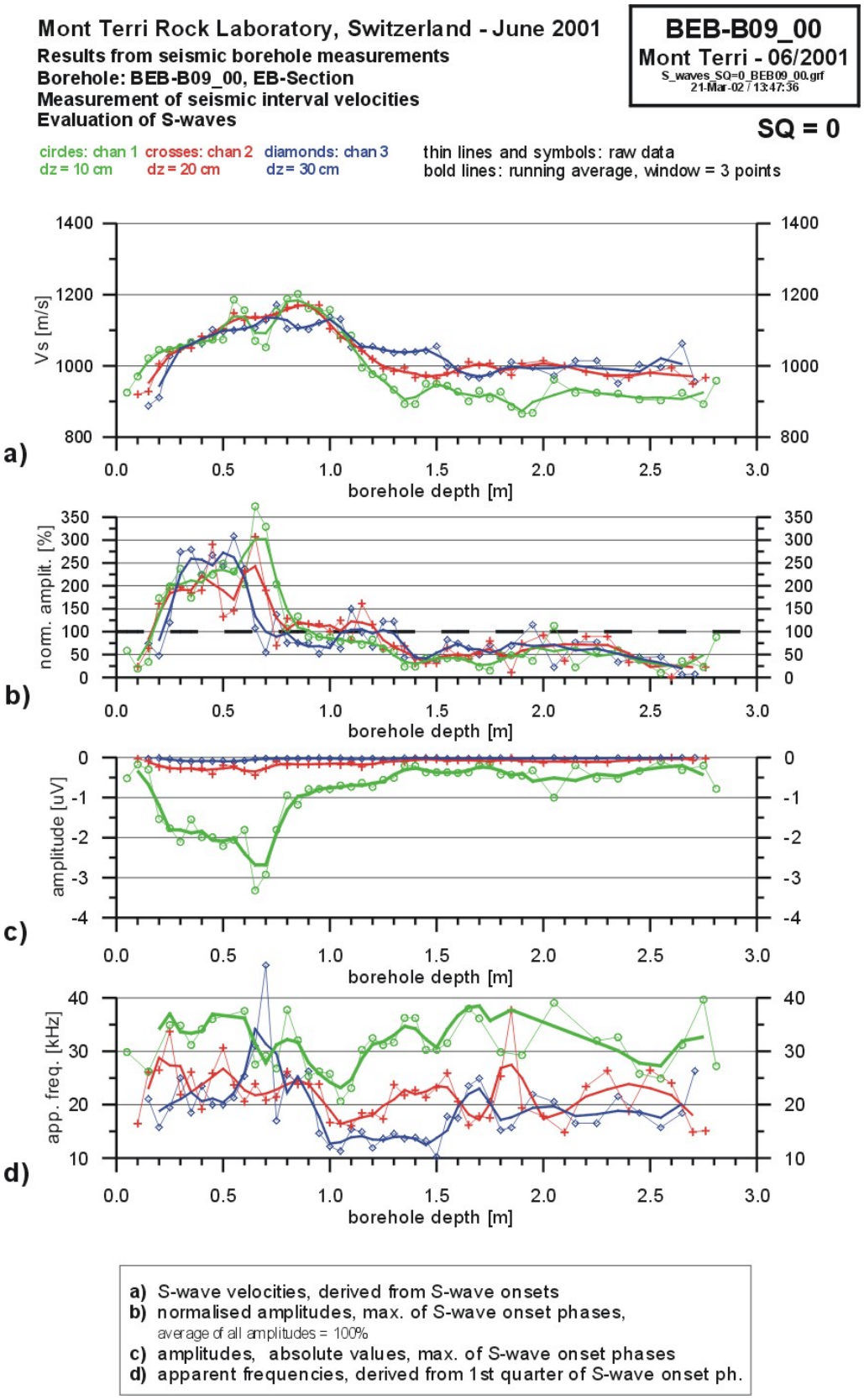

Fig. 2.1-13: Borehole BEB-B09, June 2001: Seismic parameters derived from analyses of S-waves from interval velocity measurements.

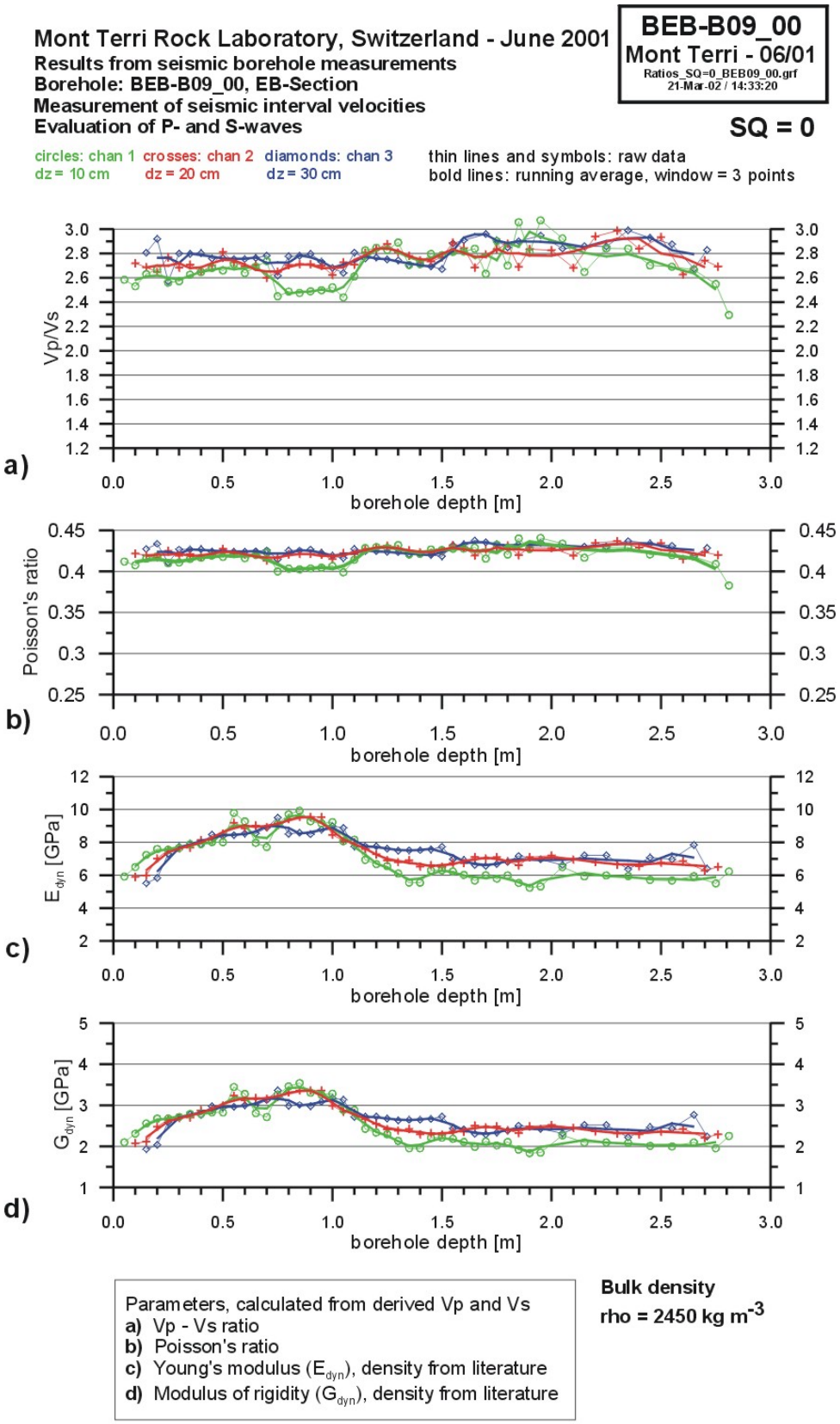

Fig. 2.1-14: Borehole BEB-B09, June 2001: Seismic and elastic parameters derived from analyses of P- and S-waves from interval velocity measurements.

Figures 2.1-9a and 2.1-12a show the **P-wave velocity distribution** along the boreholes. P-waves velocities, apparent frequencies and amplitudes were determined for all three receivers for different interval lengths (10 cm, 20 cm and 30 cm). Different colours were used for the results derived from the analyses of the three channels, which means that three different interval lengths were evaluated (channel 1: Δz =10cm, **green**; channel 2: Δz = 20cm, **red**; channel 3: Δz =30cm, **blue**). In order to smooth small scale fluctuations additionally a running average (window of 3 points) is displayed in the graphs (bold lines).
It is obvious from Figure 2.1-12a that the velocities increase with increasing interval length (10, 20, 30 cm). These differences will be discussed in chap. 2.1.3.2.4 and chap. 2.1.3.3.3.

The **first peak amplitudes** of the first arrival phases were used for the calculation of the amplitude distribution along the boreholes (Fig. 2.1-9c and Fig. 2.1-12c). According to the different travel paths amplitudes from channel 1 data (shortest path) are stronger than amplitudes derived from channel 2 and channel 3 data. In Figures 2.1-9b and 2.1-12b these amplitude values were **normalised** by using the mean value of all amplitudes from the corresponding borehole. Values smaller than 100 % lie below the average whereas values greater than 100 % lie above the average. The normalisation was done in order to make results from different boreholes comparable. Hence the influence of different coupling conditions in different boreholes can be minimised. Amplitudes show no significant systematic change with the length of the interval in this type of display because they are normalised.
Apparent frequencies as shown in Fig. 2.1-9d and Fig. 2.1-12d were derived from the first quarter of the first arrival phase. As expected we see in general the same trend as in the amplitude distribution, higher apparent frequencies for the channel 1 data than for channel 2 and 3 data. For the actual interpretation this parameter is of minor importance.

All graphs in Fig. 2.1-9 are relatively smooth. P-wave velocities increase from less than 1600 m/s to 2700 m/s within the first meter. This can be seen as a strong indication for the existence of an EDZ. With some small scale undulations the veloc-

ity increases slightly up to a maximum value of 2850 m/s. Normalised amplitudes give a similar picture. Up to 0.6 m the very low normalised amplitude values give an indication for a distinct damage of the rock. The loss of data for distances below 0.3 m means that the data quality was very bad what can be traced back of a severe damage of the rock in this part.

On the contrary the graphs in Fig. 2.1-12 show more variations. P-wave velocities starts already at 0.2 m with values of 2700 m/s. They reach maximum values between 0.3 m and 1.0 m (3100 m/s - 3200 m/s) before they fall back to a relative stable plateau of 2900 m/s for channel 3 data. The related normalised amplitudes show also between 0.3 m and 1.0 m higher values. According to these observations the extent of the EDZ is shorter than 0.25 m.

The above discussed parameters were also derived from **S-wave onsets**. They are compiled in the same way as the P-wave parameters in Fig. 2.1-10 (borehole BEB-B10) and Fig. 2.1-13 (borehole BEB-B09). The general trend in the distribution of P-wave parameters (Fig. 2.1-9 and Fig. 2.1-12) is, except of some small deviations, also discernible in the parameters derived from S-waves.

The knowledge of seismic **P- and S-wave velocities** along the borehole allows the calculation of the **P- to S-wave velocity ratios**. These ratios are shown in Fig. 2.1-11a (BEB-B10) and Figure 2.1-14a (BEB-B09). For depth greater 1 m the values lie around 2.1 (BEB-B10) and 2.8 (BEB-B09), what is a big difference.
Furthermore elastic parameters like Poisson's ratio, Young's modulus and the modulus of rigidity can be calculated. We did it with the up to now processed data for plane 1 (signal quality for P-waves: SQ=2, for S-waves: SQ=1 and even 0).
For a general interpretation of the derived elastic parameters one have to keep in mind, that the values are dependent on the direction of measurements (perpendicular to the wall, and most probably perpendicular to the micro fracturing of the EDZ). Furthermore they may be influenced by a small scale EDZ around the borehole wall (cf. chap. 2.1.3.2.4 and 2.1.3.3.3).

Due to the fact that the P- and S- wave distributions of both boreholes in each case are very similar, also the derived elastic parameters resemble.

The **Poisson's ratio** was calculated and displayed in Fig. 2.1-11b and Fig. 2.1-14b. For borehole BEB-B10 the values increase steep up to 0.4 m, than they increase only gentle to a stable plateau of approx. 0.35. With a mean value of 0.425 for borehole BEB-B09 the value is very high.

For the estimation of two further elastic rock parameters a mean value for the bulk density (under natural conditions) was taken from Bock (2001). With this bulk density the **Young's modulus** (E_{dyn}) and the **modulus of rigidity** (G_{dyn}) were calculated along the borehole depth.

The results are shown in Figures 2.1-11c, d and Figures 2.1-14c, d. Values for E_{dyn} vary between 11 GPa and 12 GPa for borehole BEB-B10 data for depths greater than 0.7 m. For smaller depths they drop down drastically. In borehole BEB-B09 the values show maxima between 0.5 m and 1.1 m, than they stay stable around 7 GPa. Values for G_{dyn} and depth greater 1 m increase to 4.5 GPa (BEB-B10) and 2.5 GPa (BEB-B09).

In order to complete the detailed presentation of results derived from the first measurement plane (boreholes BEB-B09, BEB-B10, BEB-B11) in Fig. A-1 to Fig. A-3 (see appendix) results obtained from borehole BEB-B11 are shown uncommented in the same manner.

In Fig. A-4 to Fig. A-6 in the appendix the derived P-wave parameters from the **second plane** are presented. Similarities to plane 1 data are obvious. S-waves are not yet analysed.

Fig. 2.1-15 comprises all band pass filtered (BP, Butterworth: 5 - 100 kHz) channel 2 data form June 2001 measured along both planes. They are presented with colour coded amplitudes in a time window between 0 and 400 μs, which includes the first arrival phases (approx. 80 μs) and the S-wave onsets (approx. 180 μs).

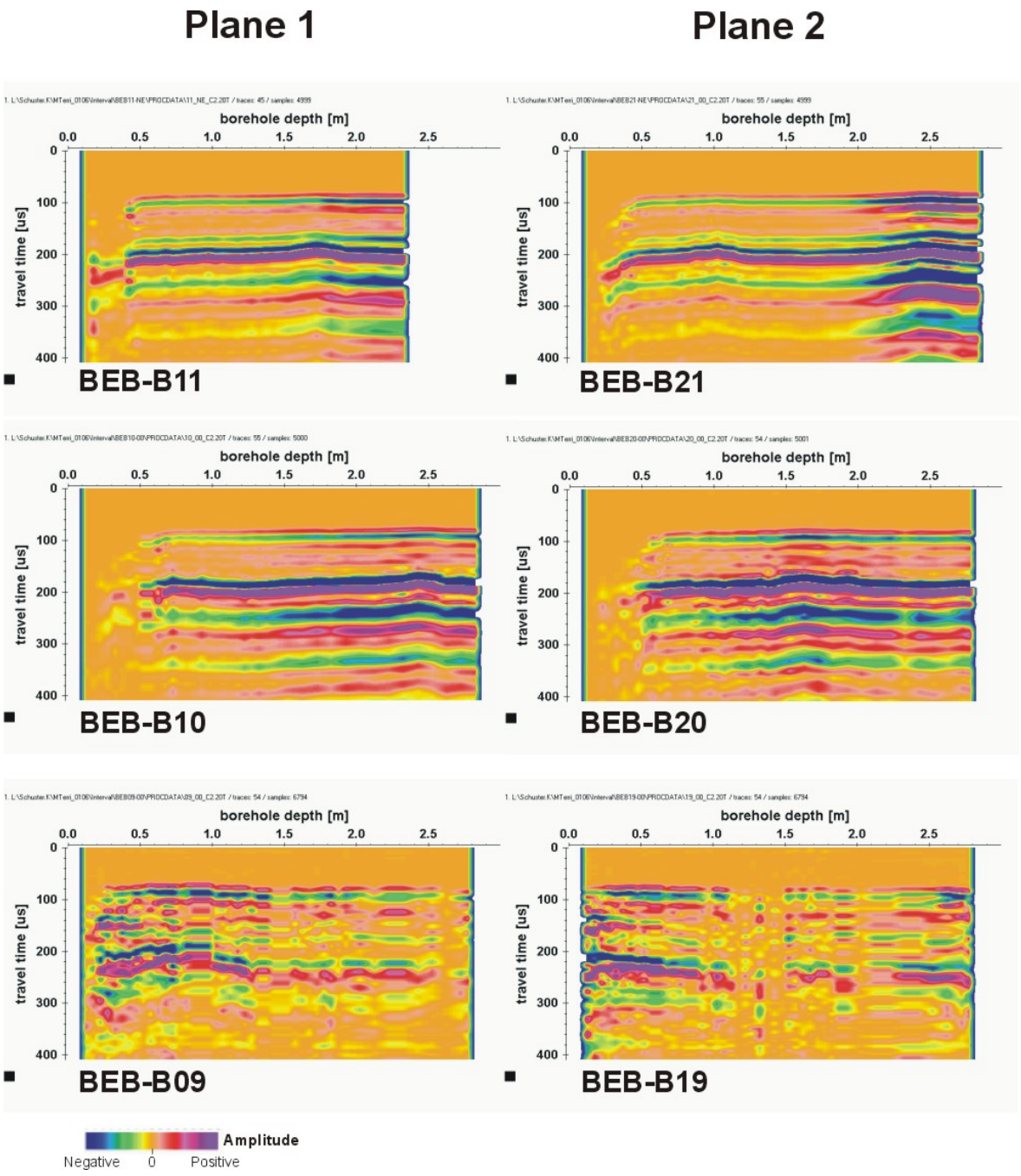

Fig. 2.1-15: Data sets from interval velocity measurements for all boreholes in plane 1 and plane 2 measured in June 2001 in the EB niche of the Mont Terri Rock Laboratory. Channel 2 data (source receiver distance = 20 cm). Bandpass filtered 5 - 100 kHz, point mode display, amplitudes colour coded, ensemble normalised.

Fig. 2.1-16 shows in the same representation and scale all channel 2 data measured during the second campaign in October 2001. In both subhorizontal boreholes (BEB-B09 and -B19) access was possible only to depth of 1.25 m. The boreholes were collapsed beyond this depth. The comparison of these two data

sets shows already that they are similar and it seems that big differences in the derived parameters can not be expected.

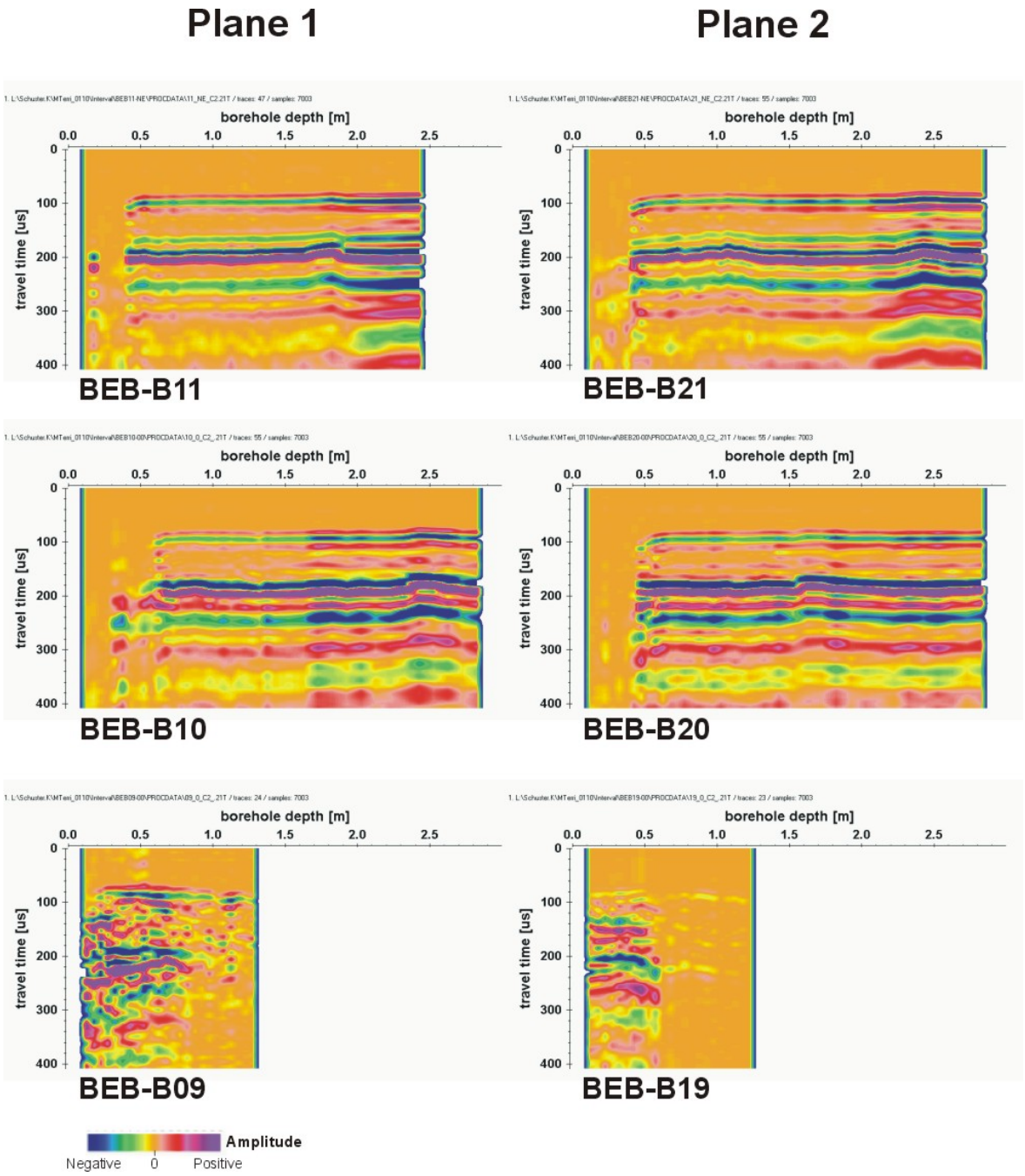

Fig. 2.1-16: Data sets from interval velocity measurements for all boreholes in plane 1 and plane 2 measured in October 2001 in the EB niche of the Mont Terri Rock Laboratory. Channel 2 data (source receiver distance = 20 cm). Bandpass filtered 5 - 100 kHz, point mode display, amplitudes colour coded, ensemble normalised.

Fig. A-7 to Fig. A-12 in the appendix show all derived P-wave parameters from measurements in October 2001 in the up to now presented manner. For all graphs, the same axis scaling was used for better comparison. The differences between both data sets will be discussed in chap. 2.1.3.3.2.

2.1.3.2.3 Determination of the Extent of the EDZ

It is characteristic for damaged zones that they are very good reflected in decreased seismic P-wave velocities and reduced amplitude values.
The seismic and elastic parameter distributions for all boreholes were determined from the data of seismic interval velocity measurements as shown and discussed in detail exemplary for boreholes BEB-B10 and BEB-B09 above (Fig. 2.1-9 to 2.1-14). The **extent of the EDZ** was determined using three criteria:

- The **zone of reduced velocities** until an almost constant velocity or very smooth velocity increase is observed independent of the absolute value.
- The extent of **zones of increased damping** was determined as the distance from which the relative amplitudes stay almost constant.
- Additional information can be recovered from the complete characteristics of the seismograms. For each borehole, the extension of a **zone of disturbed seismograms** was obtained from graphs showing the complete seismogram section where amplitudes are colour coded (cf. Fig. 2.1-7b and Fig. 2.1-8b).

With the help of these criteria all derived parameter distributions were analysed. The results for the estimation of the extent of the EDZ are summarised in Table 2.1-1 (June 2001) and Table 2.1-2 (October 2001) in chap. 2.1.3.3.1.

2.1.3.2.4 Influence of Interval Length

The differences in the derived parameters, especially the velocities, between chan. 1, 2 and 3, as can be seen in Fig. 2.1-12 for example, can be interpreted as an effect of different depths of penetration of seismic waves. According to greater interval length (spacing between source and receiver) the penetration of seismic waves into the rock increases under conditions where a velocity gradient, perpen-

dicular to the borehole axis, exists. In these cases the seismic waves reach less damaged parts of the rock. These disturbances are caused most probably by the drilling of the borehole and the following unloading. This can be regarded as the effect of a "small scale EDZ (excavation damaged zone)" around the borehole under investigation.

2.1.3.2.5 Uncertainties and Errors

For the interval velocity measurements we have to take into account an uncertainty of ± 0.5 to max. ± 1.5 microseconds for the determination of the onsets of the P-waves and between ± 1 and max. ± 4 microseconds in the worst case for the S-waves. This results in an uncertainty for P-wave velocities in the range between ± 9 % for channel 1 data and ± 3 % for channel 3 data. For S-waves the uncertainties in the velocity determination lies between ± 12 % for channel 1 data and ± 4 % for channel 3 data. The mentioned maximum values should be regarded as exceptions which occur only in some parts of the data with bad signal quality. Possible errors for the elastic parameters derived from channel 3 data are in the range of ± 7 % in the worst case. An error for the determination of the extent of the EDZ can only be estimated roughly. It should not exceed ± 10 cm.

2.1.3.3 Results of Interval Velocity Measurements

2.1.3.3.1 Extent of the EDZ

Seismic P-wave parameters derived from interval velocity measurements, as discussed by means of Fig. 2.1-9 to Fig. 2.1-14, form the basis for the formulation of a set of criteria (cf. chap. 2.1.3.2.3) which were used to assess the extent of the EDZ for boreholes BEB-B09 - BEB-B21. Concerning the determination of the extent of the EDZ Table 2.1-1 (June 2001) and Table 2.1-2 (Oct. 2001) and Fig. 2.1-17a (June 2001) and Fig. 2.1-17b (Oct. 2001) summarise the results of the interpretations according to three criteria which were explained above. The results obtained from these different criteria generally demonstrate good accordance. The average of the three values were calculated and rounded. They yield the values of

the final assessment of the extent of the EDZ. They are listed also in the last columns of Tab. 2.1-1 and Tab. 2.1-2 and they are visualised in Fig. 2.1-18a and Fig. 2.1-18b, where they are sorted corresponding to the orientation of the boreholes. The largest values (0.65 m) for the extent of the EDZ are reached in the 45° inclined boreholes (BEB-B10 and BEB.B20) whereas the shortest values, between 0.1 m and 0.2 m were obtained in the subhorizontal boreholes BEB-B09 and BEB-B19.

Borehole	Constant Velocity (all channels)	Normalised Amplitude (all channels)	Seismogram Characteristic (channel 2)	Final Extent
Plane 1 BEB-B09	0.15	0.20	0.25	0.20
BEB-B10	0.70	0.60	0.65	0.65
BEB-B11	0.55	0.45	0.45	0.50
Plane 2 BEB-B19	<0.10	0.20	0.20	0.15
BEB-B20	0.70	0.60	0.65	0.65
BEB-B21	0.50	0.50	0.45	0.50

Tab. 2.1-1: Extent of the EDZ in meters according to different criteria.
Derived from seismic P-wave parameters, measured in June 2001.

Borehole	Constant Velocity (all channels)	Normalised Amplitude (all channels)	Seismogram Characteristic (channel 2)	Final Extent
Plane 1 BEB-B09	0.20	0.20	0.25	0.20
BEB-B10	0.65	0.60	0.65	0.65
BEB-B11	0.50	0.45	0.45	0.45
Plane 2 BEB-B19	0.10	0.15	0.10	0.10
BEB-B20	0.70	0.55	0.55	0.60
BEB-B21	0.65	0.45	0.45	0.50

Tab. 2.1-2: Extent of the EDZ in meters according to different criteria.
Derived from seismic P-wave parameters, measured in October 2001.

No significant changes in the extent of the EDZ between both measurement campaigns can be observed. But values for P-wave velocities changed slightly. This will be analysed in the following chapter.

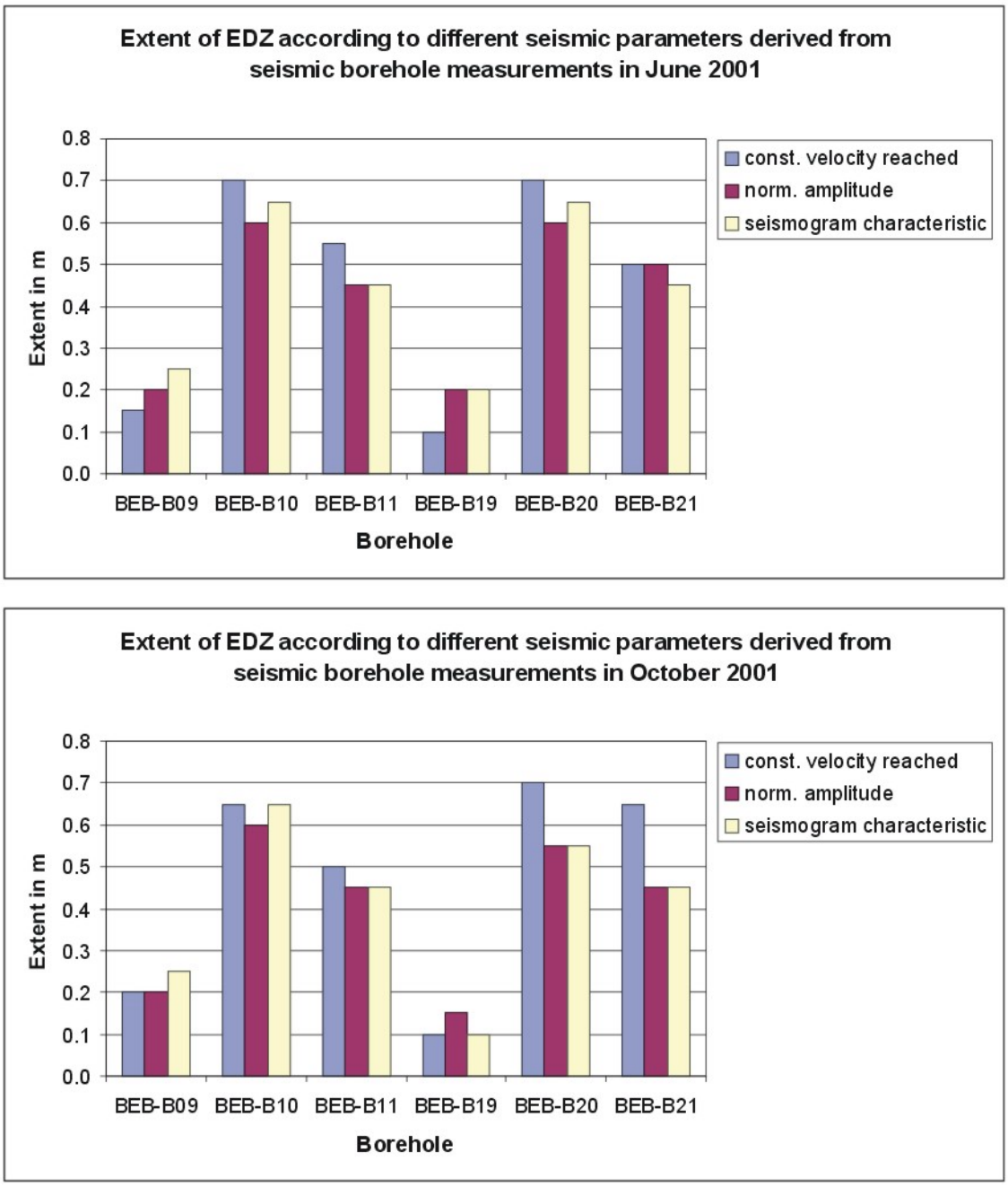

Fig. 2.1-17: Extent of the EDZ according to different criteria. Top (a): June 2001, Below (b): October 2001.

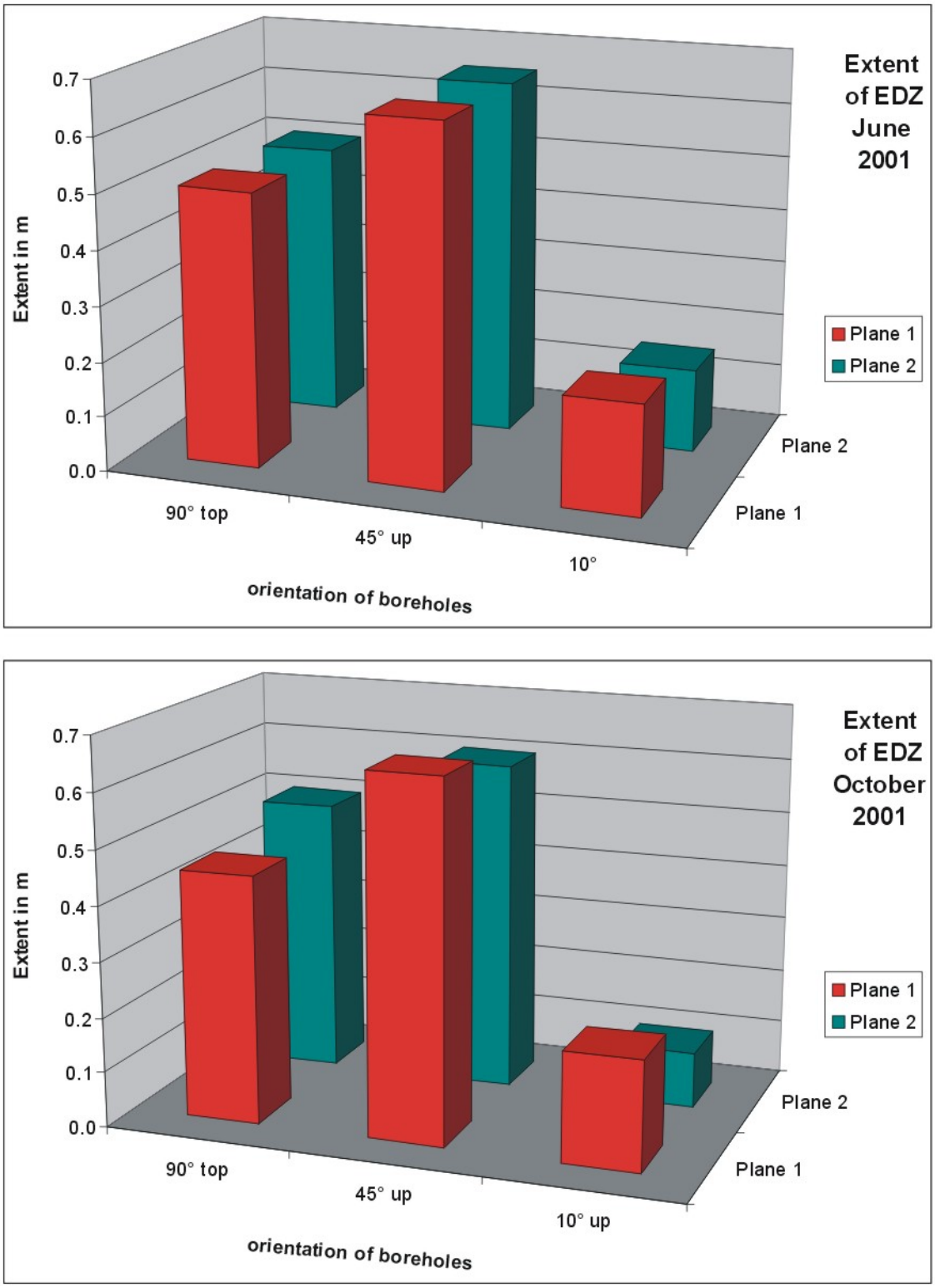

Fig. 2.1-18: Illustration of the extent of the EDZ for boreholes BEB-B09 - BEB-B11 (plane 1) and BEB-B19 - BEB-B21 (plane 2). Top (a): drilled and measured in June 2001, Below (b): drilled and measured in October 2001.

2.1.3.3.2 Comparison between Results Derived in June and October 2001

That the repetition of interval velocity measurements after longer periods can provide sensible results will be demonstrated with Fig. 2.1-19 and Fig. 2.1-20. Measurements taken in June and October 2001 are compared. For a better comparison the already shown P-wave velocity distributions (cf. Fig. 2.1-12a / A-7a for BEB-B09 and Fig. A-1a/A-9a for BEB-B11) are displayed again, but with a higher vertical resolution and in one figure. Due to the collapse of both subhorizontal boreholes in October measurements could be done only to depths of 1.25 m. All seismic data from both campaigns were already shown for comparison in an ensemble normalised amplitude colour coded display in Fig. 2.1-15 (June 2001) and Fig. 2.1-16 (October 2001).

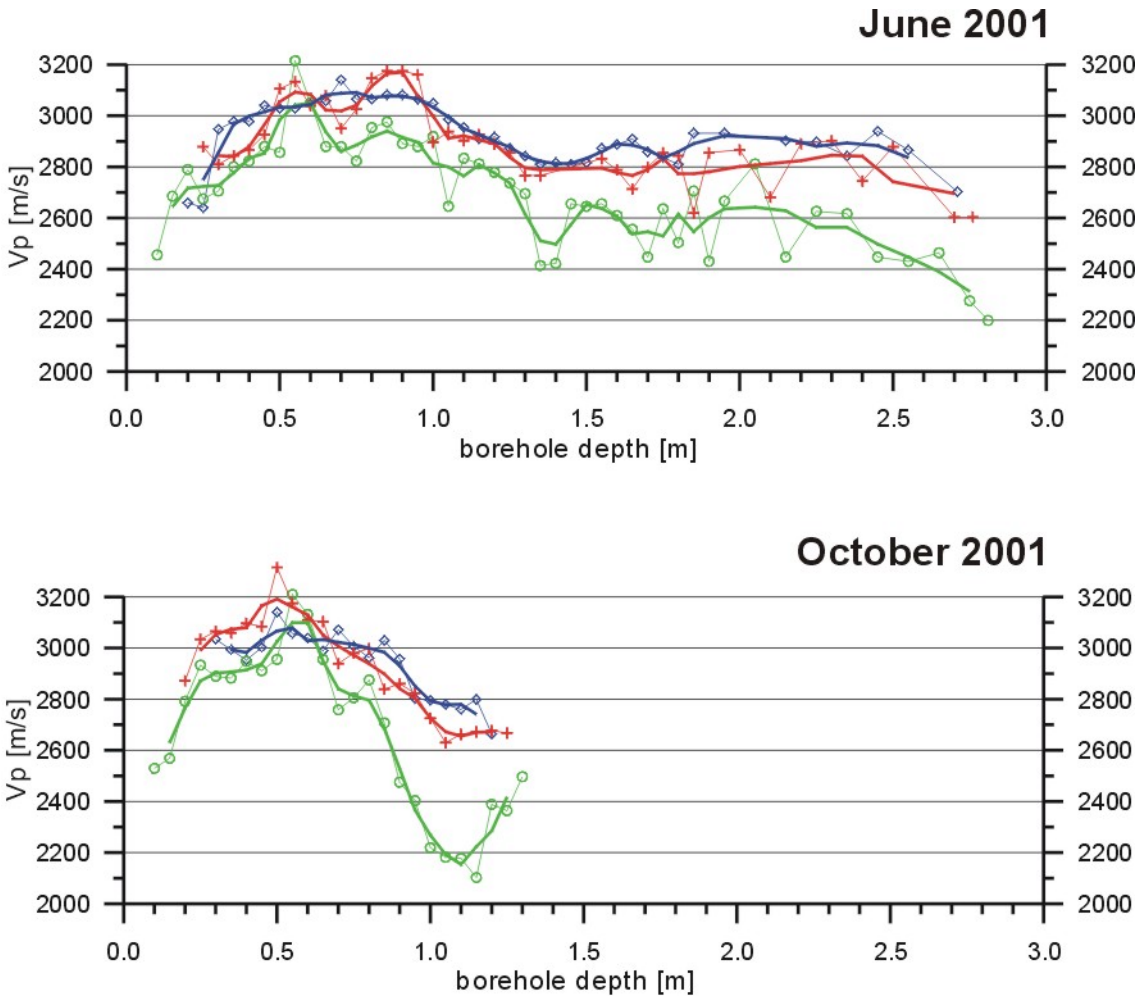

Fig. 2.1-19: Comparison of interval velocities derived from measurements in June 2001 (top) and October 2001 (below) in borehole BEB-B09.

For borehole BEB-B09 the high velocity range with P-wave velocities greater 2900 m/s, measured in June 2001, between 0.3 m and 1.2 m seems to be shrunk to a range between 0.25 m and 0.9 m. For the P-wave velocities measured in borehole BEB-B11 no remarkable differences between the two measurement campaigns can be seen.

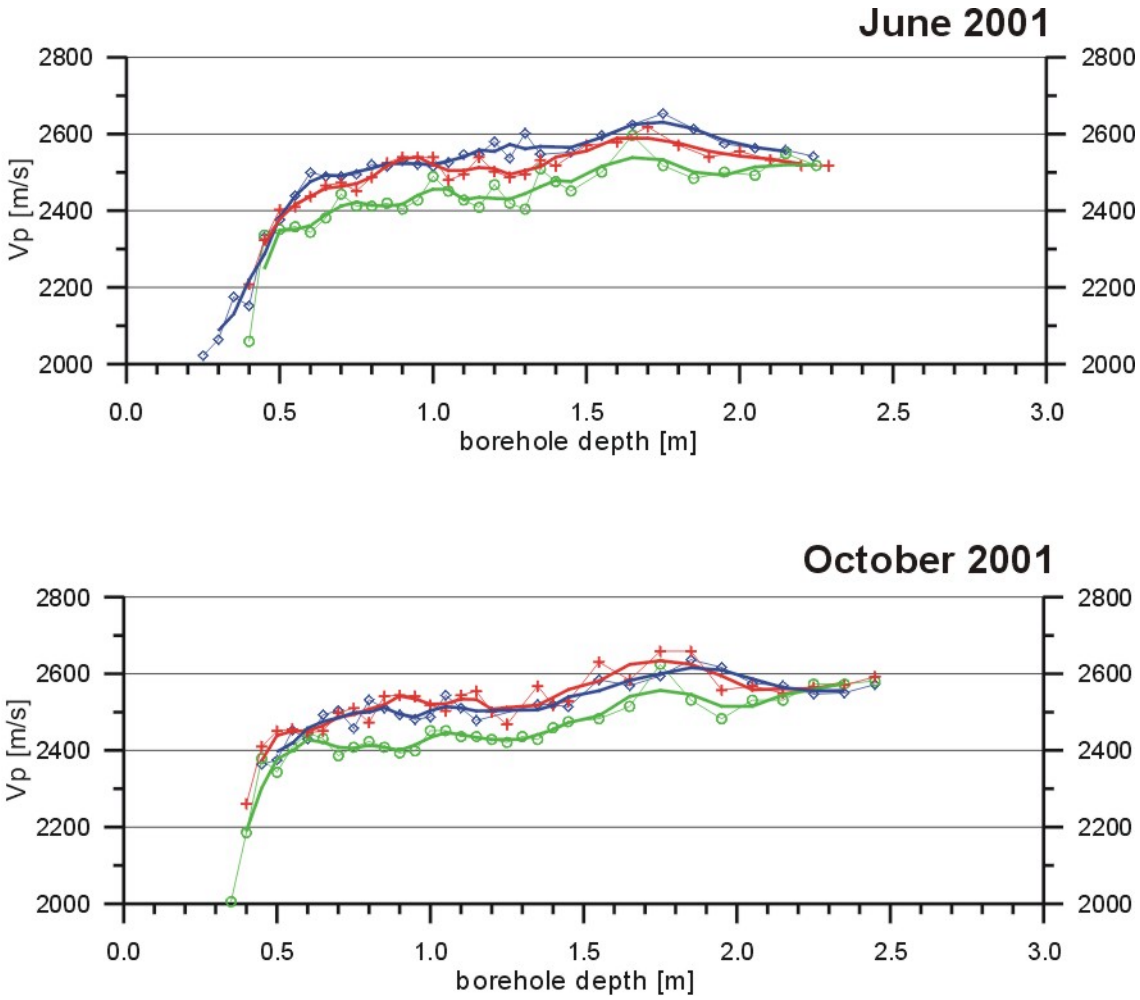

Fig. 2.1-20: Comparison of interval velocities derived from measurements in June 2001 (top) and October 2001 (below) in borehole BEB-B11.

Differences in the P-wave velocity distribution along the boreholes between both campaigns are summarised in Fig. 2.1-21 for plane 1 data and Fig. 2.1-22 for plane 2 data. Differences were calculated and expressed as a percentage deviation of the October results from the results obtained in June 2001. Apart from some minor deviations we can state that for both planes the differences in the roof

(BEB-B11 and BEB-B21) are very small (plane 1) or slightly positive (plane 2) whereas they are negative in both planes for the 45° upward direction for depths greater 0.9 m. For depths smaller 0.8 m only for BEB-B20 (plane 2) values are positive. In the subhorizontal boreholes the values also up to 0.6 m depth are positive and beyond this depth they are negative.
For a certain rock volume under homogeneous isotropic conditions we can assume that an increase of P-wave velocity can be correlated with a "consolidation" of the rock whereas a decrease of P-wave velocity for the same sample is related to a "loosening" of the rock. In this context areas with lower velocities can be regarded as an indication for a greater damage of the Opalinus Clay. Contrary, areas with higher velocities indicate less damaged or intact clay stone. Taking this interpretation into account, we observe a gentle loosening of the rock in the roof and a consolidation in the 45° direction. In the subhorizontal direction up to 0.6 m the rock seems to be loosened and for greater depth more consolidated.

This has to be seen as a result of local importance. More data sets have to be investigated in order to clarify some open questions and the significance of these results. How representative are these results? What is the influence of the small scale EDZ around the borehole? In some cases differences in the general trend between channel 2 and channel 3 data can be observed. What are the reasons for it? Can the results be explained by numerical modelling? But nevertheless such results open the opportunity to evaluate the development of the extent of the EDZ with time.

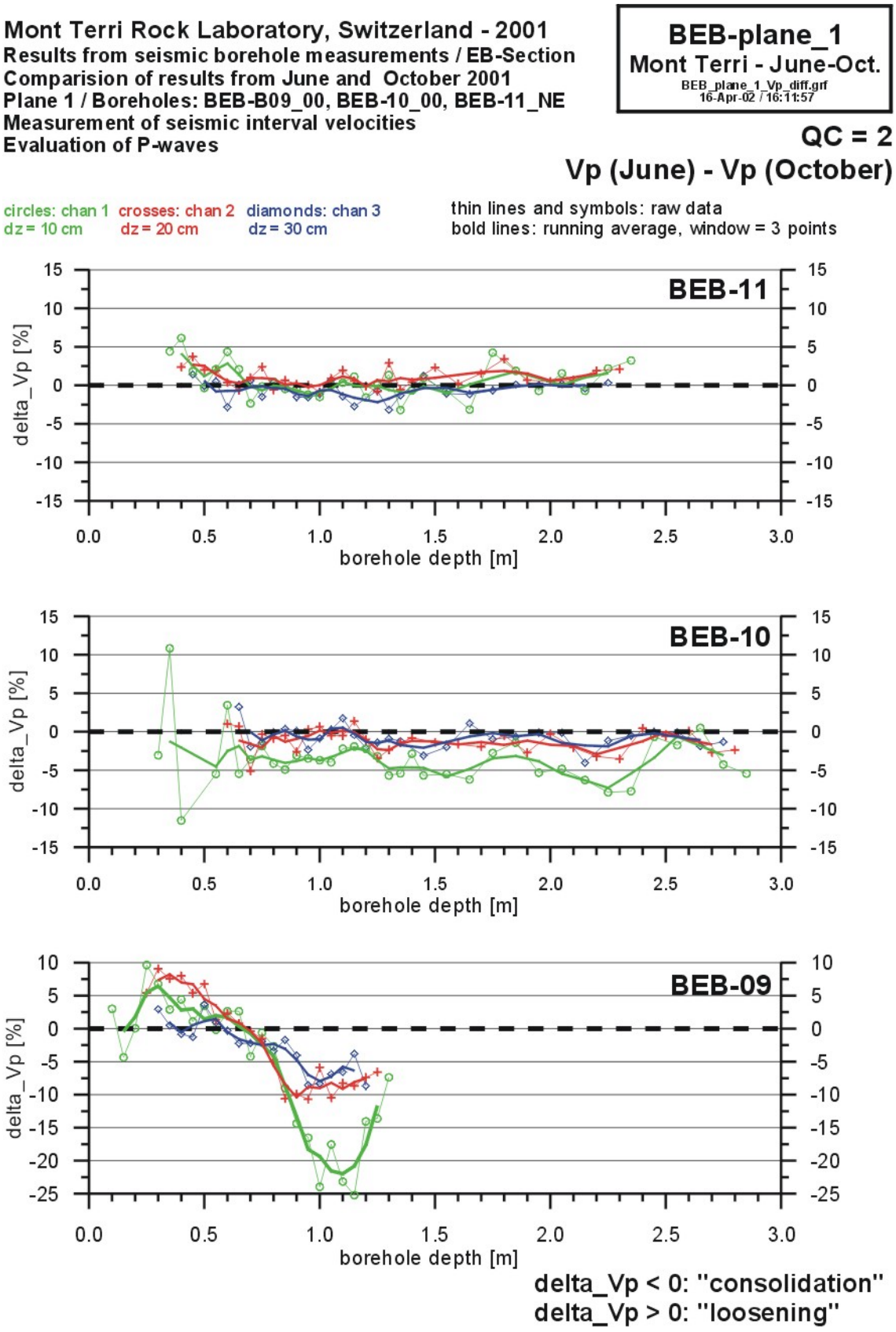

Fig. 2.1-21: Differences in P-wave interval velocities measured in June and October 2001 along plane 1. Differences are expressed in percentage deviation relative to the results from June 2001.

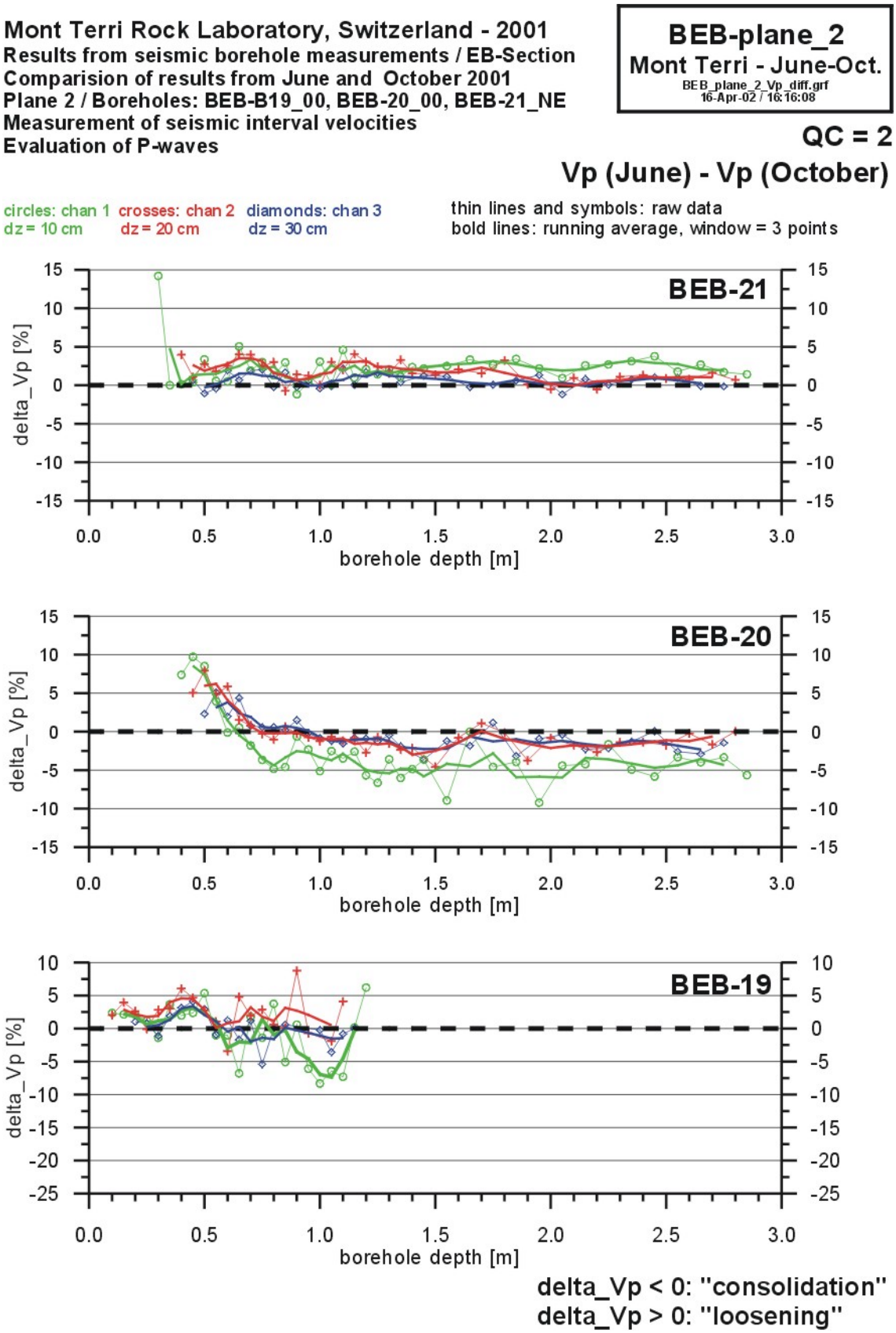

Fig. 2.1-22: Differences in P-wave interval velocities measured in June and October 2001 along plane 2. Differences are expressed in percentage deviation relative to the results from June 2001.

2.1.3.3.3 P-wave Velocity Gradients Around the Boreholes

Remarkable are differences in the three P-wave velocity graphs for one borehole, derived from channel 1, 2 and 3 data. In some boreholes the differences are very small (e.g. BEB-B10, cf. Fig. 2.1-9a) whereas they are great in borehole BEB-B09 (cf. Fig. 2.1-12a). This can be explained with a small scale EDZ around the borehole (cf. chap. 2.1.3.2.4). Differences between the boreholes are indications for the existence of different P-wave velocity gradients perpendicular to the borehole axis.

Because the boreholes which shall be compared under this aspect were drilled with identical drilling techniques (different drilling techniques would influence the vicinity of the borehole wall in different ways) one can assume, that local stress redistribution is related to the change in size of P- and S-wave velocity gradients. Therefore a correlation between the velocity gradients and elastic rock parameters should exist.

As an attempt to get a mean value of these gradients for every borehole the average of the P-wave velocity from channel 1 data was subtracted from the average of the P-wave velocity of channel 3 data. The results are shown in Fig. 2.1-23a (June 2001) and in Fig. 2.1-23b (October 2001). For the June 2001 data the gradients derived in the 45° inclined boreholes are smallest whereas they are greatest in the subhorizontal oriented boreholes. The trend in both planes is the same. Results from the measurements performed in October 2001 are different as can be seen in Fig. 2.1-23b.

For plane 1 data, measured in June 2001, the already discussed elastic parameters Poisson's ratio (ν), Young's modulus (E_{dyn}) and modulus of rigidity (G_{dyn}) of the three boreholes are compiled in Fig. 2.1-24. As for the velocity gradients also for these parameters an average value was calculated in order to compare them with the derived velocity gradients.

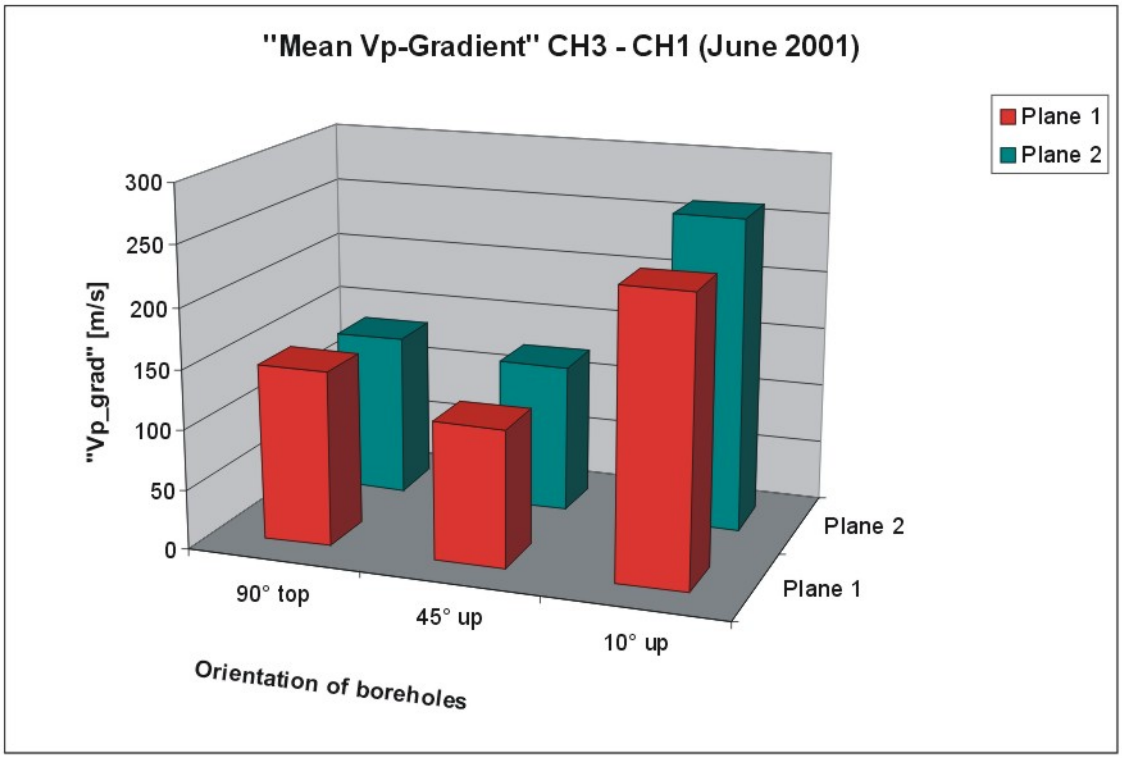

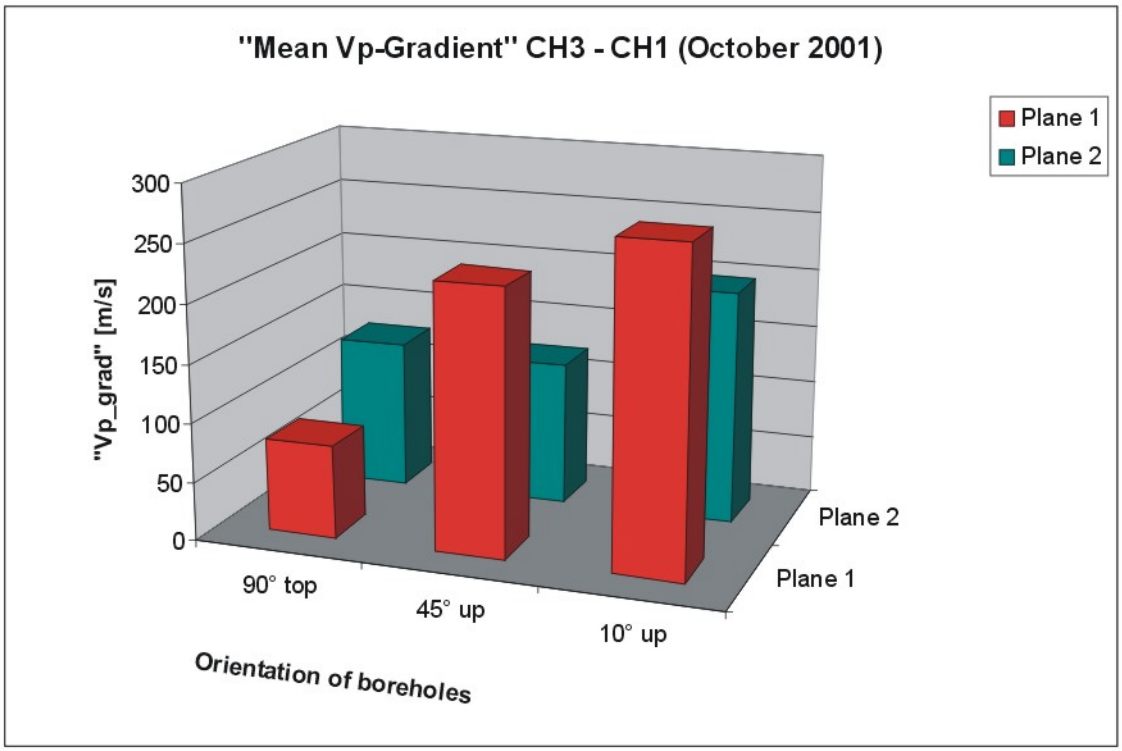

Fig. 2.1-23: Mean P-wave velocity gradient for boreholes BEB-B09 - BEB-B11 (plane 1) and BEB-B19 - BEB-B21 (plane 2). Top (a): drilled and measured in June 2001, Below (b): drilled and measured in October 2001.

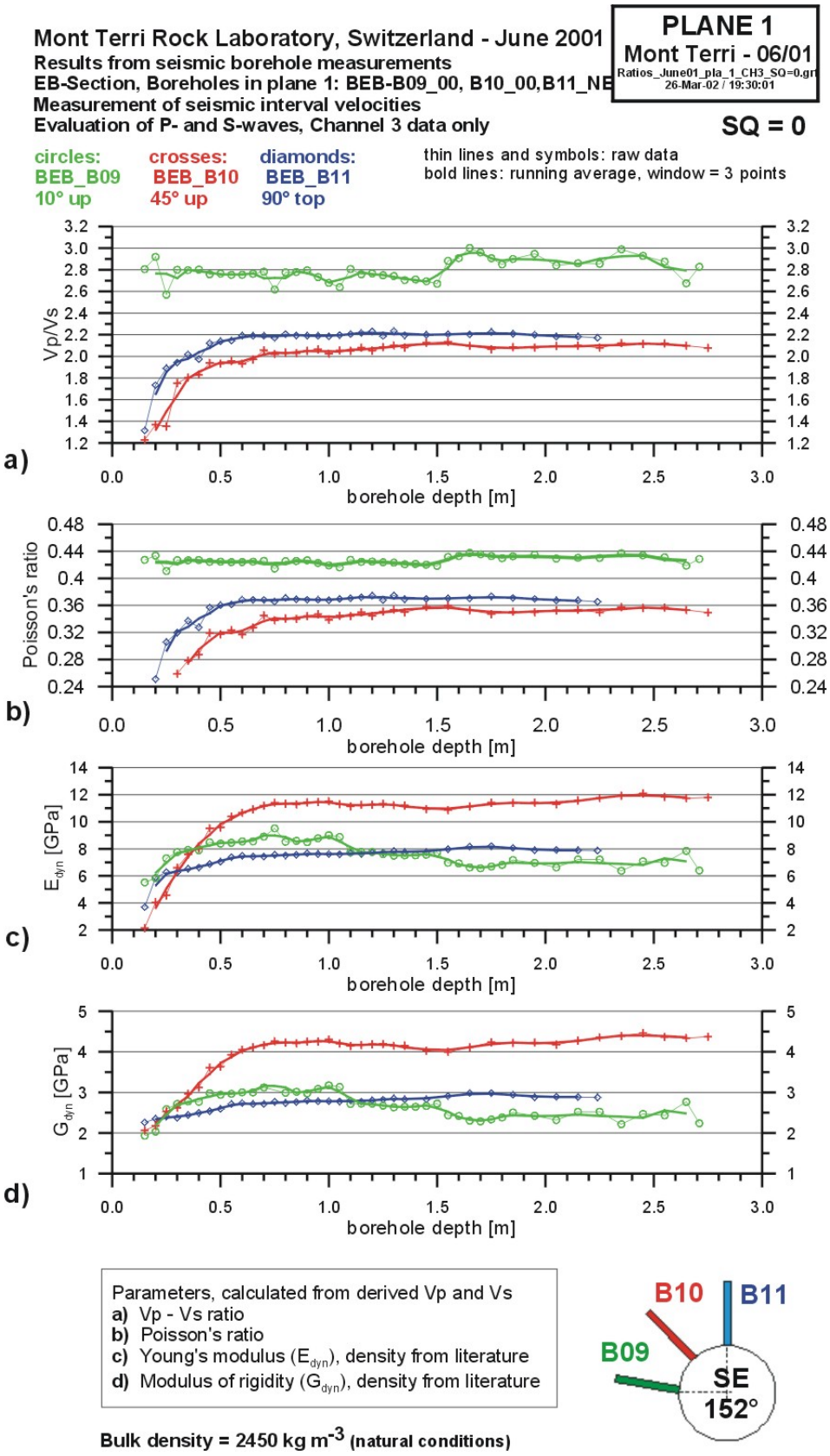

Fig. 2.1-24: Compilation of elastic parameters derived from interval velocity measurements along plane 1 in June 2001.

An overall comparison can be done with the help of Fig. 2.1-25 where all results are plotted. The highest mean gradient was observed in borehole BEB-B09 (sub-horizontal). Consequently for this direction one would expect under "normal conditions" also the lowest value for E_{dyn} and G_{dyn} and on the other hand highest values for Poisson's ratio (ν). It is valid for G_{dyn} and ν. E_{dyn} has nearly the same value as E_{dyn} which is related to the second highest value for the gradient. For the lowest value for the mean P-wave velocity gradient (BEB-B10, drilled 45° up) the relation fulfil the expectation. The lowest value for the mean gradient goes conform with the highest values for E_{dyn} and G_{dyn} and the lowest value for the Poisson's ratio.

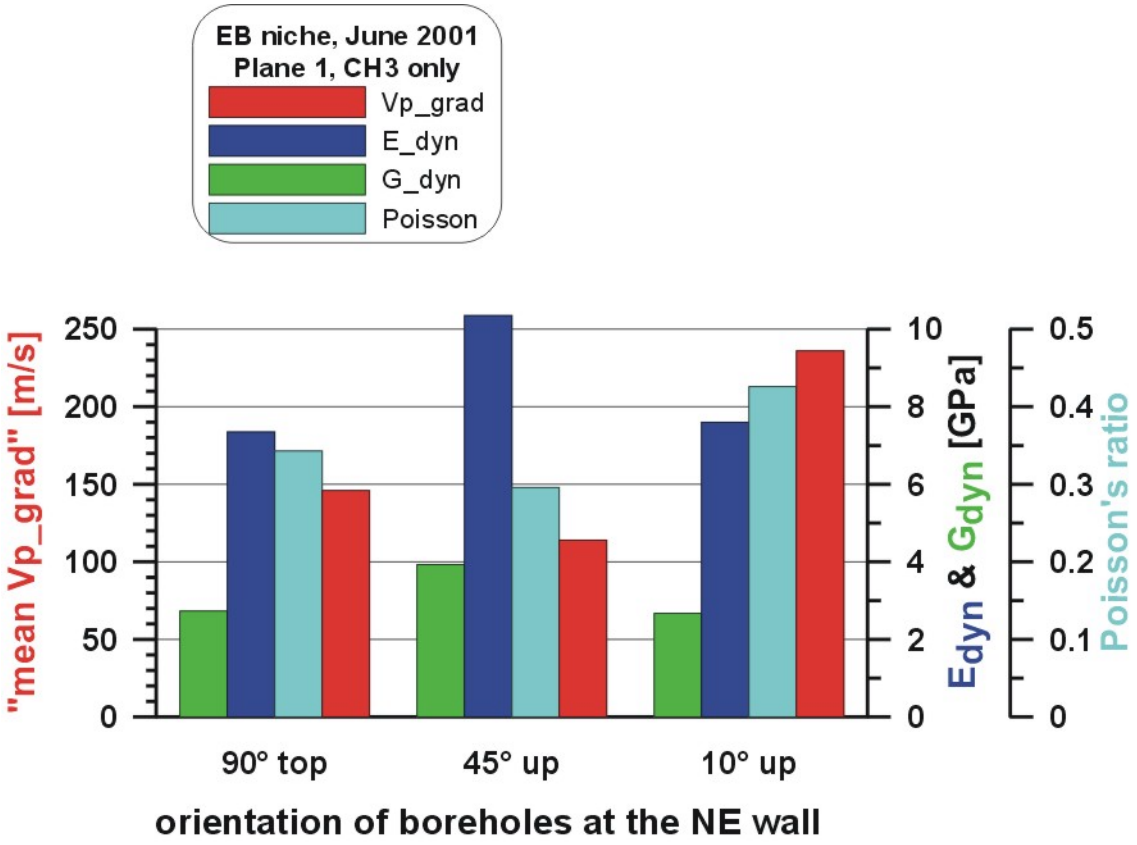

Fig. 2.1-25: Comparison between "mean P-wave velocity gradients" and elastic parameters derived from interval velocity measurements along plane 1 in June 2001.

In the future the remaining data will be analysed. For a better understanding also numerical modelling should be performed. At the moment these results can contribute at least as a qualitative support for an interpretation.

2.1.3.3.4 Correlation with Core Sample Data

A drillcore mapping was done immediately after the taking of the cores (Nussbaum et al., in prep.). As a main feature the occurrence of sandy layers in some cores can be regarded. Furthermore many artificial discontinuities (code: ad) were observed. Only in one core sample (BEB-B09) a slickenside (code: sst) was reported. In Figures 2.1-9, 2.1-12, A-1 and A-4 to A-6 these observations are plotted in the P-wave velocity graphs at corresponding depths. Because the core samples were not taken oriented, for the corresponding depth a mean value was taken from the protocols and used for the plots.

A good correlation between the occurrence of sandy layers and higher P-wave velocities in the graphs can be seen. Up to now no correlation analyses between the artificial discontinuities (ad) and seismic parameters were done. But it can not be expected to find significant correlations, because the "finger print" of the artificial discontinuities in the rock is most probably too weak and the chosen spatial measurement resolution (shortest distance between source and receiver was 10 cm, measured in steps of 5 cm and 10 cm) was too coarse.

2.1.4 Cross Hole Measurements

In order to extent the investigation on a bigger rock volume cross hole measurements between two boreholes were performed. The orientation of both boreholes (BEB-B09 and BEB-B19) are subhorizontal (10° up) and they are 1 m apart.

2.1.4.1 Data Acquisition and Analyses

After a small modification of the above described BGR mini-sonic borehole probe and the use of an additional piezoelectric transducer as a source used in a second borehole, cross hole measurements could be performed between boreholes BEB-B09 and BEB-B19. The distance between both boreholes is 0.99 m at the wall of the niche and 1.04 m at the end of the boreholes. Both, source and receivers are positioned at the same depth in both boreholes and orientated towards each other.

In steps of 10 cm both, source and receivers were moved towards the end of the borehole.

The borehole coordinates were provided by the BGR in situ measurement team.

The measured data are shown in a colour coded amplitude display in Fig. 2.1-26. In the upper part of Fig 2.1-26 the data which were received in borehole BEB-B19 (shots in BEB-B09) are shown whereas in the lower part of Fig. 2.1-26 data from the reverse experiment (shot in BEB-B19 and receivers in BEB-B09) are shown. For depth greater than 0.25 m for both shot-receiver directions the signal quality was very good, except of some traces with weaker amplitudes. This do not affect the evaluation of travel times at all, because in an other data representation the first arrival times can be picked exactly. The source signal was emitted with 5 kHz. No S-waves could be registered with this source - receiver configuration.

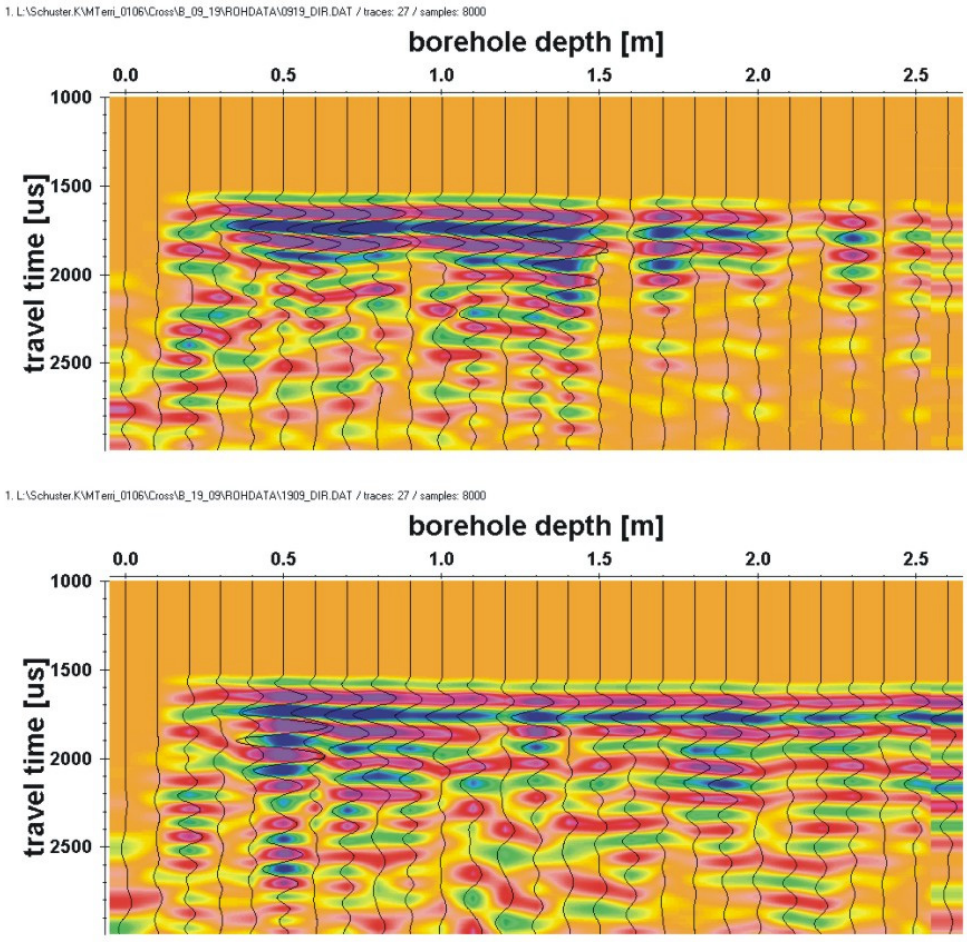

Fig. 2.1-26: Data example from cross hole measurements between boreholes BEB-B09 (source) and BEB-B19 (receiver) (top) and the reverse direction (below). Ensemble normalised display with colour coded amplitudes. For colour code see Fig. 2.1-7.

2.1.4.2 Results of Cross Hole Measurements

Similar to the evaluation of interval velocity data results for the cross hole data are summarised as distributions of P-wave velocities in Fig. 2.1-27. The derived P-wave velocities from the forward and reverse experiment should be identical presupposed the measurements took place under ideal conditions so that travel paths of seismic waves between source and receivers are identical for the forward and reverse experiment. The velocity graphs are very good in line especially the running average curve. For depth greater than 2 m they start to differ. Main features can be seen in both graphs, for example the steep increase in P-wave velocity within the first centimeters to a maximum value and the following decrease.

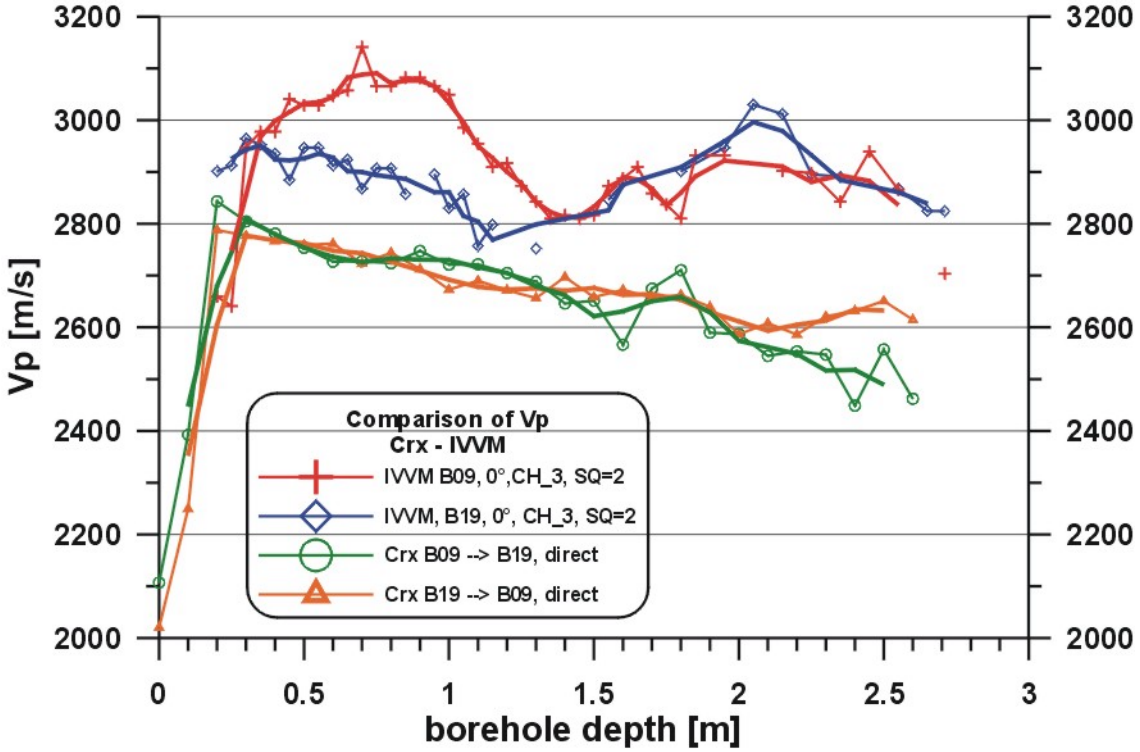

Fig. 2.1-27: Comparison of P-wave velocities derived from interval velovity measurements (IVVM) in boreholes BEB-B09 and BEB-B19 and from cross hole measurements (CRX) between both boreholes (measured in June 2001).

In addition results from the interval velocity measurements are plotted. Obviously we see differences between the graphs. To explain this, one have to take into account, that for the cross hole measurements a bigger rock volume was scanned and the exact ray paths are not known. Furthermore for the interval velocity measurements the sensors were oriented upwards in the boreholes (nearly parallel to

bedding planes) whereas for the cross hole measurements they stood in 90° and 270° direction, respectively (nearly perpendicular to bedding planes). Of course, for the calculation of distances the orientation of source and receives were taken into account.

Nevertheless these results give very strong hints for the existence of seismic anisotropy which was investigated in a special experiment and will be described in chapter 2.1.5.

2.1.4.3 Uncertainties and Errors

There are some reasons which cause errors in the calculation of seismic velocities from cross hole measurements. First of all we have to mention possible uncertainties in the determination of borehole coordinates. They were measured by the in situ measurement team. A possible error of ± 5 cm (!) for the determination of the distance between both boreholes would result in an error in the P-wave velocities of ± 5 %. All other influences, e.g. different coupling conditions or uncertainties in the determination of arrival times can be neglected in this connection. For this type of cross hole measurements a straight and direct ray path between source and receivers are assumed. According to the theory, the ray paths not compelling run geometrically the shortest way. Instead they "find" the shortest way in time (Kertz 1969). The real travel path remains unknown. This problem can only be solved with the application of seismic tomography methods with a sufficient ray coverage. Also in this case it can not be guaranteed that waves travel only in the plane between the boreholes (2 dimensional).

2.1.5 Seismic Tomography

The above discussed differences between P-wave velocities derived from interval velocity and cross hole measurements gave indications of the existence of seismic anisotropy. Also from the geological point of view we have to assume a strong anisotropy effect, because the strike of the bedding of the Opalinus Clay is approximately perpendicular to the tunnel axis orientation. The measurements were per-

formed within the first 1.5 m from the wall between boreholes BEB-B09 and BEB-B19.

A seismic anisotropy study was undertaken in 1999 with data from interval velocity measurements in eight radial drilled boreholes in the New Gallery (Schuster et al. 2000b).

2.1.5.1 Data Acquisition and Analyses

In principal seismic tomography measurements are similar to cross hole measurements. But the density of measurement points has to be increased. An appropriate ray coverage has to be chosen in order to cover all parts of the area between both boreholes.

Fig. 2.1-28 shows the ray coverage which was used for our experiment. Within this experiment no receivers could be placed along the wall of the EB niche, what would increased the coverage. So we can state already at this stage, that some directions are not covered by rays.

The measurements were done in the following way. The source was placed in borehole BEB-B09 at z = 0 cm and at 18 receiver positions between 0 cm and 170 cm in steps of 10 cm signals were received in borehole BEB-B19. This was repeated for source positions between 10 cm and 150 cm. Afterwards the source was used in borehole BEB-B19 and receivers were placed in borehole BEB-B09 and the same procedure was repeated. The total number of rays is 576. Source and receivers were oriented towards each other (orientation of 90° and 270°).

For the tomography the same equipment was used as for the cross hole measurements. Signals were emitted with a frequency of 5 kHz. A data set (source in BEB-B09 at z = 0 cm, receivers in BEB-B19) are shown in Fig. 2.1-29. Traces are sorted according to the distance between source and receiver. The first arrival phases can be identified very clear. First arrival times were picked manually and together with the calculated distances P-wave velocities were derived.

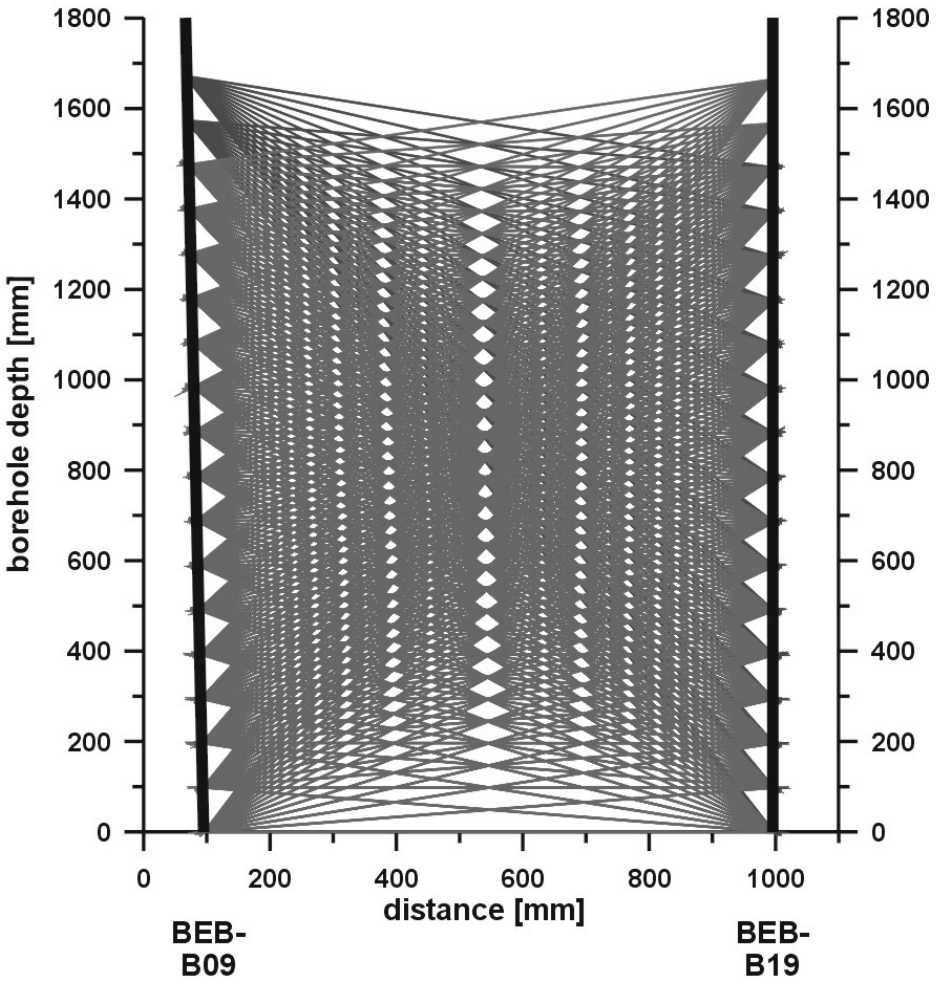

Fig. 2.1-28: Ray coverage from seismic tomography measurements between boreholes BEB-B09 and BEB-B19 (June 2001).

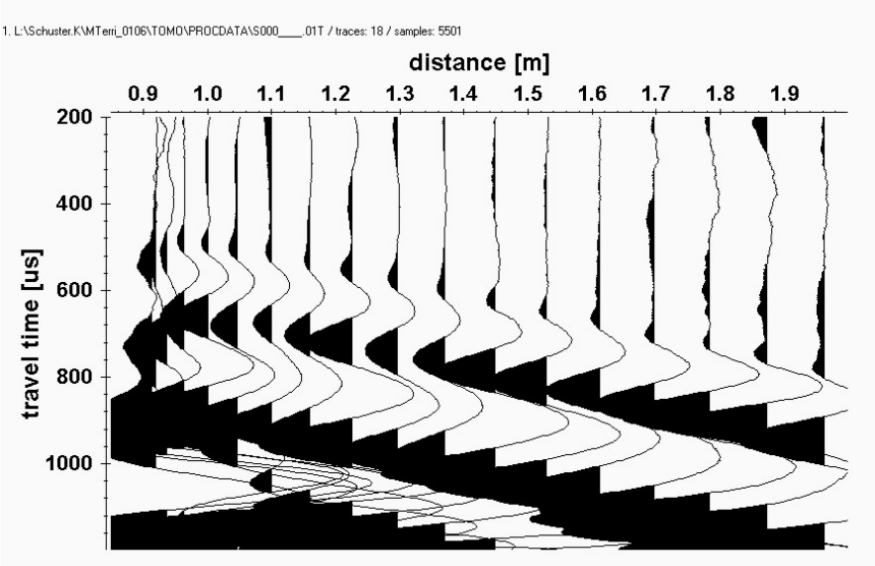

Fig. 2.1-29: Data example from seismic tomography measurements between boreholes BEB-B09 and BEB-B19 (measured in June 2001). Source at z=0 in borehole BEB-B09, receivers moved between 0 and 1.7 m in borehole BEB-B19.

2.1.5.2 Results of Seismic Tomography Measurements

How the P-wave velocities depend on the direction of transmission can be seen in Fig. 2.1-30, were the sources are placed in borehole BEB-B09 and receivers in BEB-B19 as well as in the reverse case (sources in BEB-19 and receivers in BEB-B09) in Fig. 2.1-31. The differences in the derived P-wave velocities are tremendous. They vary between 1900 m/s and nearly 3200 m/s. For a isotropic homogeneous media with a P-wave velocity of 2500 m/s for example, all eight data sets would plot on a single vertical line at 2500 m/s.

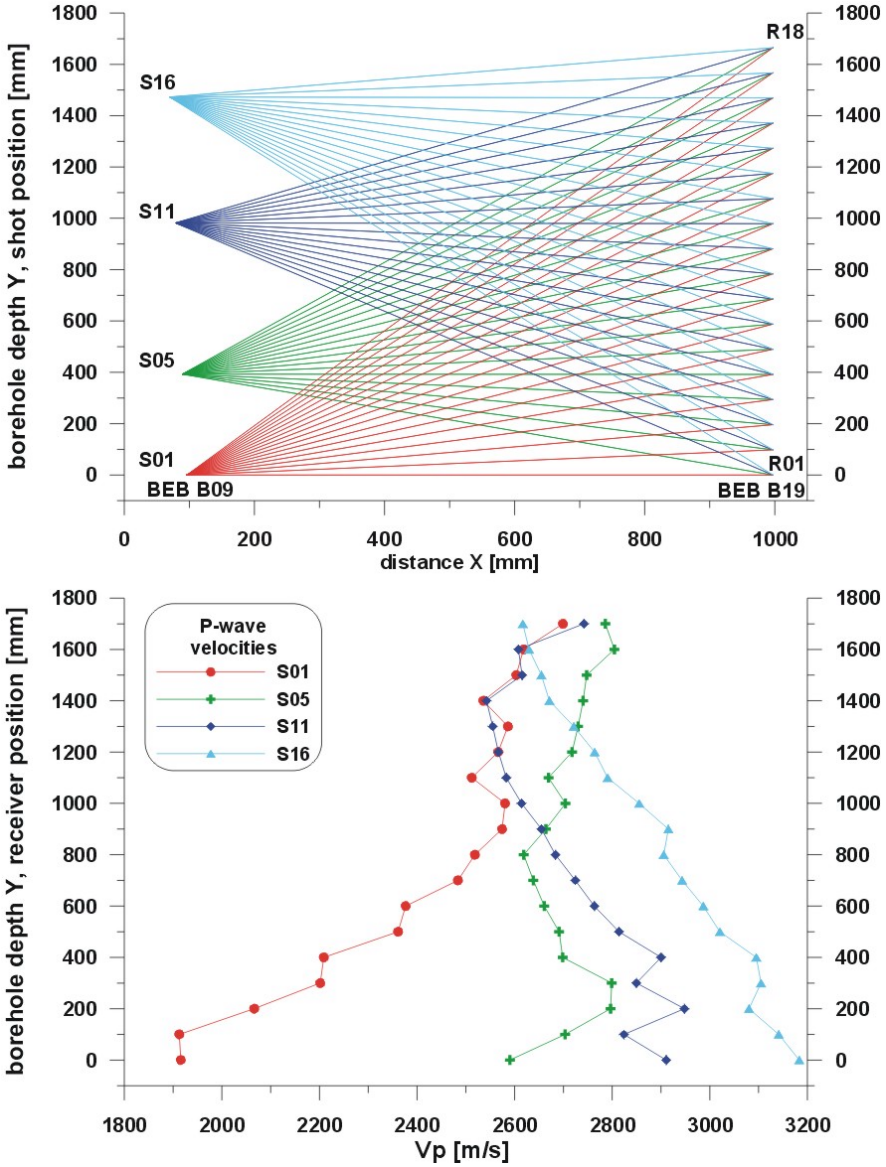

Fig. 2.1-30: Ray coverage (top) and derived P-wave velocities (below) from seismic tomography measurements between boreholes BEB-B09 and BEB-B19 (measured in June 2001). Examples are shown for sources in borehole BEB-B09 at z = 0, 0.4 m, 1 m and 1.5 m and all receiver positions in borehole BEB-B09 (R01 – R18). Velocities vary remarkable. They are influenced mainly by the anisotropy structure (e.g. bedding planes).

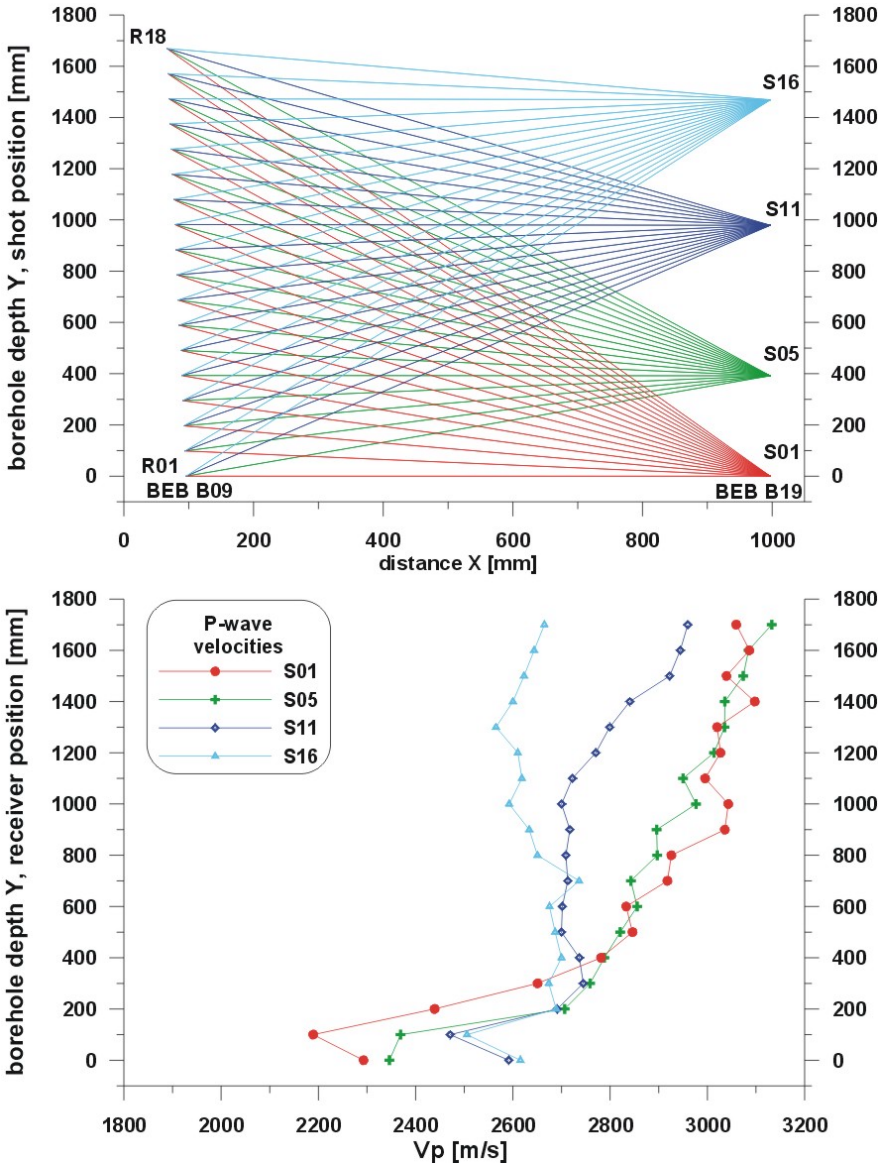

Fig. 2.1-31: Ray coverage (top) and derived P-wave velocities from seismic tomography measurements between boreholes BEB-B19 and BEB-B09 (measured in June 2001). Examples are shown for sources in borehole BEB-B19 at z = 0, 0.4 m, 1 m and 1.5 m and all receiver positions in borehole BEB-B19 (R01 – R18). Velocities vary remarkable. They are influenced mainly by the anisotropy structure (e.g. bedding planes).

P-wave velocities can also be plotted as a function of the angle between source and receiver positions. For four shotpoints results are presented in Fig. 2.1-32 in a polar diagram. The orientation 0° - 180° corresponds to the wall of the EB niche and consequently approx. to the axis of the EB niche. The relationship between source - receiver positions according to the angle can be taken from the four small sketches.

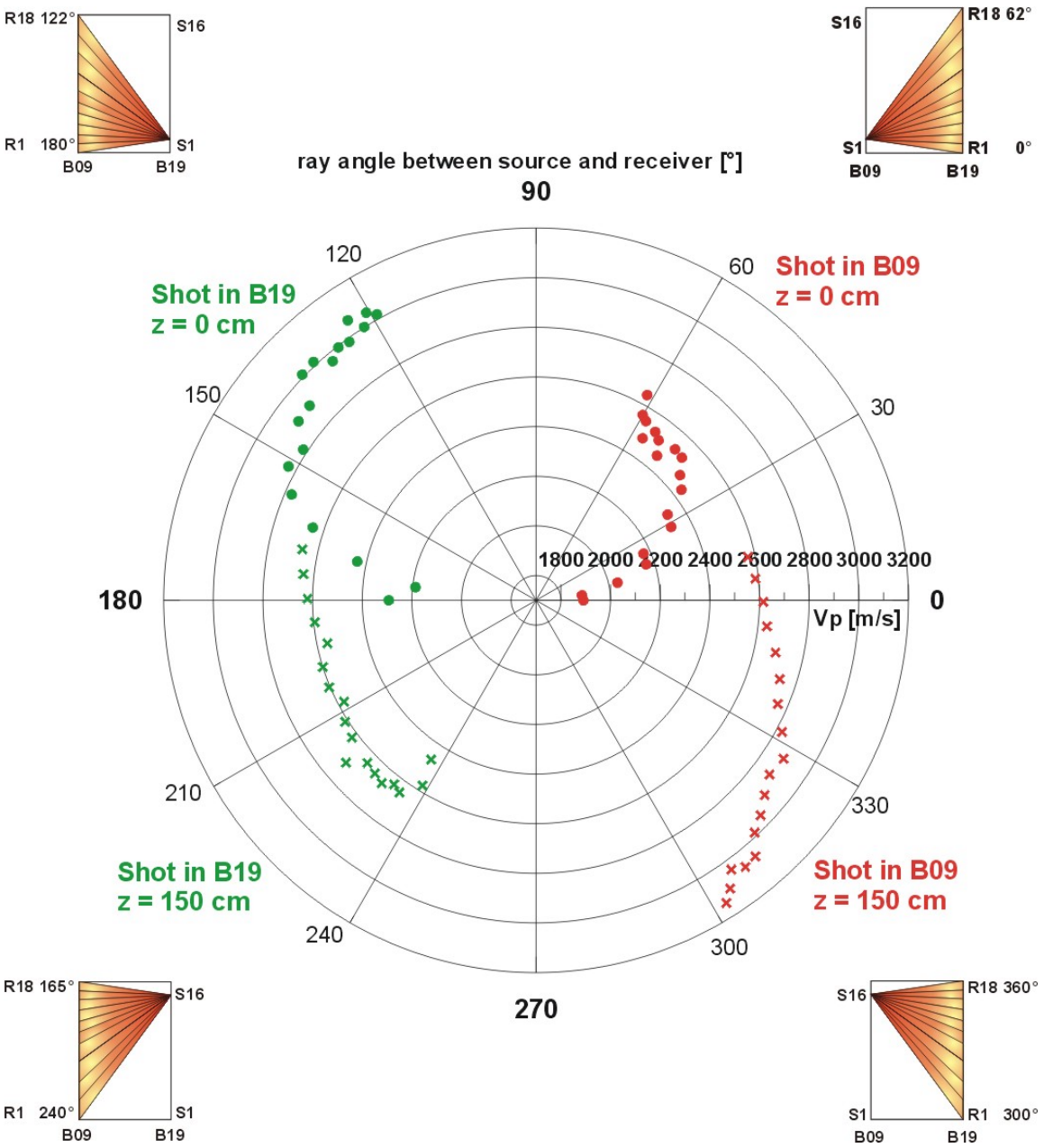

Fig. 2.1-32: Derived P-wave velocities from seismic tomography measurements between boreholes BEB-B09 and BEB-B19 (measured in June 2001). Data from two source positions in borehole BEB-B09 and two in borehole BEB-B19 are plotted over the ray angle. The 0° - 180° direction is approx. in parallel with the axis of the EB niche. A strong anisotropy of velocity is visible. The connection between the relative orientation of ray paths and the ray angle can be taken from the four small sketches.

In Fig. 2.1-33 all data points for the 576 rays are plotted. In addition the strike directions of the bedding is marked in light green (90° - 112°). Only for a better orientation also the perpendicular directions are marked (light yellow). Because no receivers were placed on the wall of the EB niche no data can be expected in the

range between 60° to 120° and 240° to 300° (see also Fig. 2.1-34). The data are superimposed with an ellipse like curve in order to mark a very rough fit (not calculated) of the data. According to this curve minimum values for the P-wave velocity can be found, as expected, in the direction perpendicular to the bedding. Maximum values seem to tend towards the strike direction of the bedding.

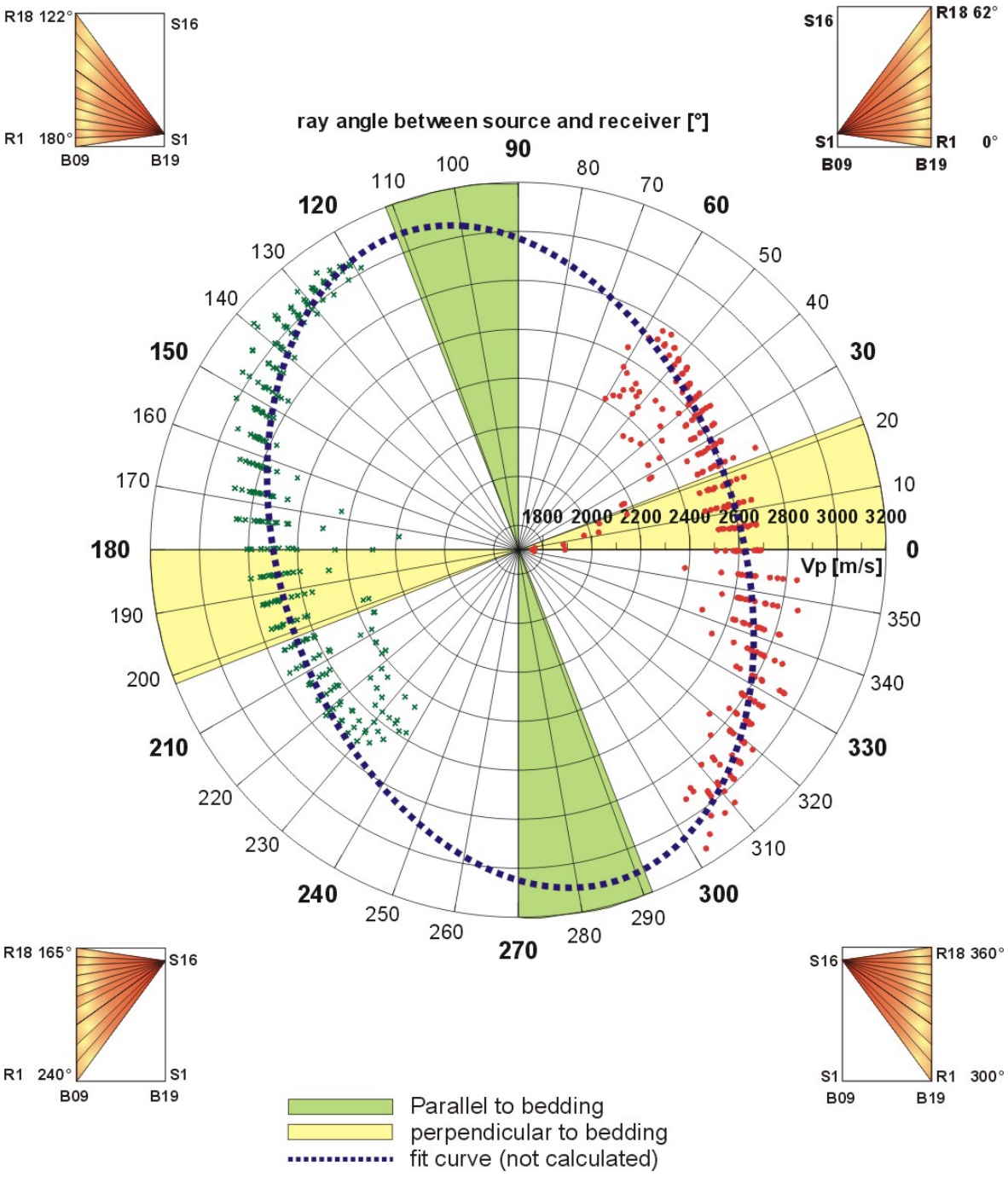

Fig. 2.1-33: As Fig. 2.1-32 but here all 576 rays used for the calculation. The main strike directions of the bedding is marked in light green, the perpendicular direction in light yellow. An ellipse which could be a fit (not calculated) of the data emphasises the seismic anisotropy. The main axis of the ellipse is slightly deviated against the bedding parallel direction.

Differing from this trend regions with very low velocities can be found between 0° and 22° (Vp < 2200 m/s). This correspond with directions were mainly the EDZ is covered. Surprisingly this can not be observed in the reverse direction (approx. 180°). Furthermore two regions with lower velocities deviate from the general trend, (20° to 60° and the corresponding reverse direction 200° to 240°). This "anomalous" region can not be explained with the anisotropy caused by the bedding. This has to be studied in the future.

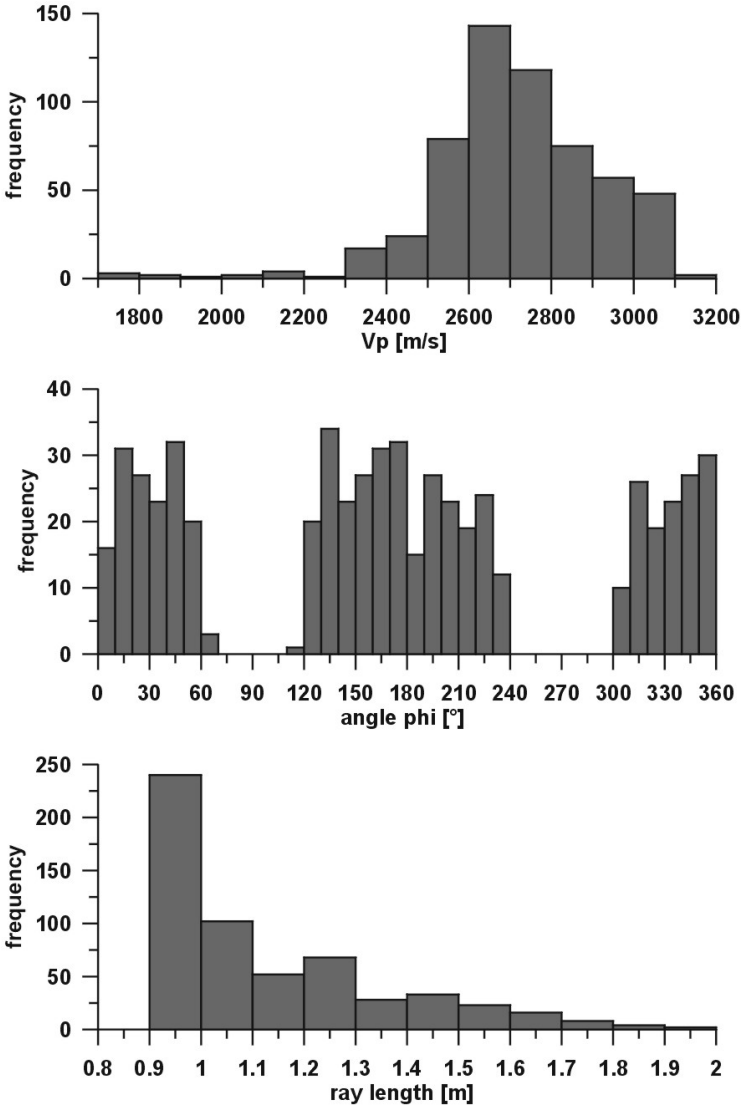

Fig. 2.1-34: Histograms with the frequencies of occurrence of derived P-wave velocities (top), ray angle (middle) and the used ray lengths (straight lines) (below). Data belong to the seismic tomography measurements between boreholes BEB-B09 and BEB-B19.

In Fig. 2.1-34 some statistical data are summarised. The histogram in Fig. 2.1-34a show the frequency of occurrence of P-wave velocities in bins of 100 m/s. Velocities between 2600 m/s and 2700 m/s dominate. Fig. 2.1-34b shows the directions with poor or no ray coverage at all (63° - 117° and 240° - 303°). For the remaining

directions the coverage is balanced. Finally Fig. 2.1-34c gives an impression of the ray length which were used for the calculations.

The mentioned insufficient ray coverage permits by rights the application of a tomography algorithm to the collected data. Although knowing that the data are not sufficiently dense sampled for a reliable tomography result the calculations were performed. Data were evaluated with a seismic tomography program which is part of the seismic software REFLEXW (Sandmeier Software).
Because the ray coverage in the vicinity of both borehole walls is very poor two data sets originating from two special interval velocity measurements along boreholes BEB-B09 and BEB-B19 were added to the above discussed data. This increases the ray coverage in the vicinity of both boreholes. The interval velocity measurements were performed in that way that source and receivers were orientated 90° in borehole BEB-B09 and 270° in borehole BEB-B19. Furthermore data from shot-receiver positions greater than 1.5 m were not used for the tomography inversion.

Poor or not covered parts remain. Still missing are the coverage of the 63° - 117° and 240° - 303° directions. To avoid this in the future receivers should also be used between both boreholes along the wall. Within the first and last 20 cm in the middle part between both boreholes the coverage is very poor.
The result of the tomography inversion is displayed in Fig. 2.1-35 as a 2-dimensional P-wave velocity distribution of the rock between both boreholes. It should only be seen as a demonstration of the potential of this method. Due to the mentioned circumstances the result has to be treated carefully. A asymmetry can be explained as it was discussed above. The anisotropy can be caused by the bedding and secondly by local inhomogeneity. The EDZ is not sufficiently covered with rays.

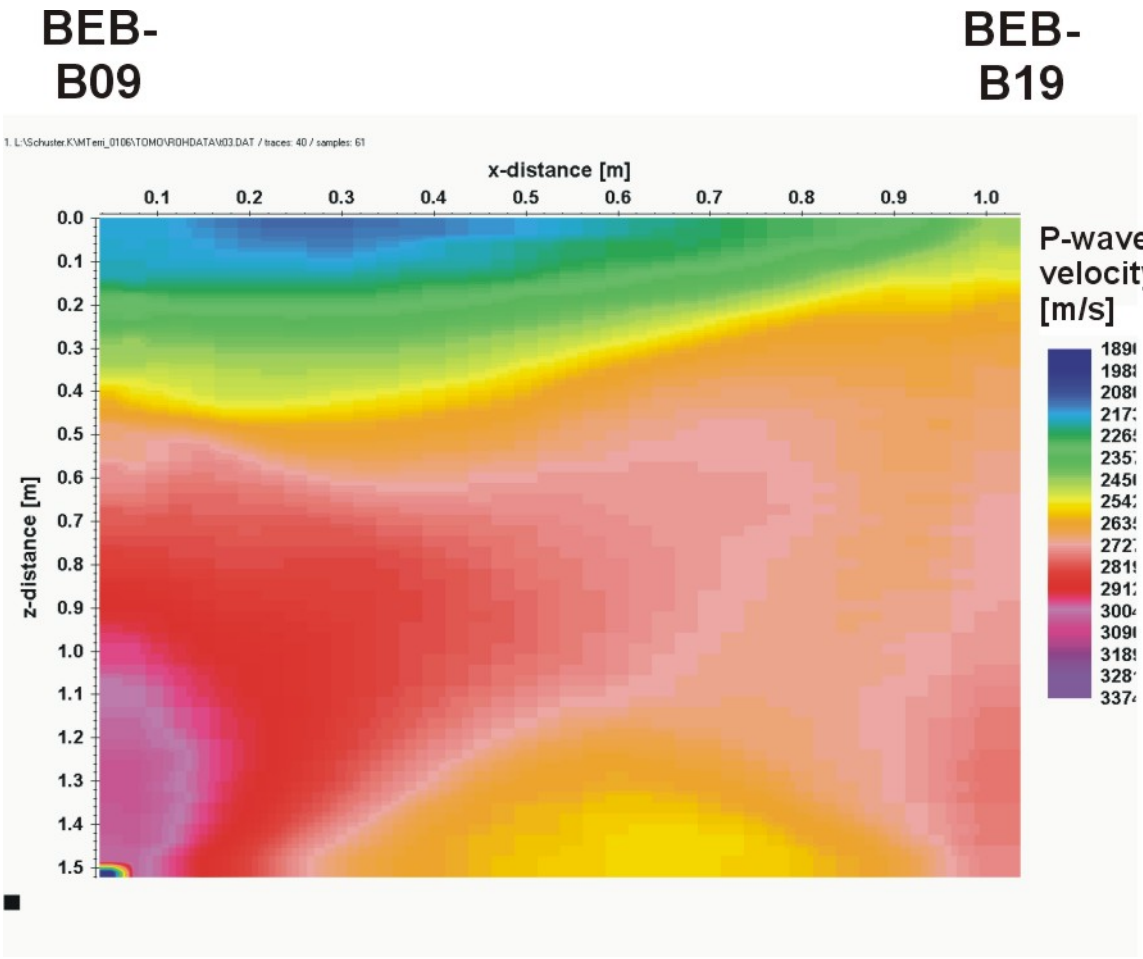

Fig. 2.1-35: Seismic tomography measurements between borehole BEB-B09 and BEB-B19. 2-dimensional P-wave velocity distribution as a result of a tomography inversion with an inadequate data set. For details see text.

2.1.5.3 Uncertainties and Errors

The same uncertainties as discussed for the cross hole measurements have to be taken into account (cf. chap. 2.1.4.3). Furthermore the ray coverage, as discussed above, has to be considered very seriously.

2.1.6 Summary of Results from Borehole Measurements

The combined application of different seismic borehole methods, as discussed up to now, led to a comprehensive characterisation of the EDZ and the surrounding of the EB niche with the help of seismic parameters, like seismic P- and S-wave ve-

locities, seismic amplitudes, seismogram characteristics and seismic anisotropy. Furthermore geotechnical parameters like Poisson's ratio, Young's modulus and modulus of rigidity were derived from the data. Results are summarised in the following:

- The EDZ varies between 0.10 m at the sidewall, 0.5 m in the roof and 0.65 m between them (45° inclined boreholes).
- Increased P-wave velocities correlate with sandy layers identified in core samples.
- Elastic parameters like Poisson's ratio, Young's modulus and modulus of rigidity correlate with derived velocity gradients perpendicular to the borehole wall.
- A very strong anisotropy of seismic velocities in the sidewall, which can not be exclusively explained by the bedding of the Opalinus Clay, were revealed with the help of high resolution cross hole measurements (incl. seismic tomography).
- Changes in the derived P-wave velocities after four months give indications of changes in the local stress redistribution.
- At the sidewall high velocities and high amplitudes characterises a zone at depths between 0.3 and about 1.0 m. The results of the measurements are in this case not typical for the EDZ neither for the intact rock. The anomaly may be due to sandy layers observed at that specific depths and/or to the stress concentration induced by the drift itself that results in a slightly squeezed material.
- Results are in good accordance with results from geoelectric measurements at the same location (Kruschwitz 2002).

2.2 Underground Research Facility Mol (Belgium) - Boom Clay - Comparison with Observations made after Excavation

2.2.1 Introduction

At the Underground Research Facility (URF) Mol (Belgium), in the argillaceous formation of the Boom Clay, seismic measurements were performed in and between two 20 m long boreholes. A mini-sonic borehole probe was used for the seismic interval velocity and cross hole measurements. The application of both methods and the combined interpretation of the evaluated seismic parameters made it possible to determine the extent and to characterise the Excavation Damaged Zone (EDZ) as well as anomalous regions. The predictions made with the help of these results were confirmed later by geologists after excavation of the rock mass (Bernier 2002, pers. com.).

2.2.2 Objectives and Location

In the framework of the extension of the Underground Research Facility (URF) HADES (High Activity Disposal Experimental Site) at Mol (Belgium) a second shaft was constructed. HADES is part of the SCK-CEN - Nuclear Research Centre (Studiecentrum voor Kernenergie - Centre D'Etude de L'Energie Nucleaire). At a depth of 223 m a chamber was excavated which will be used as the starting point for the excavation of a connecting gallery. The URF is located almost in the middle of an approx. 100 m thick argillaceous formation, which is known as Boom Clay (formed during Lower Oligocene) (Bernier et al. 2000).

In order to characterise the rock seismically in the vicinity of the starting chamber two 20 m long boreholes were used for small scale seismic investigations. In autumn 2000 BGR - Hannover (Bundesanstalt für Geowissenschaften und Rohstoffe, Section B2.2) performed seismic interval velocity and cross hole measurements in those boreholes (Schuster et al. 2001b).

Both boreholes are sub-horizontal, nearly parallel and oriented towards the existing laboratory. The distance between both boreholes is approx. 3.6 m. A sketch of the test site is given in Fig. 2.2-1. Fig. 2.2-2 shows the test site during a measure-

ment with parts of the equipment. Due to the expected fast deformation of the boreholes (diameter of 135 mm without casing) the interval velocity measurements were carried out immediately after drilling in two steps. Interval velocity measurements started after the boreholes were drilled up to 10 m. Afterwards the boreholes were drilled up to the final depth of 20 m and the second part of the measurements started immediately. The stability of both boreholes became worse at approx. 10 m and resulted in a suspension of the interval velocity measurements at depth of 13.8 m (2000/04) and 13.2 m (2000/05) respectively. Afterwards both boreholes were cased with PVC-tubes (EUPEN-PVC - 110 x 5,3 - PN 10) to prevent further damage. Cross hole measurements between boreholes 2000/04 and 2000/05 (both cased, inner diameter of 100 mm) were carried out three weeks later.

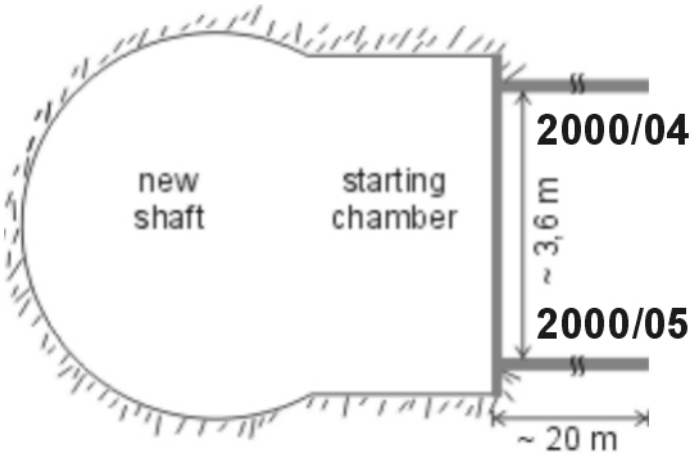

Fig. 2.2-1: Sketch of test site in the new shaft, URF Mol, Belgium.

Fig. 2.2-2: Photograph of test site in the new shaft, URF Mol, Belgium.

2.2.3 Data Acquisition

For the measurements the same seismic borehole equipment was used as described above in detail. The mini-sonic probe is designed for boreholes with a diameter of 86 mm. For the investigations at the Mol test site the mini-sonic-probe had to be adapted for 135 mm diameter boreholes and for the cased borehole with an inner diameter of 100 mm.

According to the video inspections (performed by SCK-CEN) many parts of the borehole wall were identified as mechanical unstable and therefore not suitable for the interval velocity measurements. Only the top of the borehole wall between 330° and 30° (0° means vertical upward) could be regarded as sufficient stable and in good shape. Because of this source and receivers were orientated upwards.

The evaluation of the cross hole measurements requires precise borehole coordinates. Corresponding measurements were performed by SCK-CEN and the data were placed to our disposal. We had to interpolate the coordinates for our applications.

2.2.4 Data Analyses

2.2.4.1 Interval Velocity Measurements

Velocities as well as amplitudes were derived from first arrival phases (compressional waves, P-waves) as described in chap. 2.1.3. In the following figures depths are counted from the outer side of the steel plate. The steel plate stabilises the starting chamber wall.

A compilation of all measured seismic traces along the borehole 2000/04 with a distance of 10 cm between source and receiver (channel 1) is displayed in Fig. 2.2-3a. The section is trace normalised. Already a rough visual analysis of the data reflects clear differences in the travel times. An increase of the first arrival times in the beginning and several anomalies, for example at approx. 3.8 m, can be observed. Onsets of the S-waves can be observed at times between 200 μs and 210

μs. As can be seen in Fig. 2.2-3a the quality of first arrival phases drops drastically at 9 m. S-wave onsets can not at all be observed at depth greater 9 m. One of the reasons is the instability of the borehole wall which in many cases reflects a weakening of the rock mass in that region.

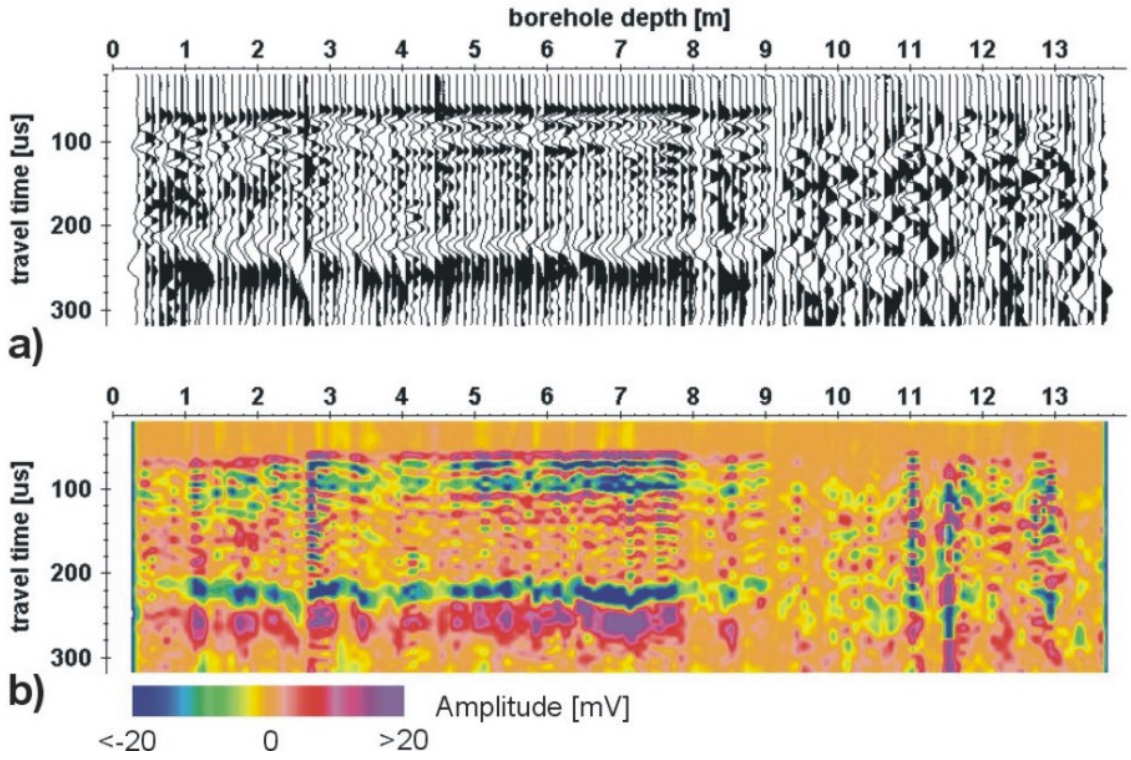

Fig. 2.2-3: Seismic section from interval velocity measurements in borehole 2000/04, channel 1 data. a: wiggle mode, trace normalised, b: point mode, ensemble normalised

For a first qualitative examination Fig. 2.2-3b gives an overview of the amplitude distribution along the borehole. Seismic traces are displayed in a point mode. The section is ensemble normalised. The amplitudes of the traces are colour coded (violet/red: positive amplitudes, blue/green: negative amplitudes, brown/yellow: zero level). The variability in the amplitude distribution as well as in the travel times are remarkable. The above mentioned anomalies, especially in the P- and S-wave distribution, can be found again very clear. According to the dynamic range of the display later phases are more emphasised.

2.2.4.2 Cross Hole Measurements

The cross hole measurements took place four weeks and three weeks after casing and grouting of borehole 2000/04 and borehole 2000/05 respectively. Depths are counted from the beginning of the tubes. The distances between the beginning of the tubes and the steel plate, which stabilises the starting chamber wall, are 5.5 cm (borehole 2000/04) and 7.5 cm (borehole 2000/05). Due to the high plasticity of the Boom Clay, a compact transition zone between tube, grouting and rock mass can be assumed. Both boreholes could be used up to a depth of nearly 20 m although parts of the casing were remarkable deformed to an elliptical cross section. The orientation of the main axis of the deformed cross section changed in addition arbitrarily with depth. Due to these diameter variations of the borehole wall source and receiver could not be oriented in the optimum direction. As the amplitudes of the signals strongly depend on source-receiver-orientation, the amplitudes measured in this part of the borehole, do not reflect the rock properties. The amplitudes of the seismic signals can not be compared each other. The corrected distances between the source and receivers are shown in Fig. 2.2-7. They vary between 3.53 m and 3.6 m.

In Fig. 2.2-4 data for the cross hole experiment with the source in borehole 2000/04 and the receivers in borehole 2000/05 are shown. Fig. 2.2-4a shows the channel 1 data in wiggle mode (trace normalised) and Fig. 2.2-4b in the equivalent point mode (ensemble normalised), were amplitudes are colour coded. Results from channel 2 and channel 3 data are very similar.

The first arrivals are in the range between 1800 μs and 2000 μs. The first arrival times decrease gradually from approx. 1 m to 6 m which is equivalent with an increase in P-wave velocity. Within the first meter the signal quality is very bad due to the extreme damage and / or the filling material in this region. At 14.8 m there is a significant drop in signal quality probably caused by unsatisfactory orientation of the transducers (see also Fig. 2.2-7e). S-waves could not be observed with cross hole measurements.

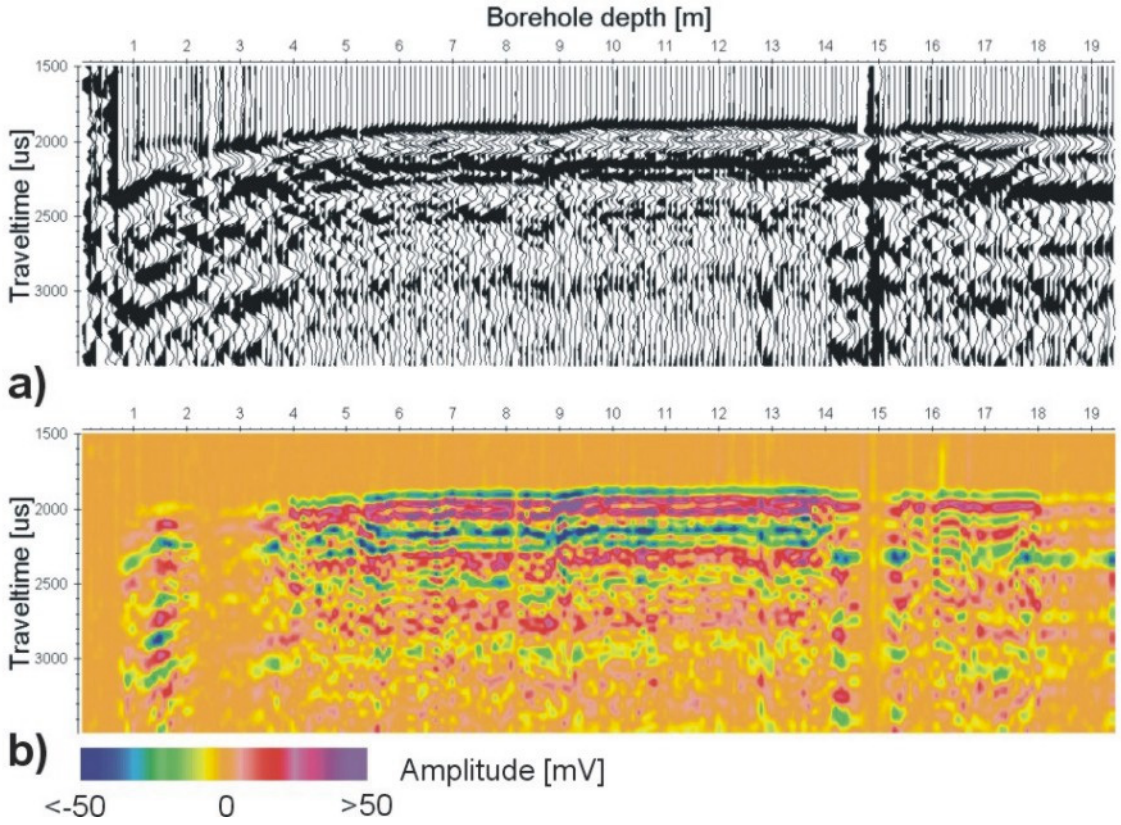

Fig. 2.2-4: Seismic section from cross hole measurements between borehole 2000/04 and borehole 2000/05, channel 1 data. a: wiggle mode, trace normalised, b: point mode, ensemble normalised.

2.2.5 Results

2.2.5.1 Interval Velocity Measurements

For quantitative analyses the distribution of the following parameters were taken into account:

1. seismic P-wave velocity (Vp),
2. normalised amplitudes of first arrival phases (norm. Amp.),
3. apparent frequency of first arrival phases,
4. seismic S-wave velocity (Vs) and
5. Vp/Vs-ratio.

In addition visual characterisations of different data plot representations (not all of them are shown here) were considered.

Results of the first arrival phase analyses from measurements in borehole 2000/04 are presented exemplary in Fig. 2.2-5a-d.

Fig. 2.2-5a shows the P-wave velocity distribution along the borehole. An increase of velocity to a level of approx. 1900 m/s in two steps to a depth of 4.6 m can be observed. At 7.2 m depth velocities starts to decrease and strong variations dominate the graph. Fig. 2.2-5b shows the distribution of normalised amplitudes. Amplitudes were normalised to the average value of all amplitudes. Values smaller than 100 % lie below the average whereas values greater than 100 % lie above the average. In the depth range 5 and 7.8 m normalised amplitudes lie substantial above 100 % and fall drastically for greater depth. In Fig. 2.2-5c the absolute values of the amplitudes are displayed. The apparent frequencies of the first arrival phases were calculated and displayed in Fig. 2.2-5d. Low frequencies indicate damaged rock as in the range 0.5 to 2 m. In the range 5 - 8 m the apparent frequencies are rather constant.

For both boreholes S-waves could be identified only up to a depth of 9 m. The S-wave velocity distribution for borehole 2000/05 for channel 1 (Δz = 10 cm) is given in Fig. 2.2-6a. The very low S-wave velocity, with an average value of about 500 m/s, is remarkable. Fig. 2.2-6b shows the ratio of the P-wave to S-wave velocity (Vp / Vs - ratio), derived for channel 1 data. Due to the low S-wave velocities the ratio is very high. With the derived P- and S-wave velocities the Poisson`s ratio can be calculated. The distribution along the borehole is given in Fig. 2.2-6c. With an average value of approx. 0.465 for depths greater than 3 m the Poisson`s ratio it is very high.

According to this parameters we conclude that up to a depth of approx. 2.8 m the rock is highly damaged. Up to approx. 5 m we observe lower P-wave velocities than the average P-wave velocity in the depth range 5 - 8 m and some anomalies which indicates smaller damages. The depth range 5 - 8 m appear relative undamaged. Only minor velocity fluctuations indicate variations in the rock. For depth greater than 8 m all parameters indicate stronger damages.

In all graphs small scale fluctuations of the parameters are obvious which have to be interpreted as disturbances due to micro cracking and / or fractures in the vicinity of the borehole wall. The extent of this disturbances towards the rock mass can not be given with this type of measurements.

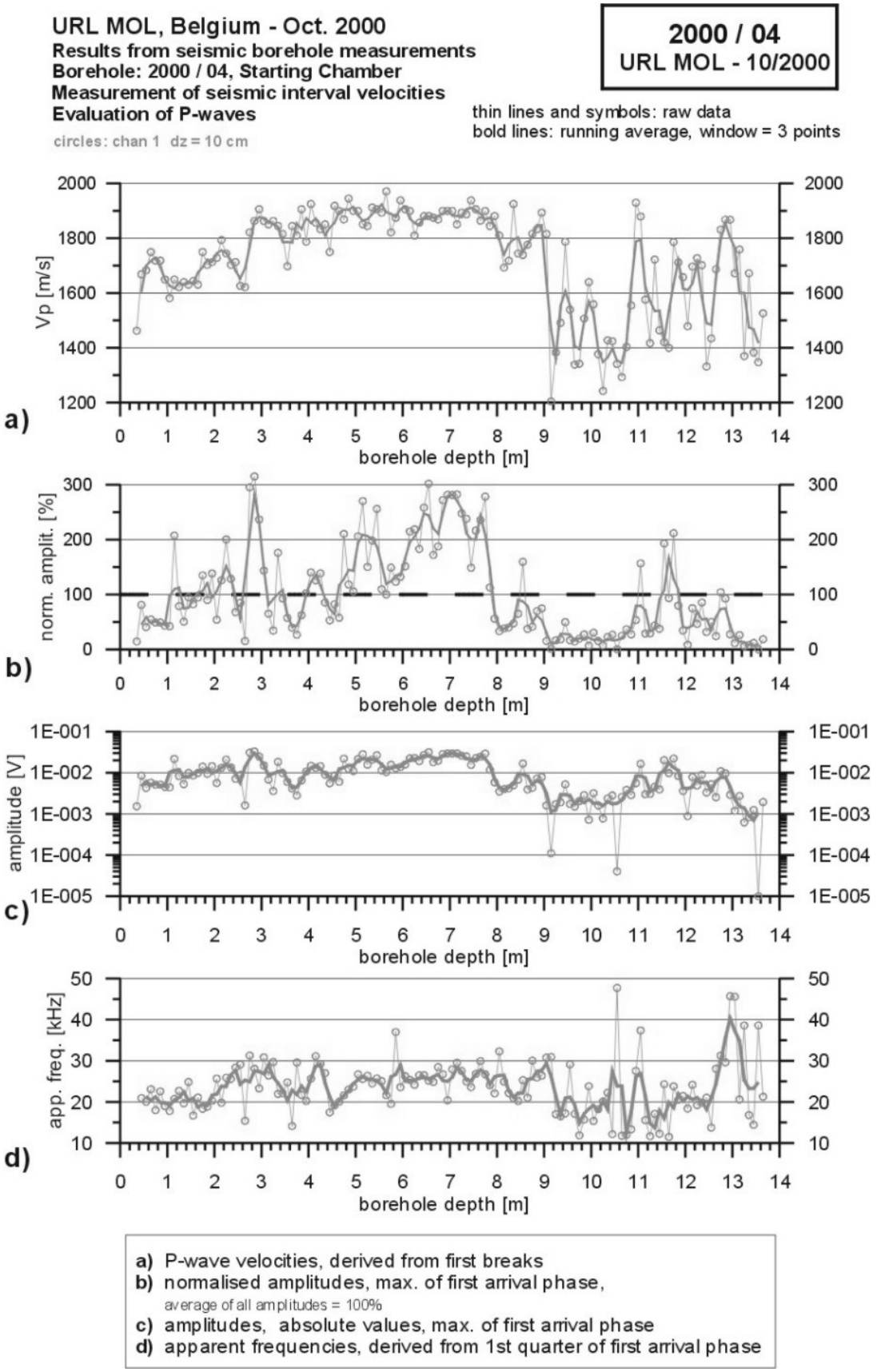

Fig. 2.2-5: Seismic parameters derived from analyses of P-waves, interval velocity measurements in borehole 2000/04.

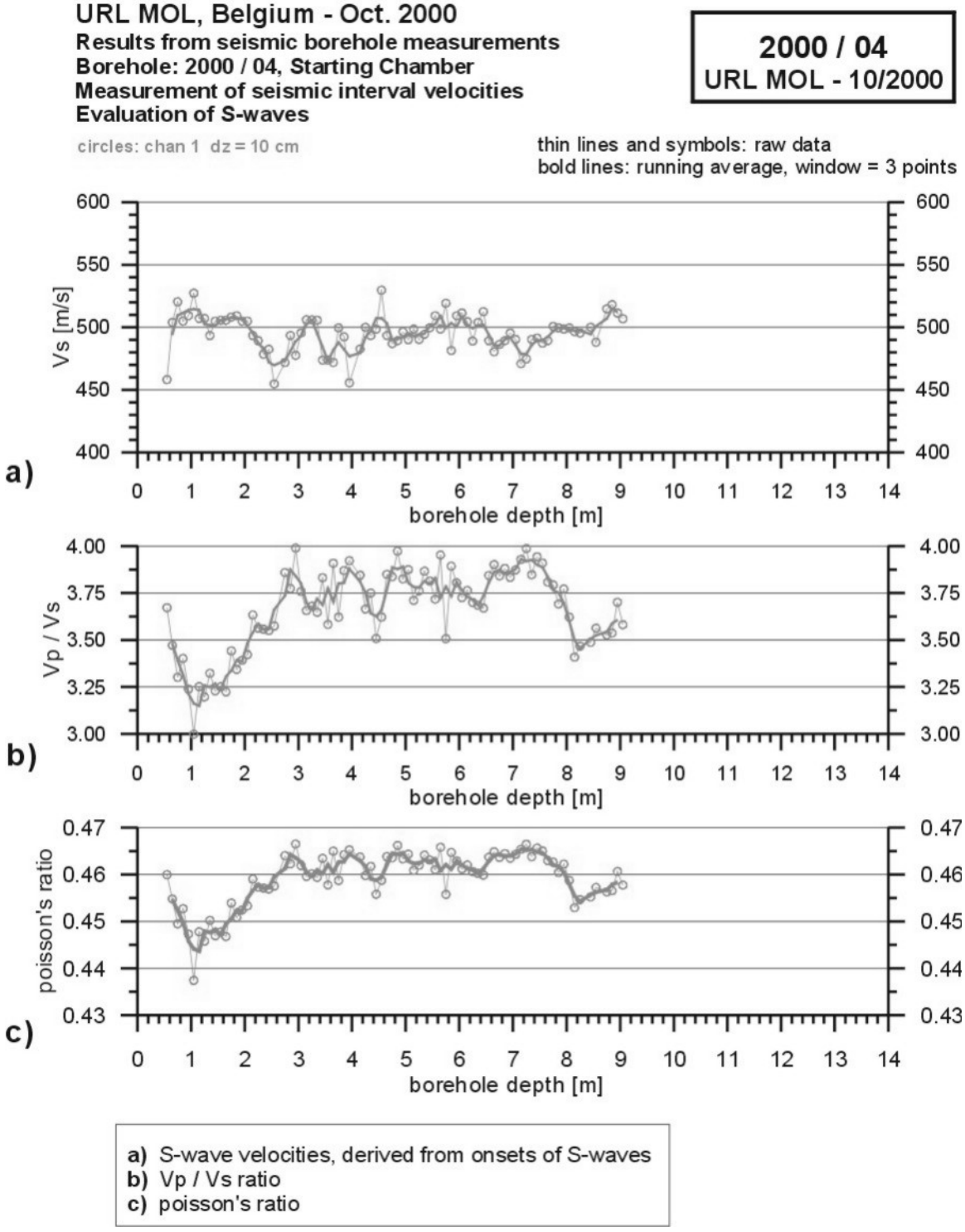

Fig. 2.2-6: Seismic parameters derived from analyses of S- and P-waves, interval velocity measurements in borehole 2000/04.

2.2.5.2 Cross Hole Measurements

Similar to the evaluation of interval velocity data results for the cross hole data are summarised as distributions of several seismic parameters in Fig. 2.2-7a-e (2000/04→2000/05).
For the cross hole experiment 2000/04→ 2000/05 the amplitudes (Fig. 2.2-7b-c) can be taken into account only up to a depth of 14 m where the problems of orientation between source and receiver started.

The derived P-wave-velocities from the forward and reverse experiment should be identical presupposed the measurements took place under ideal conditions. A straight line propagation of seismic waves between source and receivers are assumed. There are some reasons which cause errors in the estimation of seismic parameters. First of all we have to mention the differences in the tube deformation and the unknown thickness of the grouting. An uncertainty in the exact depth location, differences in the coupling of the piezo elements and last but not least the uncertainty in the travel paths of seismic waves influence the results. The velocity graphs for both measurements, forward and reverse experiment, are very good in line.

The main features of the cross hole measurements can be summarised in the following way. For borehole depths smaller 0.8 m the signal quality was very bad. No phases could be determined. Between 1 and 2 m the P-wave velocity ranges between 1800 and 1850 m/s followed by a steep increase of P-wave velocity to values around 1900 m/s which reaches at approx. 5.5 m a plateau that holds up to approx. 9 m. Then a small increase in P-wave velocity can be observed. Between 14 m and 15 m velocity falls slightly. In this depth range we have to take into account the above discussed orientation problem.

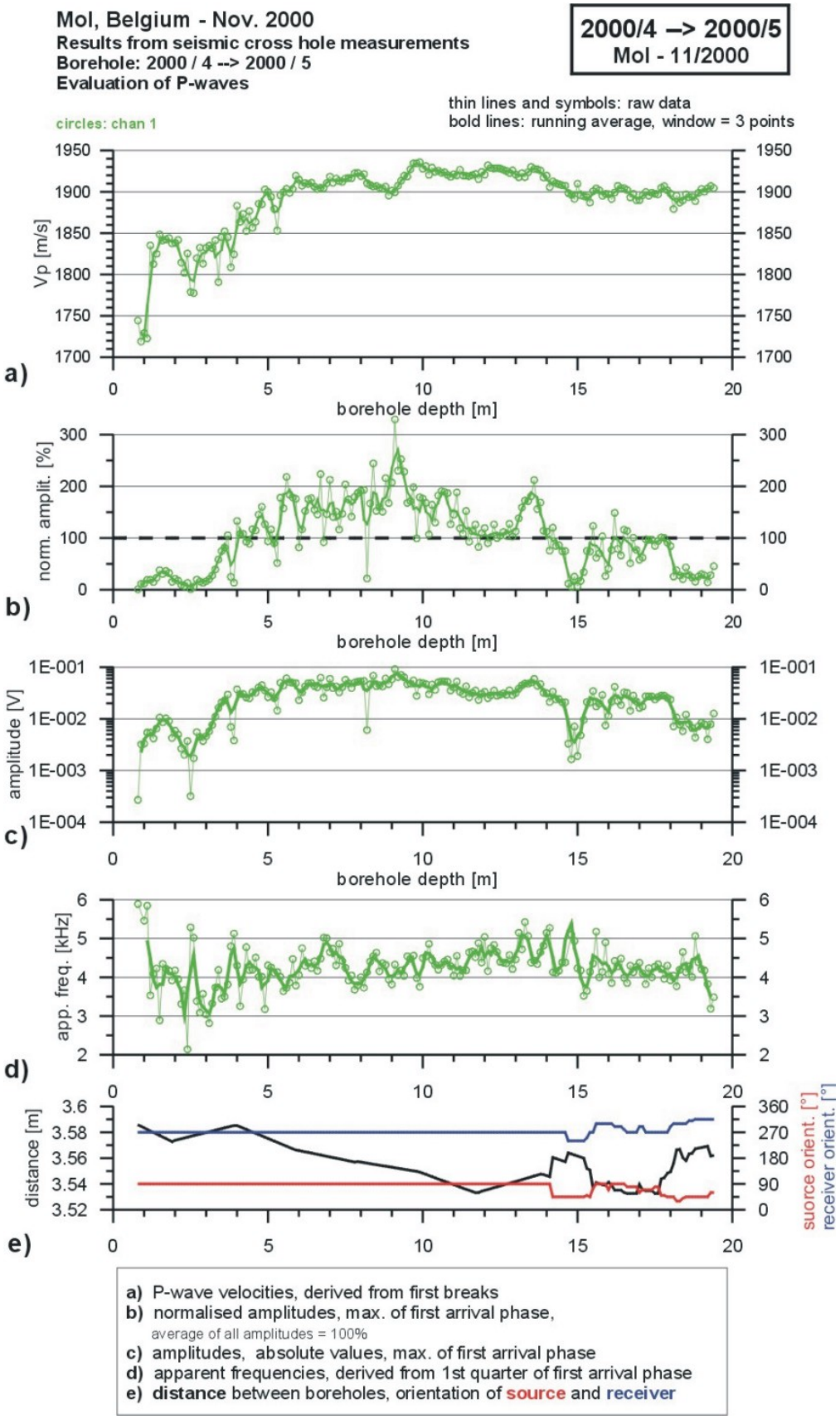

Fig. 2.2-7: Parameters derived from analyses of P-waves, cross hole measurements between borehole 2000/04 and 2000/05. (e: orientation: top is 0°, then counted clockwise).

2.2.5.3 Combined Interpretation of Results from both Methods

Averaged P-wave velocity distributions (running average of 3 points) of the performed interval velocity and cross hole measurements are summarised in Fig. 2.2-8 for depth up to 9 m. The velocity distribution which was measured in March 2000 in the test drift of the already existing part of the laboratory is included for comparison reason only (borehole 77-78 TD, sidewall, Schuster et al. 2000a). For both types of measurements the velocity increases between 3 and 6 m. The general trend is comparable in all graphs.

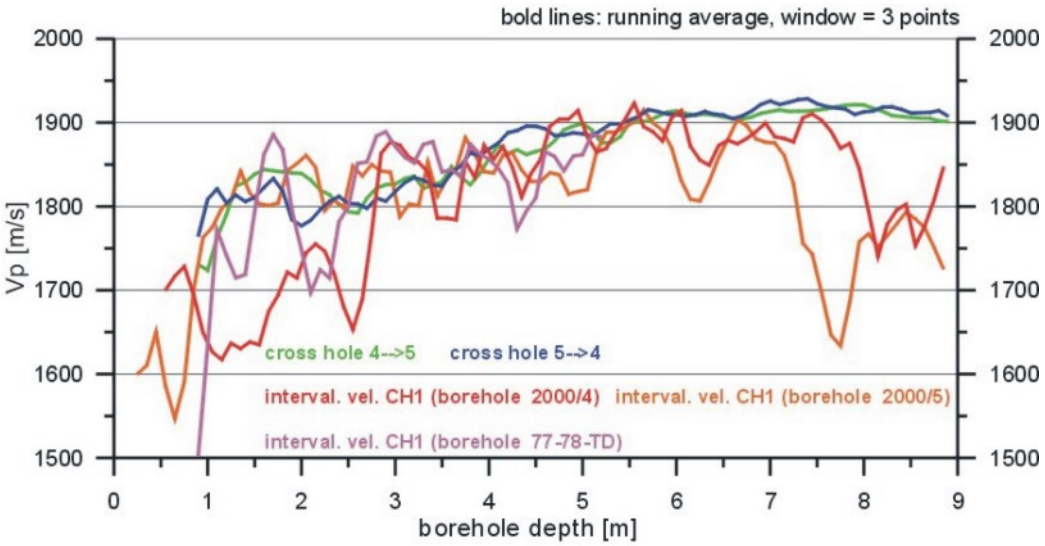

Fig. 2.2-8: Comparison of derived velocity distributions from interval velocity and cross hole measurements in and between boreholes 2000/04 and 2000/05. In addition a result from interval velocity measurements in the test drift from March 2000 is plotted (borehole 77-78-TD).

Small scale fluctuations in the graphs related to the interval velocity measurements are a striking feature. One explanation can be given when we take into account that damages caused by excavation in general created by micro cracks which are orientated parallel to the wall of a shaft or drift. Seismic waves travelling perpendicular to the shaft or drift walls are influenced very strong by this disturbances. Interval velocity measurements, performed in boreholes which are oriented perpendicular to the shaft or drift wall, reacts therefore very sensitive to such anomalies. It results in a local break down of seismic velocity as can be observed in the graphs very pronounced for depth less than 3 m and greater 7 m. The rela-

tive smooth appearance of the P-wave velocity distribution derived from cross hole measurements indicates that seismic waves which travels parallel to the shaft wall are not very strong influenced by the micro cracks (mainly orientated parallel to the shaft).
These results, derived from a combined analysis of data from both methods, can be interpreted with the existence of strong seismic anisotropy effects, created by micro cracks and / or fractures within the rock.

The compilation shown in Fig. 2.2-9 is an attempt to condense the main results and findings derived from both methods in one graph. Regions with anomalous seismic parameters, which are closely linked to petrophysical anomalous properties between both boreholes, are marked with different signatures. According to a correlation of seismic parameters derived from interval velocity measurement in each borhole the anomalies were interpolated between both boreholes. For the correlation the distribution of similar pattern of seismic parameters were used. In addition the P-wave velocity distribution derived from cross hole measurements (2000/04 → 2000/05) are plotted in.

The rock mass up to approx. 2 m (2.8 m in 2000/04 and 1 m in 2000/05) seems to be damaged with a lot of small scale disturbances. The region between 2 and 5 m shows less small scale disturbances but appear to be weak due to the ongoing gradual increase of P-wave velocity to an average level of 1900 m/s.
Consequently the EDZ extents up to approx. 5 m with a remarkable differentiation between the depth ranges 0.3 to 2 m and 2 to 5 m. Between 8.5 m (9.2 m in 2000/04 and 7.4 m in 2000/05) and 13.5 m (14 m in 2000/04 and 13 m in 2000/05), where the interval velocity measurements had to be suspended, we observe very strong velocity variations in connection with a high damping of amplitudes. The velocity derived from cross hole measurements falls for depth greater 14.5 m slightly.

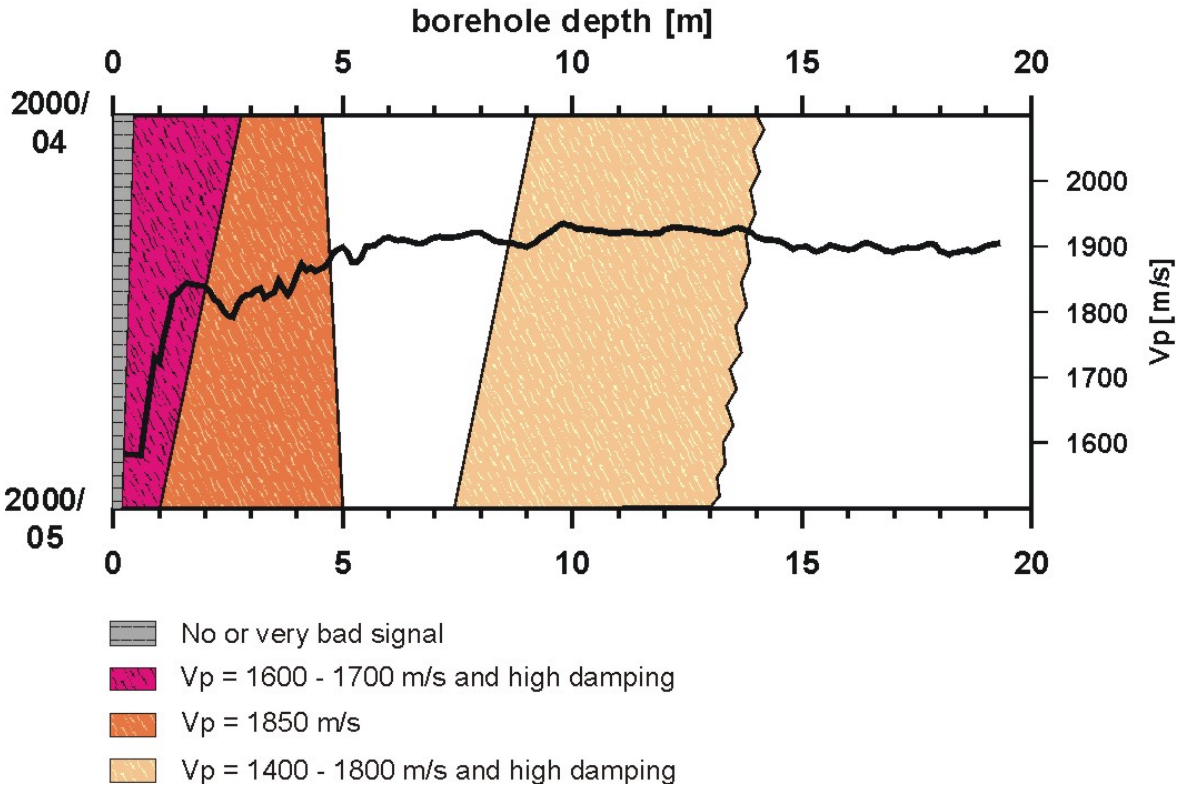

Fig. 2.2-9: Compilation of main results which describe the extent of the EDZ and the occurrence of anomalous regions. Different signatures are used.

2.2.6 Comparison between Results from Seismics and Observations made during Excavation and from Core Drilling

After seismic investigations were finished the first meters of the connecting gallery were excavated very carefully in order to map geological and tectonic features. The observations made during that excavation and results from drill core analyses can be compared with results from seismic measurements. They are summarised in the following table.

Interpretation of results from seismics (Schuster et al. 2001b)	**Observations made during excavation and results from core drilling (Bernier 2002, pers. com.)**
The rock mass up to approx. 2 m seems to be damaged with a lot of small scale disturbances.	Open fractures were observed in this zone (oxidation along fractures).
The region between 2 and 5 m shows less disturbances but appear to be weak due to the ongoing gradual increase of P-wave velocities. The EDZ extents up to approx. 5 m.	Closed fractures were observed in this zone (no oxidation). It seems that 5 - 6 m is the end of the fractured zone.
Between 8.5 and 13.5 m we observe very strong velocity variations (interval velocity measurements).	Number of fractures in cores increase in this zone with a regular pattern. From 9 m the significant increase with depth of the fracturation is probably the result of the drilling process and the present stress field.

Tab. 2.2-1: Comparison between results from seismic investigations and observations made during excavation and from core drilling.

Finally it can be said that the application of in situ seismics, especially the combination of interval velocity and cross hole measurements, revealed successfully the character and extent of the EDZ and anomalous regions of the rock mass.

2.3 Hard Rock Laboratory Äspö (Sweden) - Granite - Comparison with Fracture Scanning Tool Results

2.3.1 Introduction

At the Swedish Hard Rock Laboratory Äspö seismic in situ measurements were performed in the framework of the BGR Project "Two-Phase-Flow Experiment" (Liedtke et al. 2001). The measurements took place between the 16th and 28th of September 1998 and were carried out by BGR-Hannover - Section B2.2. The main objective of the measurement campaign was to test the application of in situ seismic methods for the detection of small scale fractures. Seismic interval velocity and cross hole measurements were performed.

2.3.2 Objectives and Location

The knowledge of petrophysical parameters of the rock mass as well as the detection and localisation are important factors for understanding and modelling of gas and fluid transport phenomena within fractured systems. This is the topic of the Two-Phase-Flow Experiment.

Seismic interval velocity and cross hole measurements were performed in the Äspö Hard Rock Laboratory (HRL) at a depth of approx. 360 m in niche 2/715 where fine grained Äspö granites are dominant. Four boreholes (borehole no.: KXP24BGR, KXP25BGR, KXP26BGR and KXP27BGR) with diameters of 86 mm and inclinations between15° and 17° were used for the investigation. The length of the boreholes ranges from 4.4 m to 8.6 m.

2.3.3 Results

In the following exemplary results from interval velocity measurements from one of the four boreholes are presented (borehole KXP24BGR, depth: 4.4 m, inclination: 17°).

The BGR mini-sonic borehole probe was used. The method and the data analysis is described in chap. 2.1.3 in full detail. The seismic interval velocities were measured successively in steps of 10 cm along the borehole, except some depth

ranges were 2 and 5 cm steps were chosen for a better lateral resolution. The source and receiver were orientated upwards. Fig. 2.3-1 shows an amplitude colour coded section measured in borehole KXP24BGR (channel 1 data, distance between source and receiver is 10 cm). Many disturbances can already be observed in this section. A differentiation between homogenous and disturbed regions can be seen very clear. The advantage of the interval velocity method is that the measurements only reflect the conditions within the measuring interval. This is especially advantageous for the detection of fractures intersecting the borehole wall.

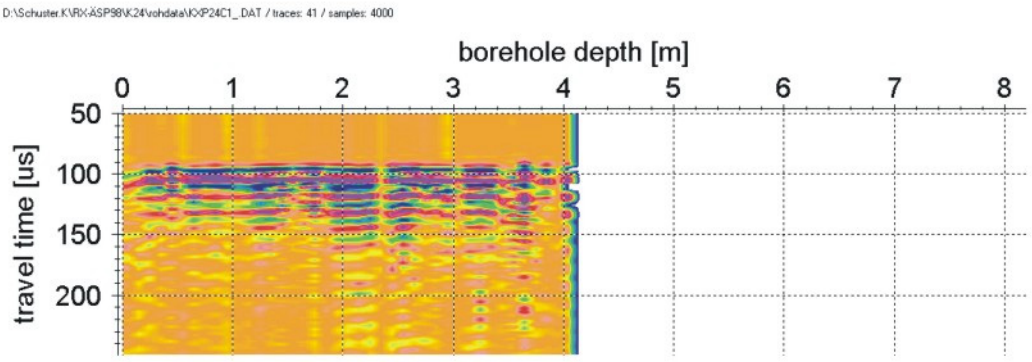

Fig. 2.3-1: Seismic section along borehole KXP24BGR for channel 1 data set. Source-receiver distance: 10 cm, measurement interval: 10 cm, point mode display, ensemble normalised, amplitudes colour coded. For colour code see Fig. 2.1-7.

In Fig. 2.3-2a the derived P- and S-wave velocities and the ratio between both are plotted. The normalised amplitude distribution, derived from first arrival phases (P-waves) are plotted below in Fig. 2.3-2b. Disturbances in the seismic wave field (see Fig. 2.3-1), which can be interpreted as the influence of fractures and / or anomalies, are also reflected in these graphs, especially in the S-wave velocities and the ratio between P- and S-wave velocity.

Three regions with different P-wave velocities can be distinguished. The step between velocity values arround 4600 m/s and 5000 m/s corresponds according to core interpretations with a Äspö diorite / finegrained granite transition. For the depth range 3.3 m to 3.7 m no change in rock material is indicated by core analyses. For the S-wave velocities the differentiation is not as clear as for the P-waves. Fig. 2.3-2b shows additionally the distribution of normalised amplitudes which represent the maximum amplitude of the first arrival phase.

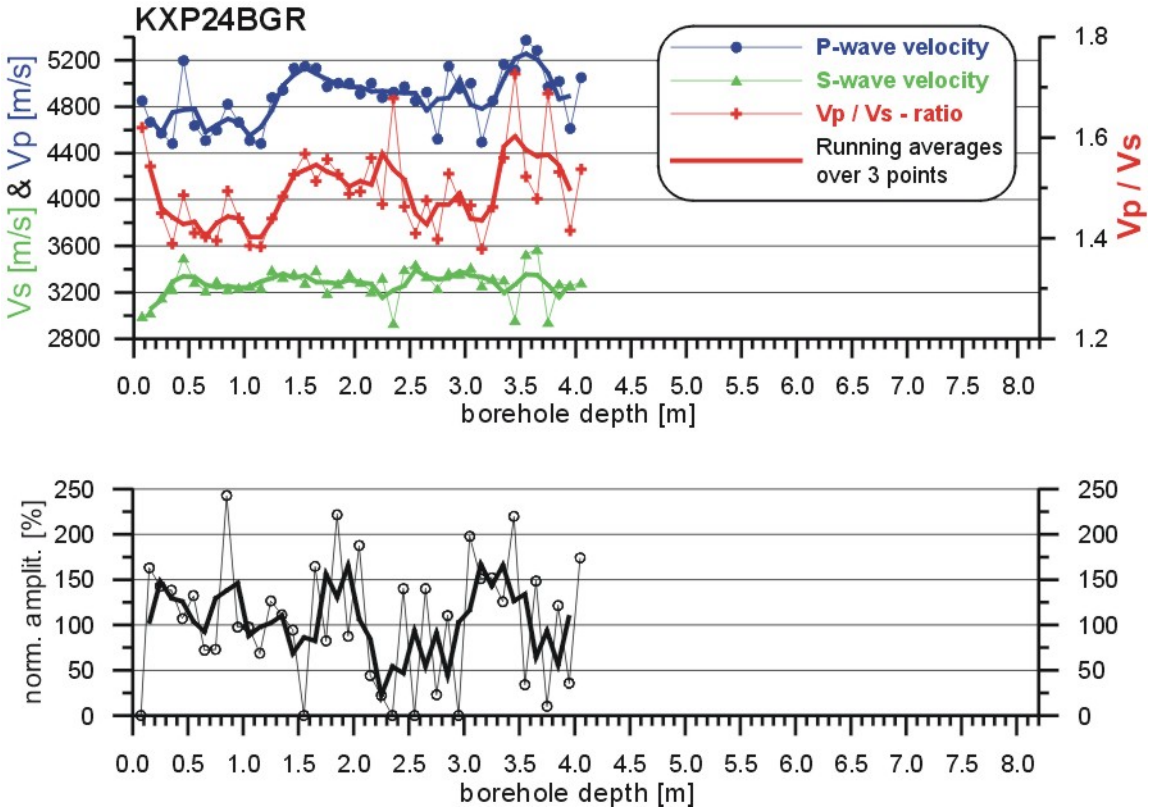

Fig. 2.3-2: Seismic parameters derived from analyses of interval velocity measurements in borehole KXP24BGR. Analyses of first arrival phases (P-waves) and S-wave onsets. Top (a): P-wave-velocity, S-wave velocity and the ratio Vp/Vs is shown. Below (b): normalised amplitude.

Fig. 2.3-3 contains a compilation of all detected fractures and disturbed regions derived from interval velocity measurements for borehole KXP24BGR. Fractures found by seismic interval velocity measurements are indicated with rectangles whereas anomalous ranges indicated with bold lines. In addition results from measurements with a Borehole Image Processing System (BIPS, fracture mapping, Contractor Raax) are plotted (diamond and cross symbols). Crosses are related to the right ordinate. Zero values for crosses correspond to closed fractures and a value of one represent open fractures. The width of the fractures (diamond symbols) varies between 1 and 8 mm and can be read off on the left ordinate.

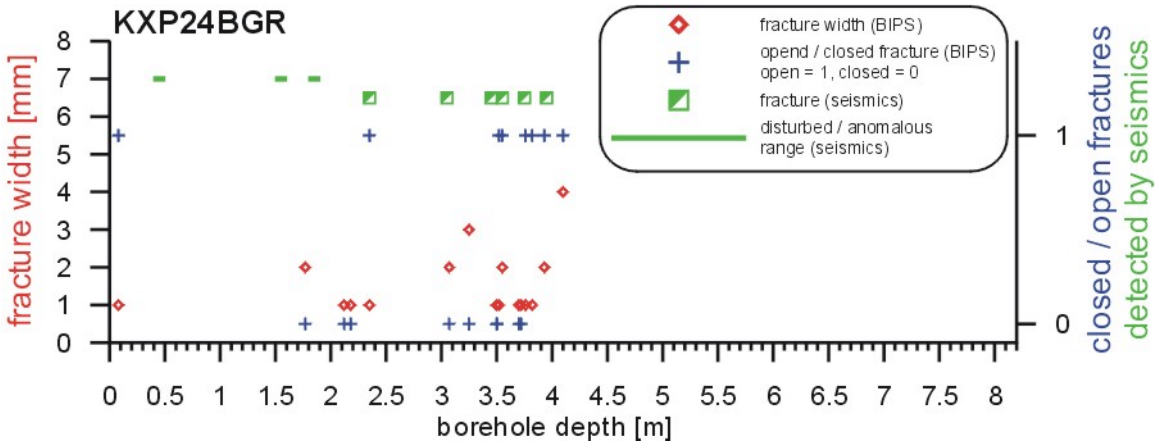

Fig. 2.3-3: Compilation of detected fractures in borehole KXP24 derived from Borehole Imaging Processing System (BIPS) and seismic interval velocity measurements.

For a comparison of both data sets (BIPS and seismics) uncertainties in depth determination have to be taken into account. First of all the depth values resulting from BIPS measurements are related to the midpoint of the borehole. For flat developed fractures there is a difference up to 12 cm between this value and the depth value where the seismic borehole probe (upward directed source and receivers) meets this fracture.

The accuracy of the localisation is, according to the distance of 10 cm between source and receiver, ± 5 cm. Furthermore an uncertainty of several centimetres (± 2 cm) for the determination of the absolute borehole depth has to be taken into account.

In spite of this in general a good correlation can be seen, especially when we focus on open fractures and closed fractures with a width greater or equal 2 mm.

In order to get a higher resolution, which is important for the detection of small fractures, an alteration of the mini-sonic probe (decrease of distances between source and receivers) is conceivable. But this is limited due to technical and physical reasons. Additionally shorter distances between the measurement points are necessary. An appropriate study was done in borehole KXP25 in the depth range between 3.1 and 3.8 m, were steps for the measurements of 2 cm instead of 10 cm were used. Fig. 2.3-4 shows the data in a wiggle and a point mode display. The depth ranges between 3.44 m and 3.68 m and greater 3.78 m have to be in-

terpreted as disturbed regions (joint set ?). Between 3.44 m and 3.56 m small disturbances of the wave field point to the existence of small fractures within the disturbed range.

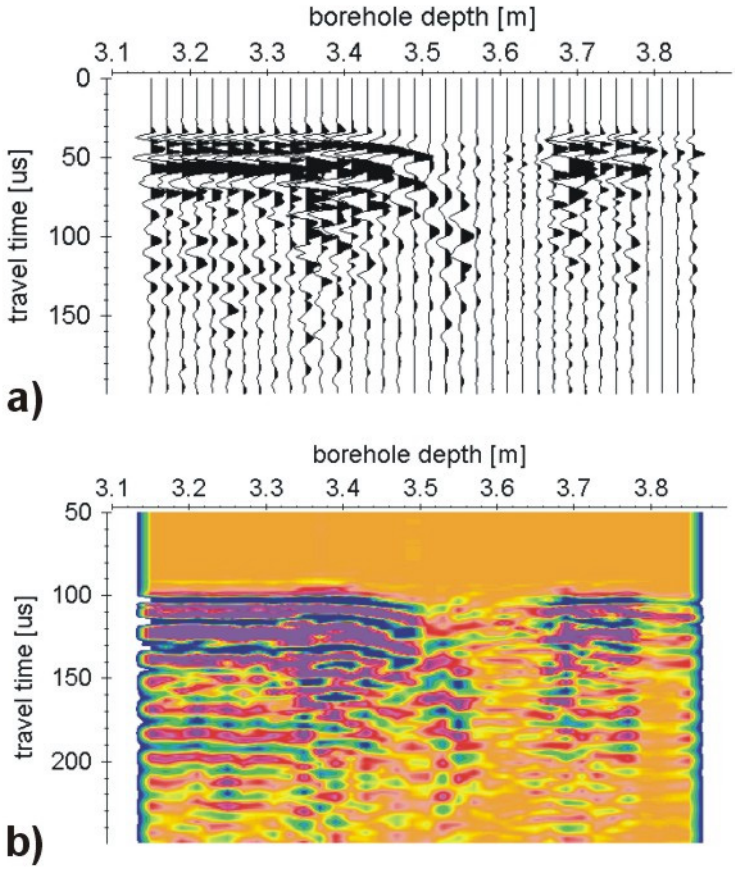

Fig. 2.3-4: Seismic section from a detailed investigation in borehole KXP25BGR. Source-receiver distance: 10 cm, measurement interval: 2 cm, real amplitudes. a: wiggle mode, b: point mode (colour code: violet/red: positive amplitudes, blue/green: negative amplitudes, amber: zero level).

2.3.4 Extent and Connectivity of Fractures

Question concerning the extent of the fractures into the rock and strongly related to that is the question concerning the connectivity between different boreholes caused by fractures were also studied.

In a first step it was searched for correlations between the seismic parameters evaluated from interval velocity measurements in the four boreholes. The analyses gave according to similar pattern in seismic parameters along different boreholes some hints for possible connectivities.

The results should help for the analysis of the seismic cross hole data set. In a second step the cross hole data sets were analysed especially with reference to

the results from the correlation analyses. Several regions in the wave field appear as shadow zones which can issue from fractures or rock anomalies.
Due to a small number of cross hole data sets only a part of the rock volume between the boreholes could be probed and therefore only a qualitative result can be given. The analyses of all data sets give several indications for fractures or rock anomalies but no clear indication for significant fractures which intersect the investigated rock volume.

2.3.5 Conclusions

The evaluation of seismic P-and S-wave signals derived from interval velocity measurements and the interpretation of different data representations (not all of them are shown here) lead to a characterisation of the four boreholes with the help of seismic parameters. The comparison between results from seismics and fracture mapping with borehole scanning tools (BIPS) can be assessed as good. To sum up it can be said that the application of in situ seismics detected and localised fractures and rock anomalies successfully.
For future seismic in situ investigations the accuracy can be improved by using shorter measurement intervals.

2.4 Rock Laboratory Grimsel (Switzerland) - Granite - Detection of Fractures

2.4.1 Introduction and Objectives

At the Swiss Rock Laboratory Grimsel seismic in situ measurements were performed within the framework of the BGR Project "*Effective Parameters*" (Himmelsbach et al., in prep.). The measurements took place during three one-week campaigns in winter and spring 1999 and were carried out by BGR-Hannover - Section B2.2. The main objective of two measurement campaigns was the detection of small scale fractures and / or joints along two 60 m and 70 m long boreholes with the help of in situ seismic methods. Both boreholes are located in the BK niche where mainly fine grained granites ("*zentraler Aaregranit*") were encountered. Seismic interval velocity measurements performed by BGR, Section B2.2 at the Swedish Rock Laboratory Äspö in 1998 gave proof of a reliable application of that method for the detection of fractures in granites (see chap. 2.3). Furthermore the extent of the Excavation Damaged Zone (EDZ) around the niche should be investigated. The third campaign aimed at a feasibility test for the application of seismic refraction methods for the determination of the EDZ along a drift wall (see chap. 3.1).

Main parameters of the used boreholes are summarised in Tab. 2.4-1. Both boreholes were drilled in the sidewall, borehole EFP98019 approx. 0.3 m above the bottom and borehole EFP98020 approx. 2.5 m above.

	Diameter [mm]	Length [m]	Inclination [°]
EFP98019	86	60.8	-15
EFP98020	86	70	30

Tab. 2.4-1: Parameters of boreholes used for seismic interval velocity measurements in the BK niche.

Measurements in borehole EFP98020 were carried out between 28th of January and 5th of February 1999. Due to a strong water influx the measurements in borehole EFP98019 had to be stopped during this first campaign. Measurements were resumed at the 27th of May 1999. A second water pump was available for this measurement campaign. From neighbouring boreholes the water level in borehole

EFP98019 could be lowered to such a level that measurements could be performed.

2.4.2 Results

Only results from interval velocity measurements are presented briefly. The applied method, data acquisition and analyses did not differ from the above described ones. Due to technical problems the acquisition parameters had to be changed for depth greater 55 m for the upward orientated borehole. Therefore the results are discussed here only to borehole depths of 55 m.

2.4.2.1 Velocity Distribution along the Boreholes

In Fig. 2.4-1 the derived P- and S-wave interval velocities are plotted for borehole EFP98020 along the borehole depth. The lines represent the running averages of 3 data points. In both velocity graphs an increase in velocity up to approx. 1.2 m can be observed very clear. Classically this would be an indication for the existence and the extent of the EDZ. Up to 8 m velocities stay relatively stable on one plateau before they jump to a slightly higher plateau. At 12.8 m both graphs indicate a distinct decrease, followed by very strong developed variations. The velocities which are characteristic for the first 12 meters are encountered only at the end of the borehole and at few single points in between.

The general drop in velocity at 12.8 m could be related to a change in material. But the very strong developed small scale variations in velocity pinpoint to the existence of many fractures and / or joints. Interval velocities are strongly influenced by fractures and / or joints. In this case we can state that as lower the velocity (compared to a typical velocity of the undamaged rock) as higher the number of fractures / joints or the thickness of a single fracture / joint encountered in this range.

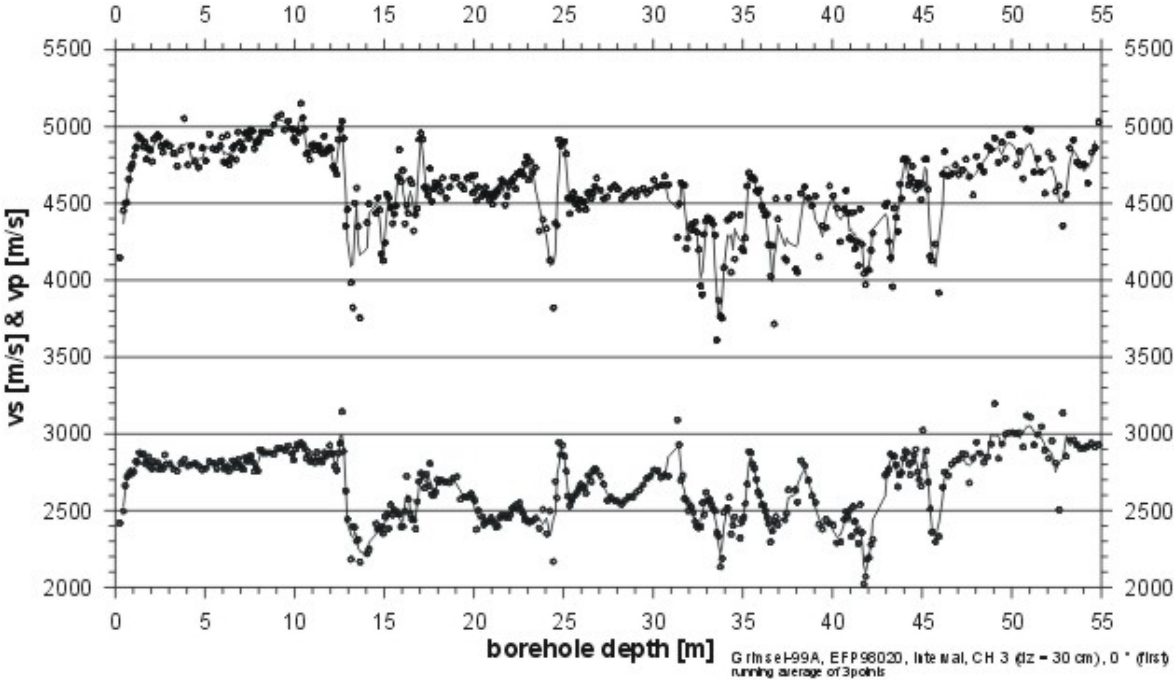

Fig. 2.4-1: Borehole EFP98020 : P-wave (top) and S-wave interval velocities (below) derived from channel 3 data (source – receiver distance of 30 cm).

The velocity distribution for borehole EFP98019 is plotted in Fig. 2.4-2. Reliable travel time picks for the velocity determination could be done only up to 36 m. Between approx. 7 and 12.5 m the velocities are relatively stable. Contrary to data from borehole EFP98020 the variations in both graphs are not so strong. Noticeable is the drop in velocity around 5 m.

In general the velocities derived in borehole EFP98020 within the first 12 meters are higher than in borehole EFP98019. When one exclude that there is no change in material within this short distance range an explanation can be found in different developed small scale EDZ around the borehole walls. Such a small scale EDZ can be caused by the drilling of boreholes. After the drilling it can be influenced for example by unloading or stress redistribution in the rock mass.

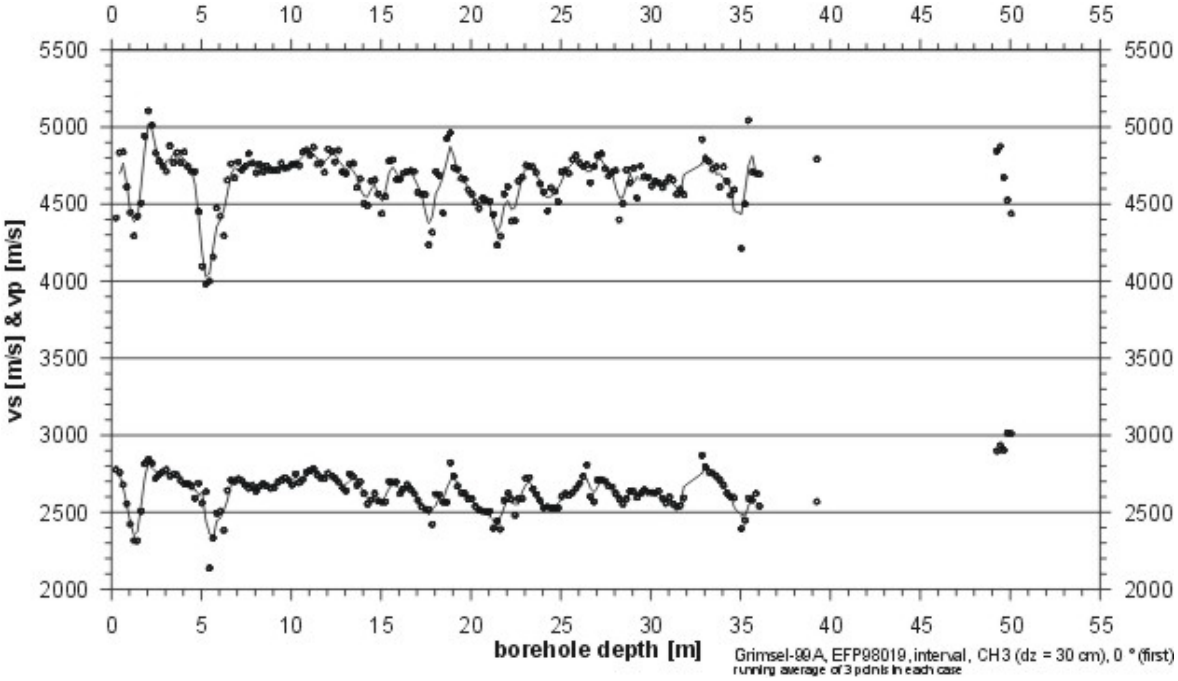

Fig. 2.4-2: Borehole EFP98019 : P-wave (top) and S-wave interval velocities (below) derived from channel 3 data (source – receiver distance of 30 cm).

2.4.2.2 Extent of EDZ

Contrary to EFP98020 data (comp. Fig. 2.4-1) P-wave velocities in borehole EFP98019 decrease from a high value of 4850 m/s to 4300 m/s within the first meter. Within the following meter P-wave velocities reach high values as they are encountered in borehole EFP98020. The P-wave velocity at a depth of 1.2 m is comparable to the P-wave velocity which was reached already after 0.15 m in borehole EFP98020. S-wave velocities show a similar pattern.

According to these observations the extent of the EDZ derived from borehole EFP98020 data would reach 1.2 m and according to borehole EFP98019 data it would be less than 0.2 m. This leads to the supposition that we see within the first two meters a superimposition of two effects which influences the interval velocities: micro cracks caused by the excavation of the niche and the occurrence of open or closed fractures / joints as they were also encountered at greater depth.

With the help of the data representation shown in Fig. 2.4-3 and Fig. 2.4-4 the EDZ do not exceed 0.4 m in both cases because only up to this depth the amplitudes are disturbed very strong or the values nearly vanished.

In March 1999 in the supply tunnel which was excavated by a tunnel boring machine seismic refraction test measurements were performed by BGR, Section B2.2. For the extent of the EDZ along a 4 m long horizontal profile values between 0.05 and 0.15 m were derived (see chap. 3.1).

2.4.2.3 Localisation of Fractures and / or Joints

The occurrence of fractures and / or joints can be very good visualised with the help of a data representation where the amplitudes are colour coded. In Fig. 2.4-3 and Fig. 2.4-4 channel 1 data are plotted that way over a range of 55 m. For borehole EFP98020 (Fig. 2.4-3) one can distinguish between undisturbed and disturbed ranges. Up to approx. 12.5 m the wave filed is very coherent which can be related to a homogeneous rock mass. Only at about 7 m a week anomaly in the S-waves (blue band) is visible. This drop in amplitude is related to a fracture encountered at this depth. Several other homogeneous ranges, with extents of more than 2 m can be observed along the borehole, for example between 18 and 20 m and 27.5 and 30.5 m. But the striking feature is the existence of many ranges where amplitudes are decreased to values nearly zero (amber / yellow colour). All this anomalies are indications for the existence of single fractures or joint sets. According to this display the fractures and joint sets can be picked on the depth axis and compared with drill core data.

In Fig. 2.4-4 channel 1 data from borehole EFP98019 are displayed. The different appearance of this data representation, compared with Fig. 2.4-3, results from different acquisition parameters which do not influence the results. Concerning the detection of fractures and / or joints in borehole EFP98019 a similar description, as it was done for borehole EFP98020 data, can be given. In comparison with EFP98020 data up to 35 m less fractures and / or joints seem to exist.

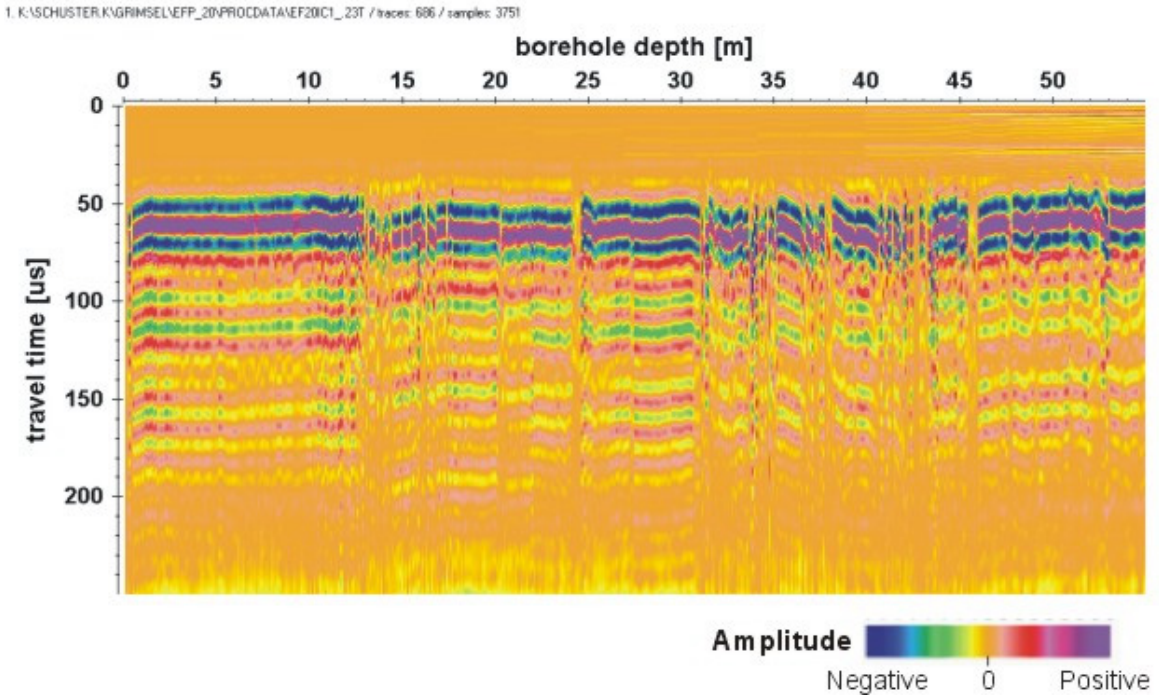

Fig. 2.4-3: Borehole EFP98020 : Ensemble normalised representation of seismic data from interval velocity measurements. Amplitudes are colour coded. Disturbances in the wave field are related to fractures and / or joints.

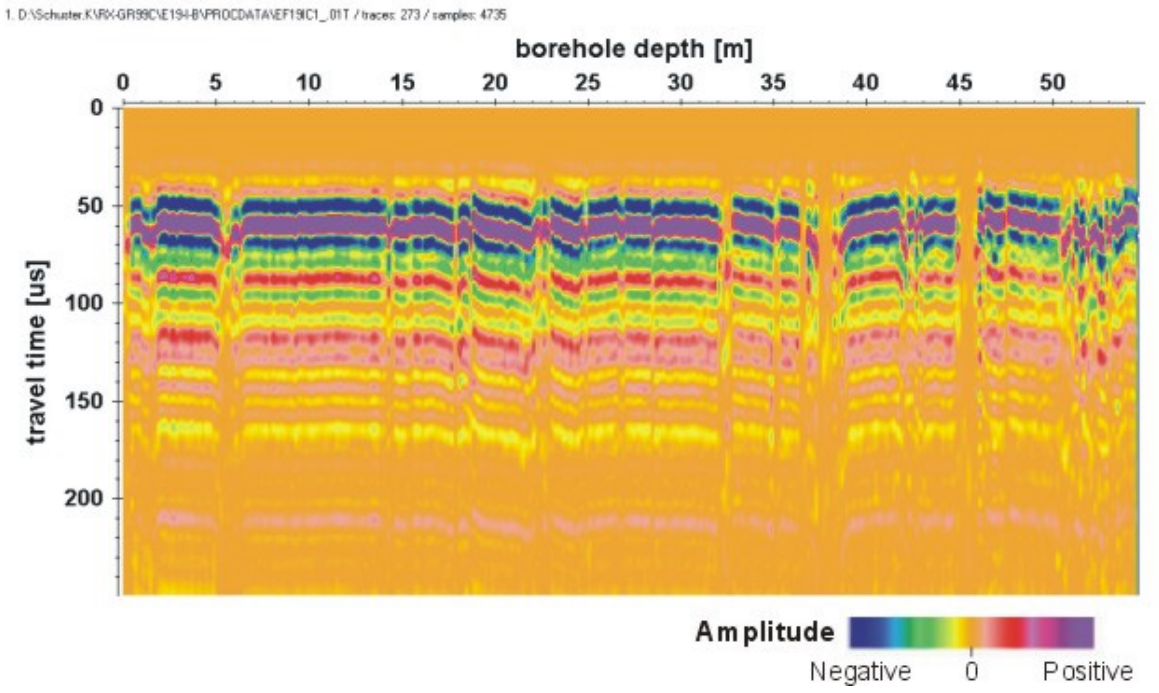

Fig. 2.4-4: Borehole EFP98019 : Ensemble normalised representation of seismic data from interval velocity measurements. Amplitudes are colour coded. Disturbances in the wave field are related to fractures and / or joints.

2.4.2.4 Conclusion

The application of seismic interval velocity measurements with a mini-sonic borehole probe revealed the existence of fractures and / or joints along two 60 and 70 m long boreholes. The localisation of the fractures and / or joints is in good accordance with onsite observations made on drill cores. The extent of EDZ in the BK niche is at least 0.4 m.

2.5 Asse Research Mine - Salt Rock - Comparison with Permeability Measurements

2.5.1 Introduction and Objectives

At the Asse Research Mine (Germany) seismic borehole measurements were carried out in spring 2000 by BGR in a 700 m deep and 90 years old drift (Schuster and Alheid 2000). The measurements took place immediately after permeability measurements which were performed by GRS (Gesellschaft für Anlagen- und Reaktorsicherheit) were finished. The aim of the measurements was to analyse the extent of the EDZ around the lined and unlined sections of the drift especially with regard to the permeability measurements.

The drift was excavated in 1911 by blasting. Four years later an approx. 20 m long section was lined with a cast iron lining. Two photographs of the seismic measurements within the lining (Fig. 2.5-1) and from the unlined section (Fig. 2.5-2) give an impression of the location.

For both measurements four radial boreholes with diameters of 86 mm were used. Boreholes were drilled in the framework of the ALOHA 2 project (Investigation of the hydraulically effective excavation disturbed zone around disposal regions, Wieczorek 2001). In the following we concentrate on the comparison of two vertical boreholes, drilled in the floor. Borehole DJ_V (accessible depth 7.3 m) is located approx. in the centre of the lined section of the drift and borehole VS_V (accessible depth 6.9 m) is approx. 18 m away from borehole DJ_V and 7 m outside the lining.

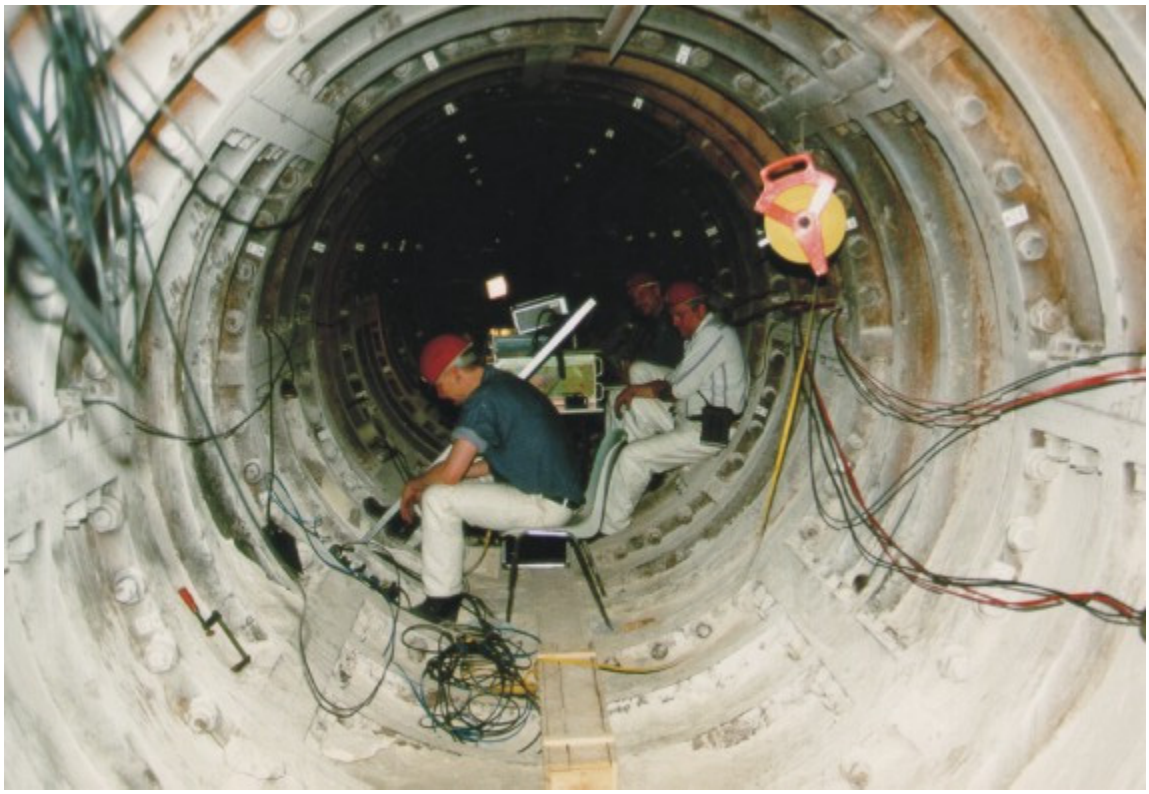

Fig. 2.5-1: Asse Research Mine, 700 m level. Seismic interval velocity measurements inside the lining (Tübbing-Strecke).

Fig. 2.5-2: Asse Research Mine, 700 m level. Seismic interval velocity measurements in the unlined section.

Seismic interval velocity measurements were applied in order to characterise the EDZ with the help of seismic parameters. The method is described in full detail in chapter 2.1.3. The orientation of the source-receiver plane was NNE, this is perpendicular to the axis of the drift.

2.5.2 Results

The quality of the signals are very high, especially the signal to noise ratios. Figures 2.5-3a and 2.5-3b show the relevant part of two data sets (borehole depth 0 - 2.1 m) measured in boreholes DJ_V and VS_V. In order to stress the variation of travel times at the beginning of the boreholes the first arrival phases are zoomed in. Traces with a distance of 20 cm between source and receiver (channel 2 data) are displayed. Each seismic section is trace normalised (wiggle mode, black lines) whereas amplitudes are interpolated and normalised over the total ensemble of traces were superimposed. They are displayed colour coded (blue: negative, ocher: zero level, red/violet: positive). Borehole VS_V had around the borehole mouth a 10 cm thick backbreak. Therefore the measurements started 10 cm below the level of the floor. The material which was encountered in the boreholes is indicated at the top of both sections (st: steel, con: concrete, salt: rock salt). A distinct decrease of travel times of the first arrival phases can be seen within the first meter in both figures.

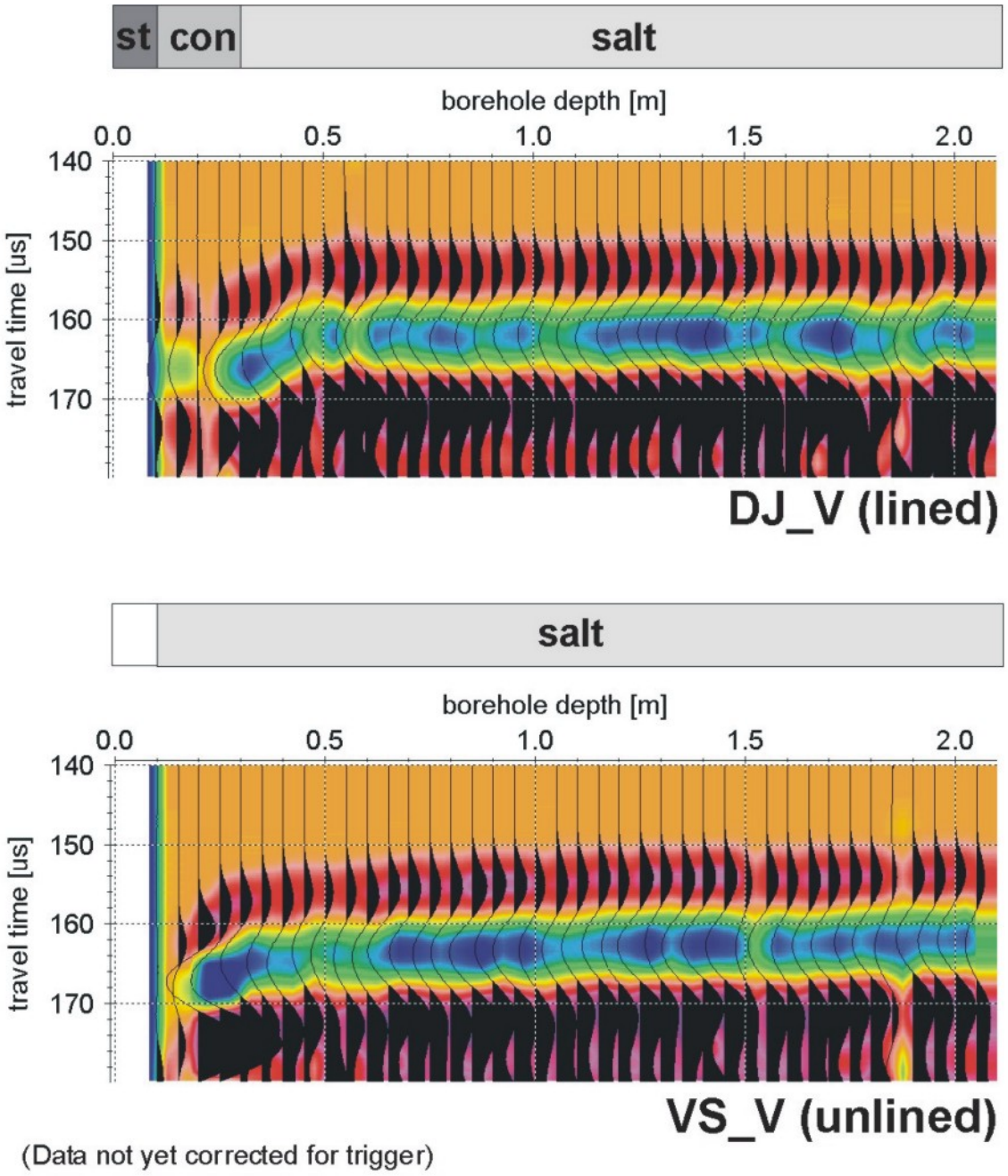

Fig. 2.5-3: Seismic sections (0 - 2.1 m) for channel 2 data (distance source - receiver 20 cm) from interval velocity measurements in vertical boreholes at the Asse Research Mine (700 m level). Wiggle mode data (trace normalised) superimposed with colour coded amplitudes (ensemble normalised). Colour code: violet/red: positive amplitudes, blue/green: negative amplitudes, amber: zero level. Top (a): data from lined section. Below (b): data from unlined section. (st: steel, con: concrete).

The related P-wave velocity distributions derived from channel 2 data are presented in Fig. 2.5-4 together with results from permeability measurements (modified after Wieczorek 2001). The left ordinate is valid for the P-wave velocity graphs and the right ordinate for the permeability data.

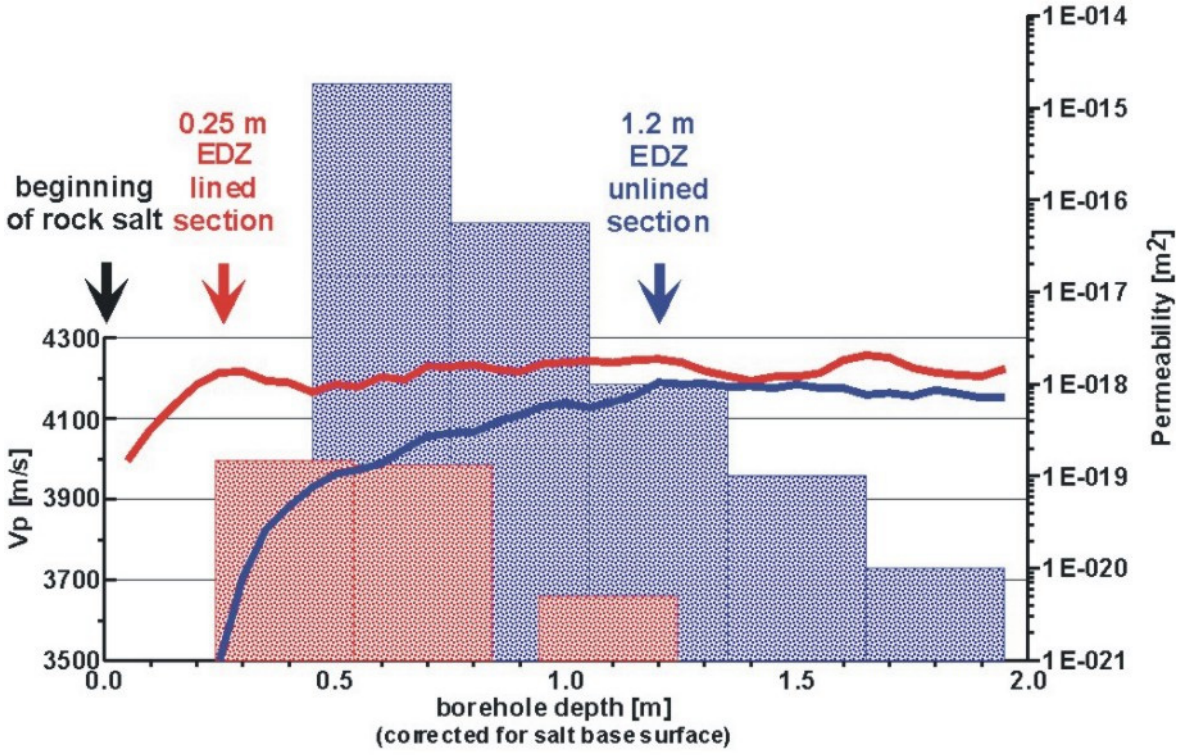

Fig. 2.5-4: Comparison between results from seismic interval velocity measurements and measurements of permeability (Project ALOHA 2, GRS, Wieczorek 2001) at the Asse Research Mine (700 m level). Results from lined section: red colours (bars and graphs). Results from unlined section: blue colours (bars and graphs).
P-wave velocities: left ordinate, permeability: right ordinate. Depths are corrected to the beginning of rock salt. Permeability lies outside the seismically identified EDZ (>0.25 m in the lined section and >1.2 m outside) below 10-18 m2.

For the P-wave velocities only the running average over three single measurements are plotted. The depth was corrected for both data sets. Both depths scales begin with zero at the point where the rock salt was encountered in the boreholes. When we subtract the thickness of the steel liner (10 cm) and the concrete layer of approx. 20 cm for borehole DJ_V the P-wave velocity reaches roughly an constant value of approx. 4200 m/s after 0.25 m, as it is shown in Fig. 2.5-4 (red line, left ordinate). Corresponding we have to add 10 cm for the data from borehole VS_V. This is the difference between the bottom floor and the borehole mouth (because

of the backbreak). Within borehole VS_V a comparable constant P-wave velocity is reached after approx. 1.2 m (blue line, left ordinate). On the basis of former measurements a P-wave velocity of 4200 m/s can be regarded as a good average velocity for the undisturbed rock. Both depth ranges with reduced P-wave velocities were interpreted as the EDZ derived from seismic parameters.

The permeability measurements (gas injection tests) were performed by GRS (Wieczorek 2001). The results were taken from Wieczorek (2001) and corrected for depth in the same way like the seismic data were corrected. For both data sets their zero point for the depth axis starts at the point where the rock salt was encountered in the borehole. The width of the bars corresponds to the test interval of the permeability borehole probe (red bars: lined section, blue bars: unlined section). The depths are assigned to the centre of the 30 cm wide bar. Below 0.4 m (borehole DJ_V) and 0.6 m (borehole VS_V) no permeability measurement were performed. We observe a gradual decrease of permeability towards greater depth.

2.5.3 Conclusion

Results from both methods are very good in line. The comparison between results from seismic and permeability measurements shows that values for the permeability outside the range of the seismically identified EDZ (0.25 m for borehole DJ_V and 1.2 m for borehole VJ_V) lie distinct below 10^{-18} m^2. Obviously the EDZ in rock salt is much more pronounced in the unlined section. The lining reduces the EDZ to a minimum value. Further investigations should clarify whether a lining even could result in a reduction (self healing) of the EDZ.

3 Refraction Seismic Methods

The major aim of the project was to modify a geophysical method for the non-destructive in situ application for the determination and petrophysical characterisation of the EDZ. As could be shown in the previous chapters seismic borehole methods gave proof of the reliable application for the determination of the EDZ. With the help of seismic parameters, as P- and S-wave velocities as well as damping of seismic amplitudes the EDZ can be characterised.

The application of the seismic refraction method and the following evaluation and interpretation of data yields a model of the underground in terms of a velocity distribution. The method uses seismic waves which travels as refracted waves (critically refracted on interfaces and / or as diving waves) through the underground. This type of seismic wave which was radiated from the surfaces, penetrated downwards until it met a seismic interface were the seismic velocities of adjoining interfaces are significantly different, then continued along this interface and finally emerge under a critical angle at the surface is called a refracted wave. For details see for example Sheriff and Geldart (1982).

The EDZ as described above with the help of seismic parameters fulfil the prerequisites for a successful application of the seismic refraction method. Due to reduced velocities in the vicinity of an excavated cavern or drift a positive velocity gradient exists. In general velocities increase gradually from the wall of a cavern or drift towards the undamaged parts of the rock mass.

A refraction seismic feasibility test with a four channel digital storage oscilloscope and three piezoelectric transducers was performed in March 1999 in the Rock Laboratory Grimsel (Switzerland). Results of this successful test are presented in chap. 3.1. In Spring 2000 a new 48 channel system was available. The equipment and test measurements in the laboratory will be described in chap. 3.2. The complete new system was used first for an in situ test measurement at the Asse Research Mine in summer 2000. This will be discussed briefly in chap. 3.3. In summer and autumn 2001 the equipment was used at the Mont Terri Rock Laboratory within the framework of an extensive seismic measurement program which offered

the opportunity of comparison of results derived from different methods. The refraction seismic data acquisition, the evaluation of data and the interpretation of results will be described in full detail in chap. 3.4. Therefore in chap. 3.1 to 3.3 the applied data acquisition method, evaluation of data and results are discussed only in brief.

3.1 Rock Laboratory Grimsel (Switzerland) - Granite - Refraction Seismic Test

As a feasibility test for the application of a non-destructive seismic method for the investigation of the EDZ in March 1999 measurements were performed in the Rock Laboratory Grimsel (Switzerland). Measurements took place at the sidewall of a supply drift (centarl Aare granites, fine grained). The drift was excavated by a tunnel boring machine. Along the sidewall a 9 m long horizontal profile was measured.

Due to the lack of a multi-channel high resolution acquisition equipment a four channel digital storage oscilloscope (DSO) was used (Nicolet 440). Contrary to a classical seismic refraction data acquisition, where many simultaneously recording receivers and few shotpoints are used, we used 91 shotpoints and three receivers. Three channels of the DSO were used for the receivers, the fourth for the trigger piezoelectric transducer. This type of data acquisition is not optimum because uncertainties in trigger accuracy influence the results. Furthermore the amplitude distribution along the total profile depends strongly on the many shotpoints with their individual characteristics.
Three piezoelectric transducers were used as receivers (PCB M353B67). Each of them was moved during the measurements to three different locations. In Fig. 3.1-1b the different locations are marked with RE-N. For example, the first piezoelement was fixed at profile locations RE-1, than at RE-4 and finally at RE-7.

As seismic source a concrete test hammer (SCHMIDT hammer) was used. The distance between the 91 shotpoints (excitation points) was 10 cm. Triggering was

done with a piezoelectric transducer which was placed at all shotpoints near the impact location of the source. The related trigger delays were later corrected.
After data were sorted and corrected for trigger delays they can be displayed as a receiver section. Due to the reciprocity of travel times this can also be regarded as the better known shot section. In Fig. 3.1-1a a data set for receiver position RE-7, located at profile coordianate 5.9 m, is plotted that way. Plotted are 91 signals from 91 excitation points which were recorded at receiver location RE-7.

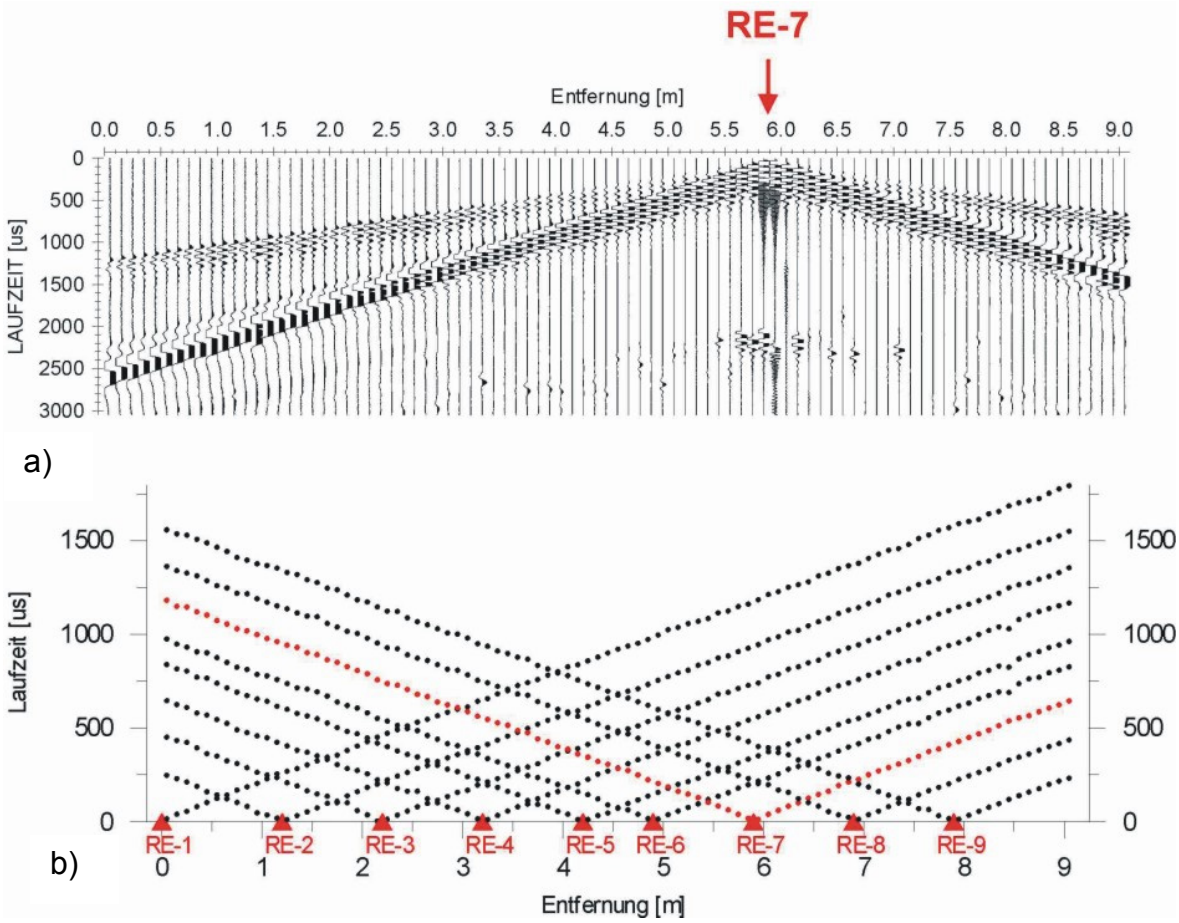

Fig. 3.1-1: First results of a seismic refraction test measurement at the Rock Laboratory Grimsel. a: all received signals at receiver position RE-7 at 5.9 m, trace normalised display. b: first arrival travel time curves for all nine receiver positions.

Very clear the first arrival phases (P-waves) can be observed. They are followed by the onsets of S-waves. For distances greater approx. 1.5 m from the "source point" both phases start to separate. Fig. 3.1-1b shows the travel time curves for the picked first arrival phases for all nine receiver locations. Variations in the travel

time curves are little, what imply that there is laterally no big change in the velocity distribution. Small variations in the curves, especially when they occur on all curves at the same profile coordinate, can be seen as indications for the existence of fractures and / or joints. But due to the used unusual acquisition method we can not exclude uncertainties in the data due to technical reasons.

The first arrival travel time curves are the basis for an inversion which yields a velocity distribution of the rock. Even though the slopes in the graphs show laterally a slight change data were inverted with the Intercept Time Method (Ewing et al. 1939). The result is a 1-dimensional P-wave velocity model of the underground. The calculated velocity-depth-curves within the profile range 4 to 8 m are plotted in Fig. 3.1-2. Eight velocity-depth-curves are compiled for velocities between 3800 and 5500 m/s and depths to 0.6 m.

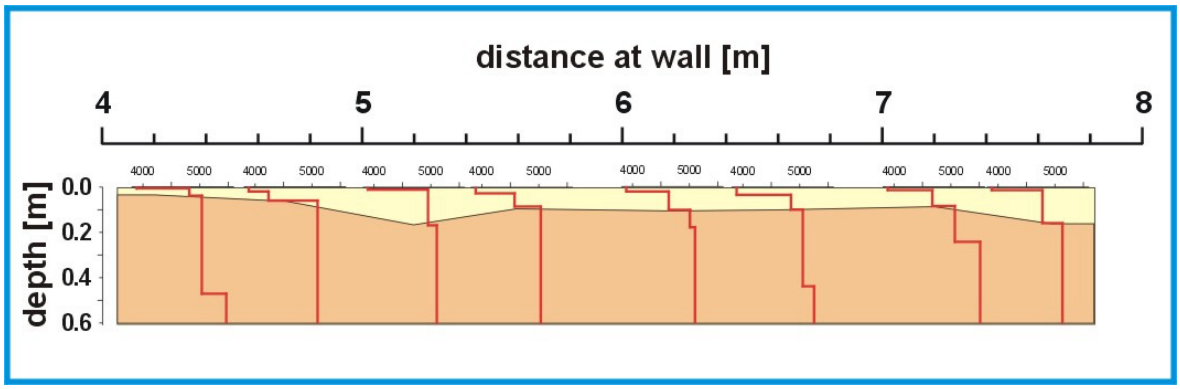

Fig. 3.1-2: Result of a 1-dimensional inversion of travel time curves in the profile range 4 - 8 m. At eight locations the depth-P-wave velocity distribution (Vp = 3800 - 5500 m/s and z = 0 - 0.6 m) are plotted. Light yellow marks the depth range with P-wave velocities < 5000 m/s.

The depths values where velocities lie below 5000 m/s are interpolated along the profile and highlighted with a light colour. Reduced P-wave velocities are characteristic for the EDZ. It reaches only a few centimeters from the sidewall into the rock (approx. 2 - 12 cm). These results are in good accordance with observations made in the Swedish Rock Laboratory Äspö, where similar extents for the EDZ were found in drifts, excavated with tunnel boring machines.

3.2 New Refraction Seismic Equipment

For the high resolution refraction seismic in situ measurements a multi-channel data acquisition system is necessary. A complete seismic recording equipment for this purpose consists of the following main components:

- High resolution (in time and amplitude) digital scope recorder with at least 24 channels, including a control unit
- Sensitive piezoelectric transducers as receivers
- Seismic source
- All components have to be robust enough in order to resist the harsh in situ conditions

As a good compromise between spatial resolution and handling of such a device a system with 48 channels was selected. Because no conventional seismographs with the demanded high sampling rates of at least 100 kHz were on the market we followed the idea of connecting three conventional DSOs to one multi-channel recording system. A disadvantage of such a solution is the fact, that the devices are designed for applications under laboratory conditions and not for harsh conditions as they are normal for example in salt mines. In order to protect the devices a protection casing has to be build.

After a market analyses the decision was made in favour of three YOKOGAWA DL 716 devices. Some of the main parameters are listed in the following:

- No. of channels: 16
- Maximum sampling rate: 10 Ms / s
- A/D conversion resolution: 12 bits

The provider of the three DSOs developed a special software for using three 16 channel DSOs as a 48 channel recording system. A synchronised sampling of data between the three units is guaranteed. A notebook computer serves as a control unit. Communication between the notebook and the DSOs is realised via three RS232 ports. The recorded data are stored after each measurement on the internal harddisk drives (capacity of 3.2 GB). After measurements are finished they are transfered via a SCSI interfaces to the notebook. From the notebooks safety copies can be transfered to ZIP-drives.

As receivers for the seismic signals 48 uniaxial or 16 triaxial piezoelectric transducers can be used. The manufacturer of the transducers is PCB - Piezotronics. Main technical parameters for uniaxial piezoelectric transducers:

- Type: PCB M352 C 67
- Voltage sensitivity [mV / g]: 100 mV/g
- Frequency range (±10%): 0.3 - 12,000 Hz

Main technical parameters for triaxial piezoelectric transducers:

- Type: PCB M356 A 15
- Voltage sensitivity [mV / g]: 100 mV/g
- Frequency range (±10%): 1 - 6,500 Hz

A power supply with an integrated preamplifier for the piezoelectric transducers (factors: 1, 10 and 100) is necessary to run the transducers (PCB Sensor Signal Conditioner Model 481 A02).

Seismic energy can be generated with a small seismic impact source. The spring driven source has to produce a seismic signal which on the one hand do not overmodulate the nearby receivers and on the other hand it has to be strong enough to produce signals of good quality at distances of about 5 m. Tests on a rock salt block in the laboratory yielded signal frequencies greater 10 kHz in the vicinity of the impact point.

In spring 2000 the three new 16 channel digital storage oscilloscopes, the notebook and the control software as well as the piezoelectric transducers were available for first test measurements in the laboratory.

A photograph of the test measurements in the laboratory is shown in Fig. 3.2-1. The DSOs are shown from the back without casing. Each DSO stands on a power supply for the piezoelectric transducers. On the right hand side is the 2.1 m long and 1 m high salt block. On top 48 uniaxial piezoelectrical transducers are deployed along a line. In Fig. 3.4-1 in the chapter after next a sketch can be seen with all components of the recording equipment.

In general this first test was successful. Some minor errors in the software had to be corrected and some improvements were made.

Fig. 3.2-1: Test measurements at the laboratory with the new 48 channel equipment. Rear view of the three digital storage oscilloscopes (without casing). 48 piezoelectric transducers are deployed on a salt block.

3.3 Asse Research Mine - Salt Rock - Refraction Seismic Measurements

For use under harsh conditions in rock laboratories and mines especially the sensitive electronic devices of the DSOs had to be protected against shocks during transportation, moisture, aggressive dust, for example in salt mines, and high temperatures. For this reason the DSOs were hermetically sealed by steel cases. Through a window in the cases the display of the DSOs can be observed. The DSOs are controled by a notebook which is connected via the serial ports.

Because the DSOs are hermetically sealed they are cooled by a Peltier element which is mounted on top of the cases.

In summer 2000 the complete system was ready for an in situ test. This first test was performed at the Asse Research Mine at the 490 m level. A 7.5 m long horizontal profile on the sidewall of a drift was measured. Fig. 3.3-1 shows the equipment at this location.

Fig. 3.3-1: Seismic refraction measurements at the Asse Research Mine (490 m level) with the new 48 channel equipment. The three digital storage oscilloscopes are protected by cases. Piezoelectric transducers are deployed along a horizontal profile at the sidewall.

The three DSOs are placed on a table. On top of each case the Peltier elements can be seen. The control notebook stands in the front on a table. The piecoelectric transducers pasted up on the sidewall with a special glue. A part of the 45 used receivers can be seen on the right side in the photograph. The three power supplies for the piezoelectric transducer stand on the bottom. The test was successful. The equipment proved their worth in spite of the very harsh conditions with temperatures above 40 °C. For future work only some changes on the seismic source and the trigger had to be made.

First qualitative analyses of the raw data show along the profile lateral variations in the P-wave velocities. Reduced P-wave velocities, which are indicators for the EDZ are restricted to the close vicinity of the sidewall. A raw data example from a registration of a nearby shot point location is shown in Fig. 3.3-2.

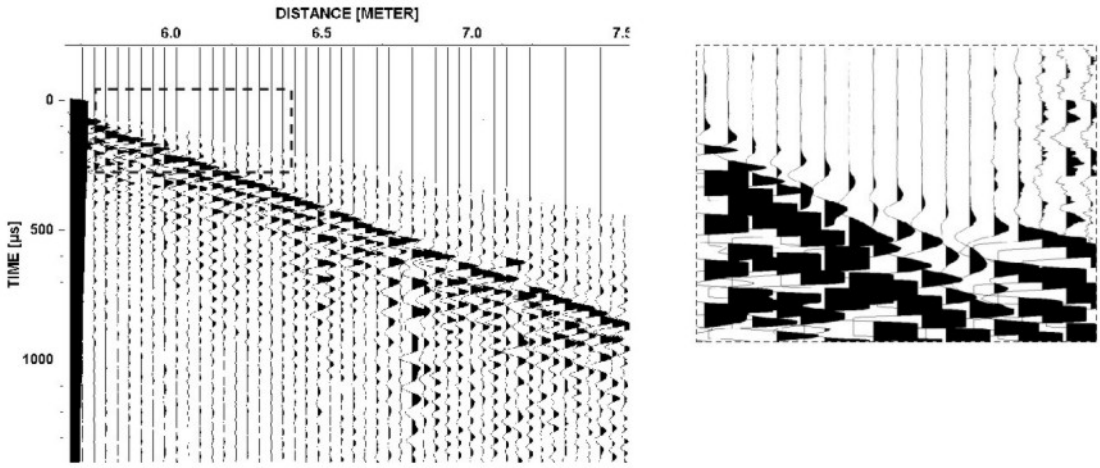

Fig. 3.3-2: Data set from seismic refraction measurements at the Asse Research Mine (490 m level). Shot position x = 5.5 m. Left: 48 traces, trace normalised display, S-waves are dominant. Right: Enlargement of the left rectangle, P-waves as first arrivals are visible.

On the left the trace normalised shot section with all traces of one record are shown. S-waves with strong amplitudes dominate the plot (slope between 0 and approx. 800 µs). P-waves appear with weaker amplitudes (slope between 0 and approx. 400 µs). On the right side the part which is marked in the left plot with a rectangle is magnified. P-waves can be identified very clear. Data evaluation is not yet finished. It will be done in the nearby future.

3.4 Mont Terri Rock Laboratory (Switzerland) - Opalinus Clay - Refraction Seismic Measurements

After the test measurements were successfully finished and corrections on the software and improvements on the seismic source were finished the equipment was ready for a routinely measurement campaign.
For a refraction seismic measurement with the new equipment the Mont Terri Rock Laboratory was chosen, because measurements could be integrated into a bigger seismic measurement campaign. Furthermore at the same location geoelectrical measurements were performed (Kruschwitz 2002). This gave the opportunity of comparison between results derived from different methods with the results obtained from refraction seismics.

The investigations in the EB niche offered the opportunity to have direct access to the rock along a distance range of about 6 m. Piezoelectric transducers could directly be placed with a special glue at the wall. This is a prerequisite for performing seismic refraction measurements. Measurements performed that way are absolutely non-destructive what can be seen as a big advantage. In the New Gallery of the Mont Terri Rock Laboratory the shotcrete prevented the performance of this type of measurements.

3.4.1 Data Acquisition

The principle of the applied measurement technique and some details about the instrumentation are outlined in Fig. 3.4-1. The equipment consists of 45 piezoelectric transducers which are used as receivers, a special power supply and preamplifier for the receivers, a small seismic impact source, three synchronised digital storage oscilloscopes (DSO, 16 channels each) and a notebook as a control unit (see also chap. 3.2).

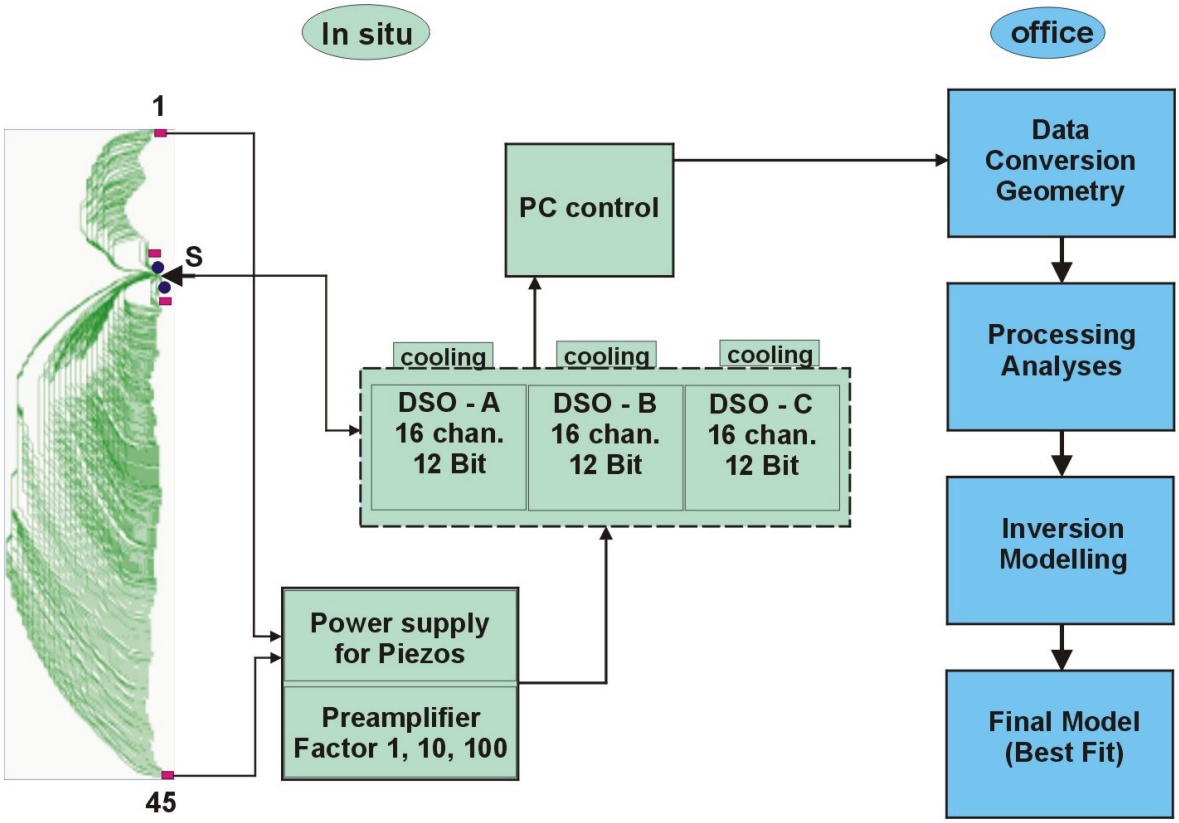

Fig. 3.4-1: Principle of high resolution seismic refraction measurements. 48 channels supported. S: Impact source, 1 - 45: receiver positions.

Three profiles were measured as listed in chap. 1. Up to now a 5.7 m long horizontal profile along the NE wall of the EB niche (see Fig. 2.1-2, blue line on the left) is analysed. A spacing of approx. 4.1 cm between the receivers was used. This narrow spacing was necessary to guarantee the desired high spatial resolution. In Fig. 3.4-2 the topography of the profile is drawn exaggerated. The total profile had to be measured along three subprofiles (A, B, C), each equipped with 45 seismic receivers. In Fig. 3.4-13 some receivers can be seen.

The 11 shotpoints were nearly equidistant distributed along the 5.7 m long profile. The distance between the shotpoints is approx. 60 cm. Seismic energy was generated by a small seismic impact source. The spring driven source has to produce a seismic signal which on the one hand do not overmodulate the nearby receivers and on the other hand it has to be strong enough to produce signals of good quality at distances of about 5 m.

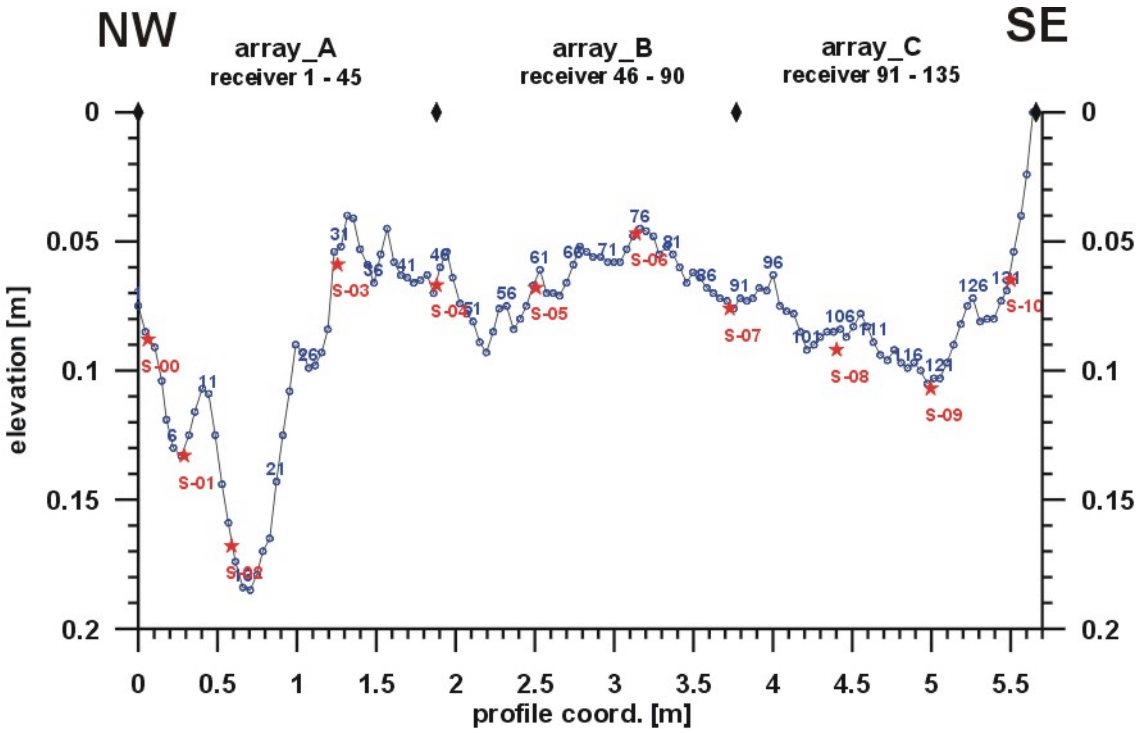

Fig. 3.4-2: Topography along the seismic refraction profile Mt05 in the EB niche (NE sidewall). Shotpoints marked with S-00 to S-10, some receiver points marked with their numbers.

The receiver as well as the shotpoint positions were smoothed slightly with a small drilling machine (smoothed circle areas of approx. 20 mm in diameter and 1 - 3 mm deep). The receivers were fixed with a special glue on this areas.

After the emission of the seismic impact pulse the generated wave field is registered simultaneous at 45 receiver positions with a sample rate which has to be adjusted to the frequency content of the expected signals, which is, of course, site dependent. A sample rate of 1 μs was used. This sample rate allows a more reliable application of filters for an improvement of the signal to noise ratio. The impact of the seismic source is also registered and serves as the trigger for the measurement system. In order to get information about the strength of the seismic impulse at different shotpoints nearby two piezoelectric transducers register the strength of the source. The individual / local impulse strength can be taken into account. This opens the possibility to analyse also the amplitudes of the seismic signals, because they provide information about the attenuation behaviour of the rock under investigation.

In Fig. 3.4-3a the raw data set registered for shotpoint 2 are compiled (seismic shot section). It consists of 135 traces. Because the maximum number of traces which can be registered simultaneously is 45 the measurements along the total profile length of 5.7 m was done in three steps. In the first step 45 receivers were deployed along a 1.9 m long subprofile (A) and signals were emitted from all 11 shotpoints. Then the 45 receivers were moved to subprofile B and again all 11 shotpoints were used. Finally subprofile C was measured in an analogous way. Later the traces of the three measurements had to be time shifted in order to eliminate the individual trigger time delays and combined to a shot gather (see Fig. 3.4-3). These data sets form the basis for the following processing steps.

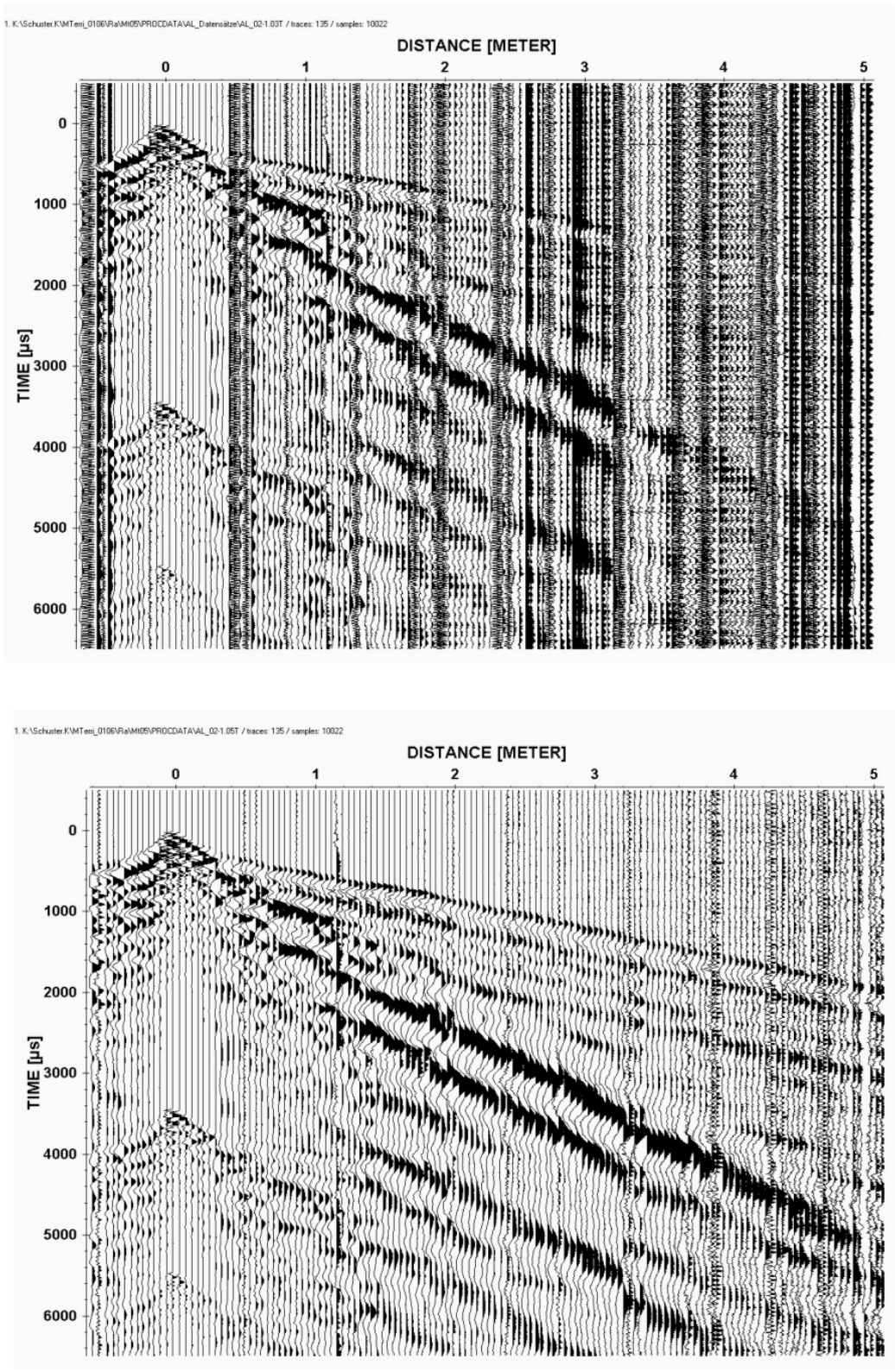

Fig. 3.4-3: Data example from seismic refraction measurements along the NE sidewall in the EB niche for shotpoint S-02 (profile Mt05). All 135 traces are distributed nearly equidistantly (spacing of approx. 4.2 cm) over the 5.64 m long horizontal profile. Top (a): raw data, below (b): filtered data (DC-shift subtracted and mean filter applied). Both data sets are trace normalised.

3.4.2 Data Analyses

The aim of the processing of the raw data is first of all the improvement of the signal to noise ratio in order to get reliable travel time information. Furthermore this is a precondition for the application of a phase correlation which forms the basis for the derivation of a one dimensional start model of the rock under investigation in terms of depths to a refracting boarder. In addition the distribution of seismic P-wave velocities along the profile can be extracted. At this stage it provides only apparent velocities.

3.4.2.1 Main processing steps

The applied main steps for the processing of seismic refraction data are listed briefly in the following:

- Insert of geometry information (profile distances, positions of receivers and shotpoints, topography) into the seismic trace headers
- Sort and combination of subprofiles
- Start time correction due to the individual trigger time delays
- Plot of shotpoint sections
- Subtraction of DC shifts
- Mean filter, 11 points
- Picking of first arrival times (P-waves) and phase correlation
- Plot of travel time curves
- 1-dimensional inversions for all travel time curves
- Creation of a 2-dimensinal start model
- Forward computation (net work ray tracing and / or Finite Differences)
- Iterative modelling till the best fit between model travel times and measured travel times is reached
- Final model

3.4.2.2 Seismogram sections

As can be seen in Fig. 3.4-3a the first arrival phases (P-waves) can only be correlated up to a distance of approx. 3.2 m from the shotpoint (between 0 and 1400 μs). The same holds for the shear waves (S-waves). They can be correlated between 1300 μs and 3400 μs. The signal to noise ratio for greater distances is very low. The signals are superimposed mainly with artificial noise. In general disturbing noise is generated not only by the measurement system but also by nearby or far away operating electrical devices like power supplies, engines, traffic noise and so on. In Fig. 3.4-3 the traces are plotted trace normalised that means that every trace is normalised to its maximum amplitude value. Otherwise all traces could not be plotted at once in this wiggle mode display. The differences in the amplitudes between the near and far offset traces are in the range of 1:10,000.

The raw data set (Fig. 3.4-3a) was filtered in two steps. First a DC shift, which sometimes is caused by a DC voltage offset during the measurements, was subtracted from all traces. Afterwards a mean filter was applied. This type of filtering was tested and compared with the application of a band pass filter (Butterworth). The band pass filter caused a not tolerable phase shift which would lead to errors in the first arrival picks. This was observed especially for the traces near the shotpoints. In order to avoid this the mean filter was applied. The result is shown in Fig. 3.4-3b. The improvement is considerable. Now signals can be traced up to the end of the profile.

In Fig. 3.4-3 at about 3400 μs and 5400 μs (for distance x = 0) an artefact can be observed. The seismic signal appears with weaker amplitudes a second and a third time. This is created by an unwanted second and third stroke of the seismic impact source. Unfortunately these signals interfere for greater times with the S-waves generated by the first stroke.
The apparent velocities (slope of the travel time curves) for P-waves are approx. 2200 m/s - 3000 m/s. For the S-waves it is between 1000 m/s and 1200 m/s.
Because we are interested mainly in the first arrival phases the data can be potted with reduced times. In these displays the travel times are reduced proportional to the horizontal distance between source and receiver (x) assuming a constant ve-

locity distribution, according to $t_{red} = t_{meas} - \frac{x}{v_{red}}$. The reduction velocity was chosen that way that the first arrival times form a horizontal line in the graphs. In Fig. 3.4-4 to Fig. 3.4-6 for all 11 shotpoints the data are plotted in a time window between -200 μs and 1400 μs. Only for this presentation data were band pass filtered (BP, Butterworth 0.3 - 16 kHz). The above mentioned phase shift can not be resolved in this display. A reduction velocity of 2700 m/s was chosen. The signal quality in general is very good. For shotpoint 0 to shotpoint 7 data the first arrival phases can be followed nearly over the complete section. Only for the last three shotpoints (SP 8 - SP 10) for greater distances the noise dominates. When one compare data from shotpoint 0 with data from shot point 10 remarkable differences can be observed. Both data sets cover the same distance range.

Several small scale disturbances are visible which can be seen as hints for the existence of joints and / or faults.

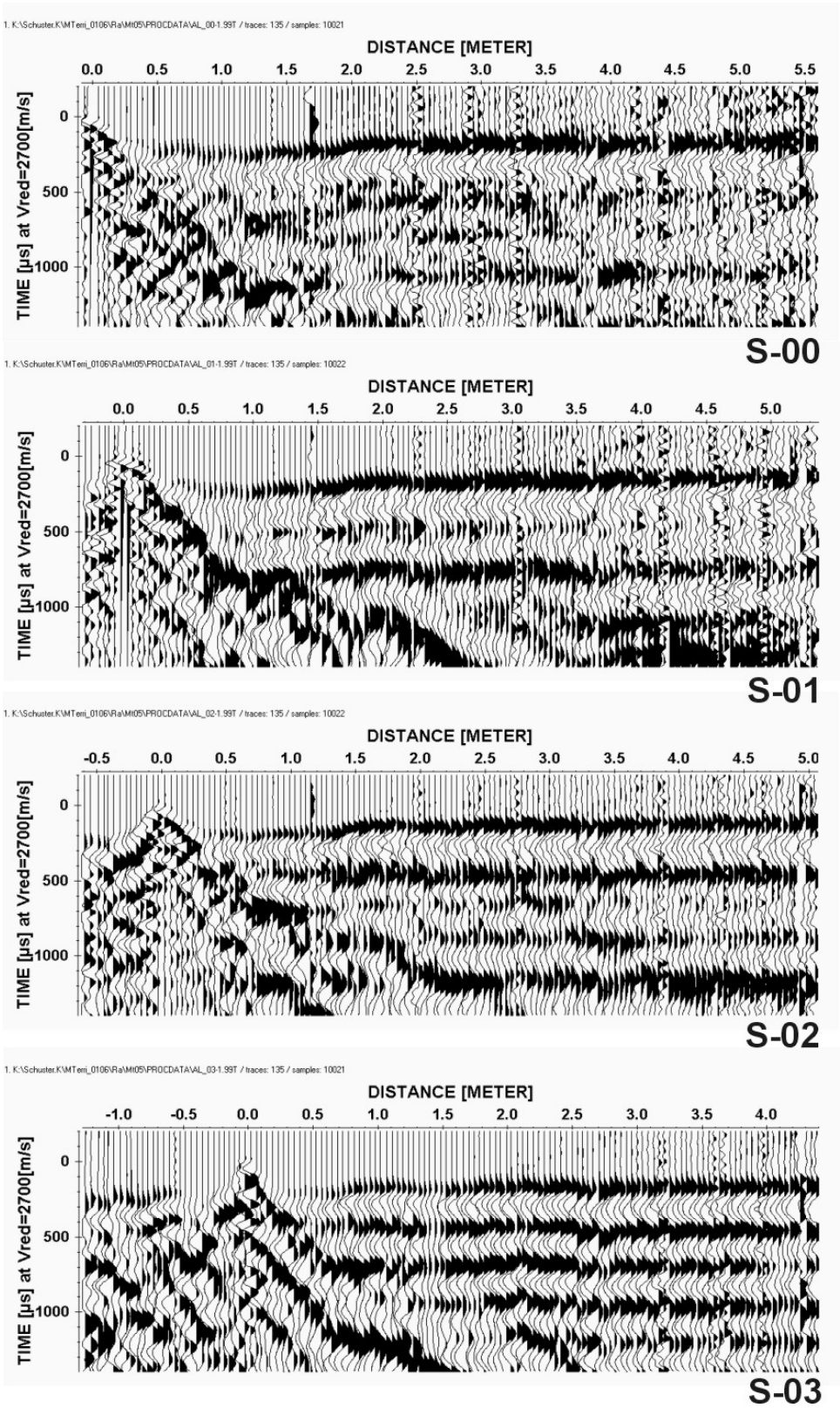

Fig. 3.4-4: Compilation of seismic shotpoint sections with reduced travel times for shotpoints S-00 - S03 in a time window between -200 µs - 1400 µs (profile Mt05). Travel times are reduced distance dependent with a velocity of 2700 m/s. P-wave first arrivals appear at about 100 µs. Data are filtered for this display (Bandpass, Butterworth 0.3 kHz - 16 kHz).

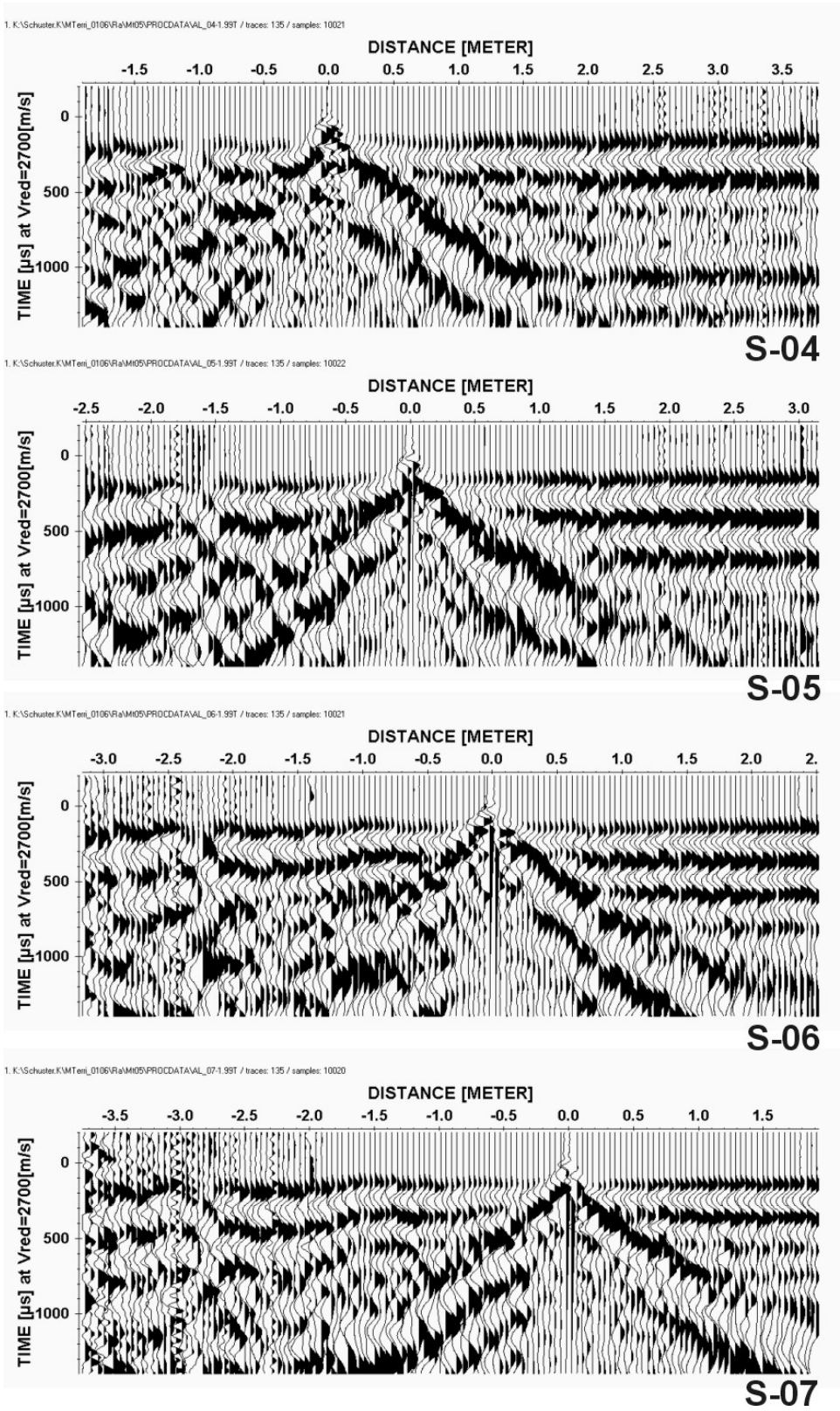

Fig. 3.4-5: Compilation of seismic shotpoint sections with reduced travel times for shotpoints S-04 - S07 in a time window between -200 µs - 1400 µs (profile Mt05). Travel times are reduced distance dependent with a velocity of 2700 m/s. P-wave first arrivals appear at about 100 µs. Data are filtered for this display (Bandpass, Butterworth 0.3 kHz - 16 kHz).

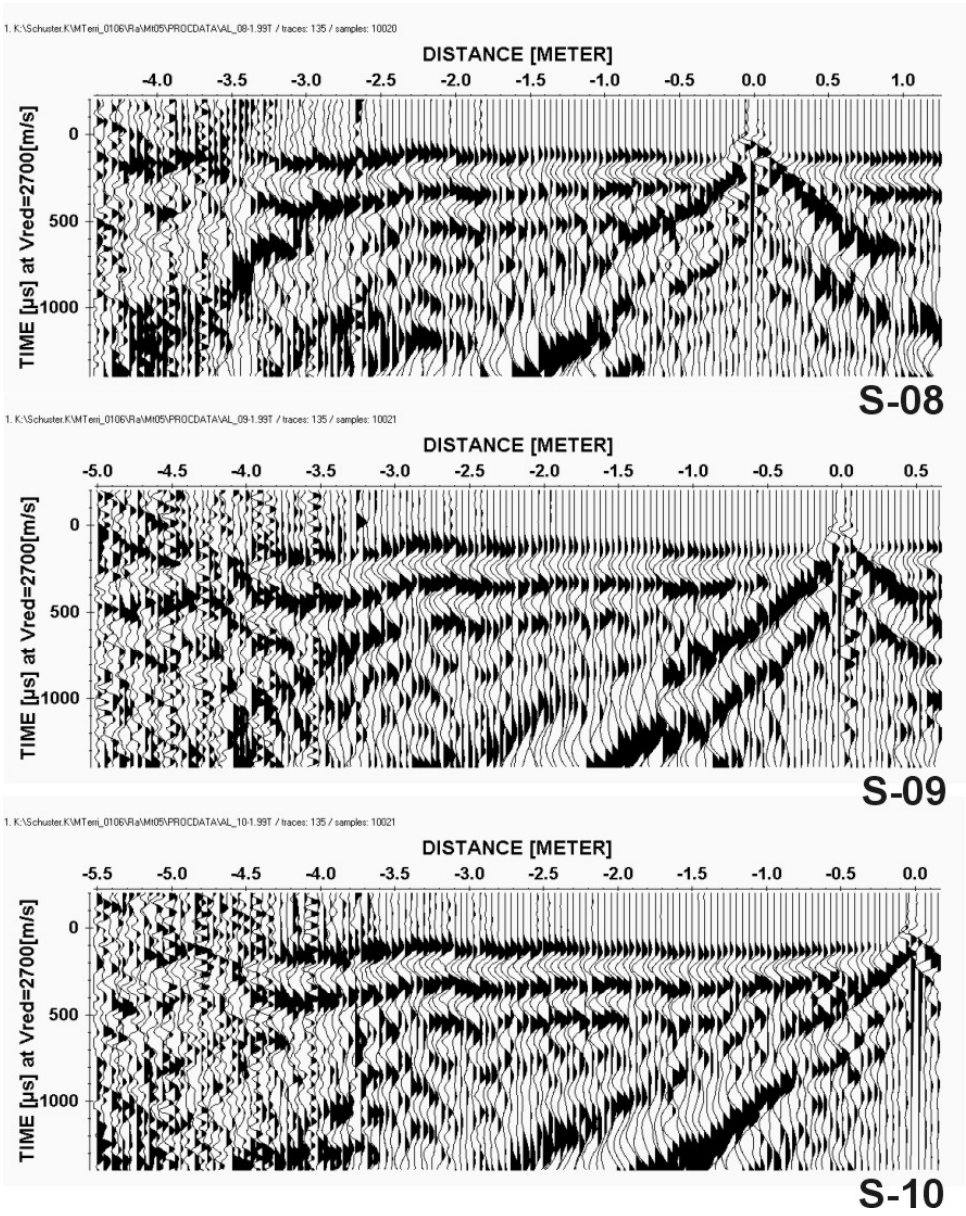

Fig. 3.4-6: Compilation of seismic shotpoint sections with reduced travel times for shotpoints S-08 - S10 in a time window between -200 µs - 1400 µs (profile Mt05). Travel times are reduced distance dependent with a velocity of 2700 m/s. P-wave first arrivals appear at about 100 µs. Data are filtered for this display (Bandpass, Butterworth 0.3 kHz - 16 kHz).

3.4.2.3 Travel time curves

First arrival times were picked manually because a high accuracy is required. Times were picked in the filtered (mean filter) data sets. In some cases also the raw data were taken into account. A compilation of all picked first arrival times is presented in Fig. 3.4-7. The most striking feature is that they are relative similar in the general trend. Of course many small scale variations along the curves can be recognised. They originate from the topography of the surface and from the existence of structural features of the rock (joints, faults, fractures).

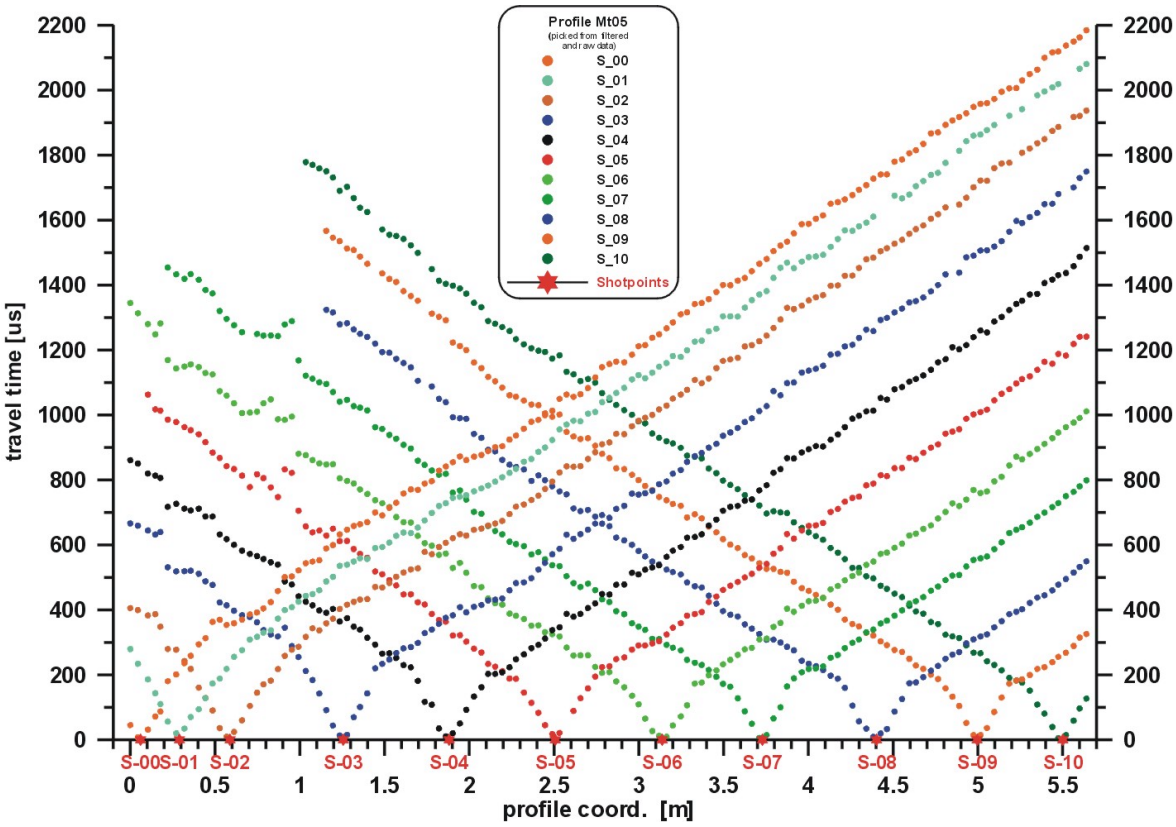

Fig. 3.4-7: First arrival travel time curves from all shotpoints along seismic refraction profile Mt05. Travel times were picked from first arrival phases (P-waves).

In all curves two slopes can be identified. A first one in the time window between 0 and 350 μs (at 0.5 m) and 200 μs at the end of the profile. The slopes correspond to apparent velocities between 900 m/s and 1400 m/s. For times greater than 350 μs and 200 μs the majority of the data points describe slopes which corresponds to apparent velocities between 2200 m/s and 3000 m/s. The similarities as well as the small scale differences between the travel time curves can be seen by

plotting all travel time data over the distance from the shotpoints in one graph, as in Fig. 3.4-8. For both slopes a graph is superimposed which represents an average apparent P-wave velocity of the first layer (EDZ, 1250 m/s) and for the intact rock (2700 m/s).

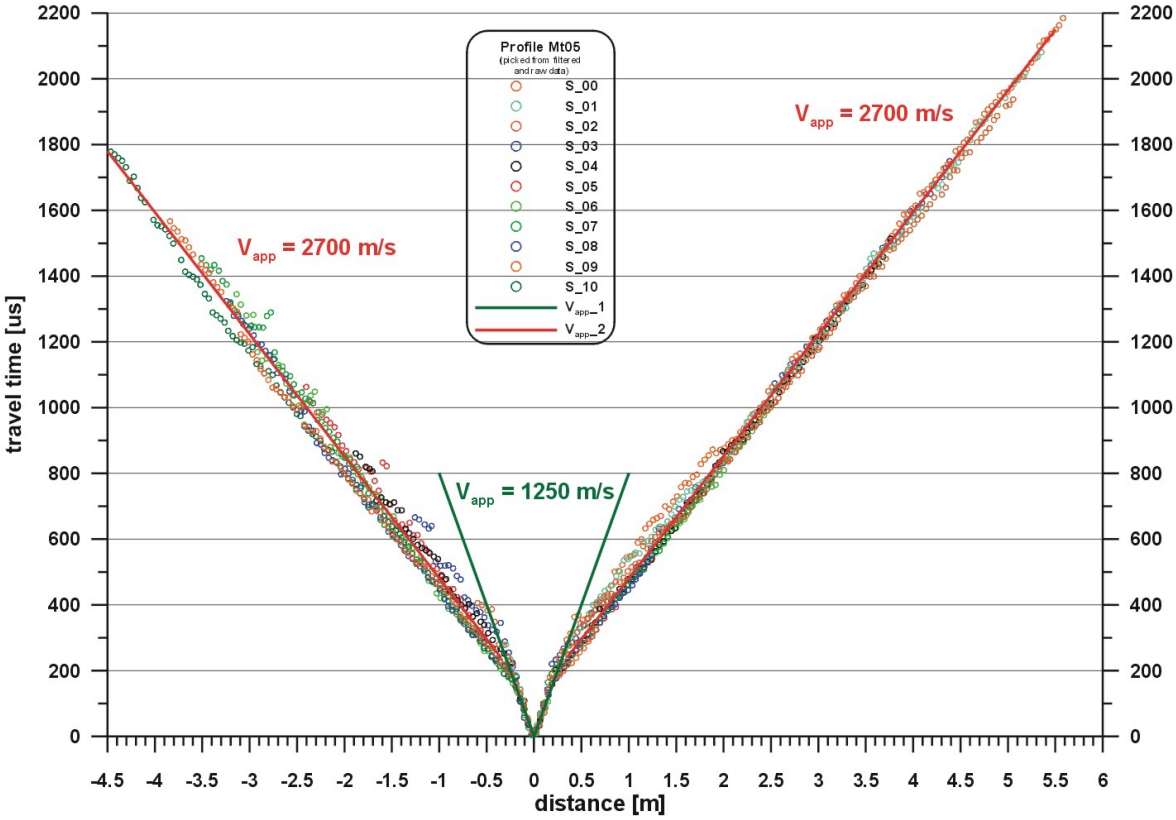

Fig. 3.4-8: Superimposition of travel time curves from all shotpoints along seismic refraction profile Mt05. For comparison apparent velocity graphs are plotted (Vapp = 1250 m/s for the first layer [EDZ] and Vapp = 2700 m/s for the undamaged rock).

3.4.2.4 Travel time analyses and 1 dimensional models

For each shotpoint an individual travel time analysis was done. With the help of linear regressions apparent velocities and intercept times (intersection of linear regression curve with the time axis) were determined. As an example the data for shotpoint S05 are shown in Fig. 3.4-9. The apparent velocities for the first layer are nearly the same (1250 m/s and 1230 m/s). Greater differences are found for the second travel time branch which is related to the interface between the first layer (EDZ) and the intact rock. The apparent velocities are 2520 m/s and 2740 m/s.

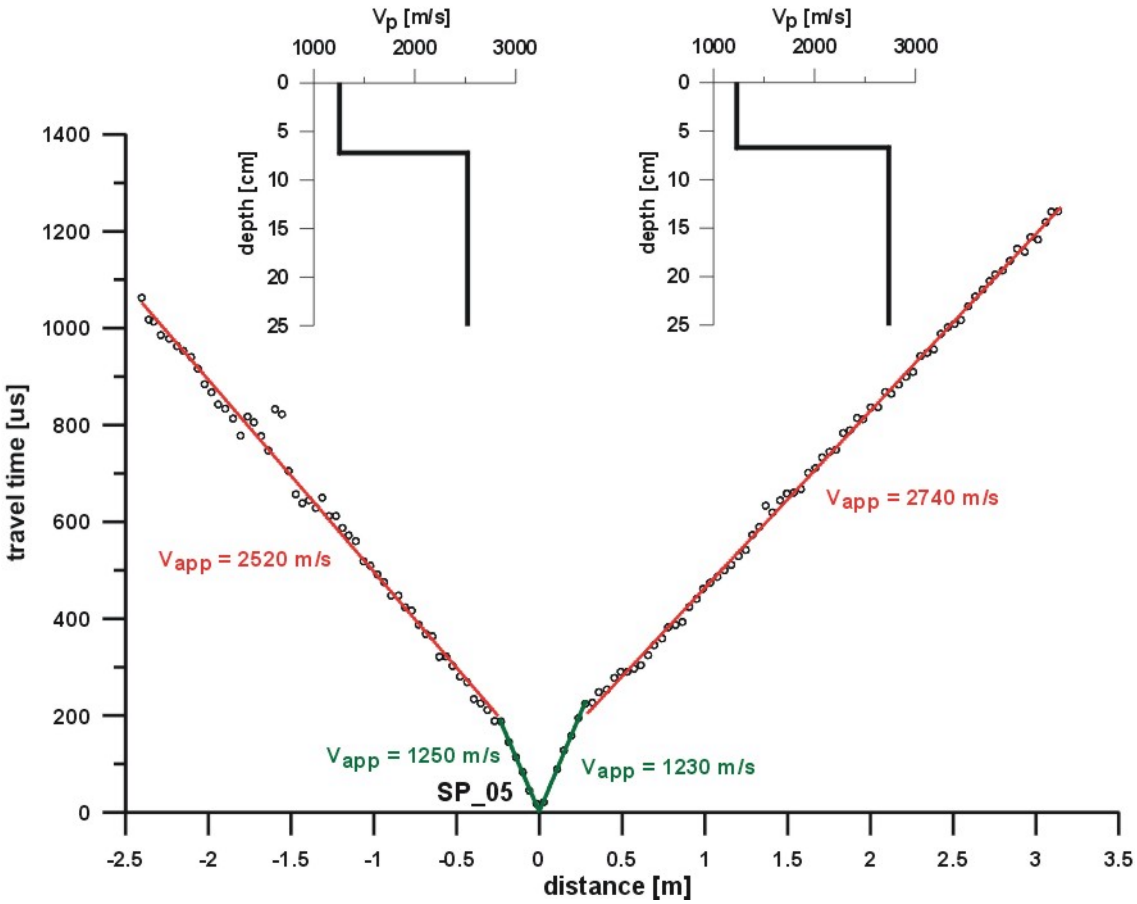

Fig. 3.4-9: Derived apparent velocities from travel time curves from shotpoint S-05 (profile Mt05). For both travel time branches a 1 dimensional model (top left and right) was calculated with the help of the Intercept time method.

The apparent velocities as well as the intercept times are used for a simple travel time inversion. The intercept time method (Ewing et al.1939) was used in order to obtain 1-dimensional models at each shotpoint. For both directions of the travel time curve of shotpoint S05 the results are plotted additionally in Fig. 3.4-9 (top). On the left hand side a velocity of 2520 m/s is reached at a depth of 7.2 cm whereas a velocity of 2740 m/s is reached already at 6.7 cm on the right hand side of shotpoint S05. The difference in depth is very little. But the difference in velocity are remarkable. This type of model is only a rough approach of the reality, because already these data show that it is a 2-dimensional structure.

3.4.2.5 2 dimensional start model and forward modelling

In the following step all 1-dimensional models are combined to a 2-dimensional model. This model serves as an start model for an iterative process which can be described briefly as follows:

- forward modelling,
- comparison between calculated and measured travel times,
- change of model parameters (depth of interfaces and / or velocities) according to the travel time residues,
- new forward modelling.

This process is done as long as the calculated travel times fit the measured travel time data within a range specified by the user.

For the creation of the 2-dimensional start model the topography (undulation of the surface) of the wall was taken into account. The exact knowledge of this topography is very important because of the small extend of the EDZ (first layer in the model) an uncertainty in the topography would falsify the derived model considerable. For the modelling (forward computations) two algorithms were used. Both are implemented in the seismic software tool REFLEXW. The first one is a net work ray tracing (Moser 1991, Dijkstra 1959) tool. The second one is a Finite Difference calculation after Vidale (1988). In Fig. 3.4-10 the ray paths which were used during the calculation are shown.

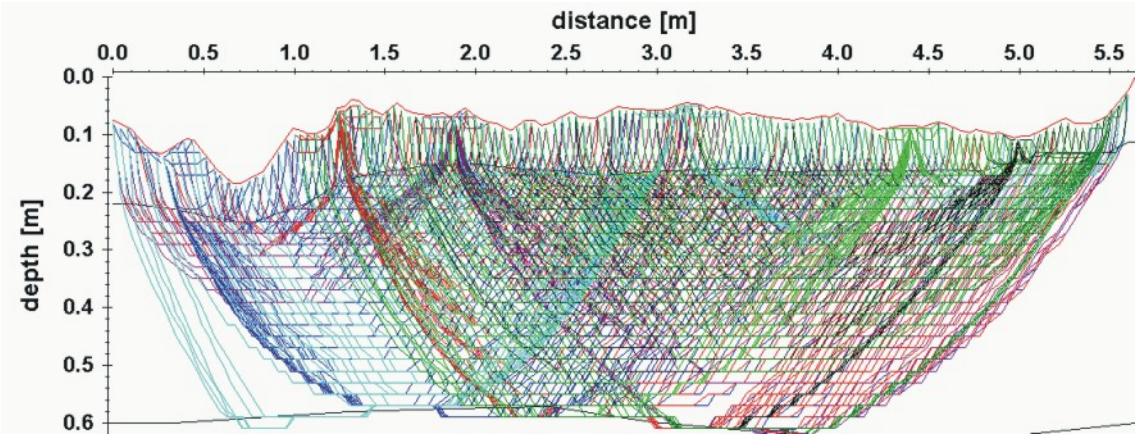

Fig. 3.4-10: Ray paths used in the 2 dimensional FD forward modelling for the determination of the final model (best fit).

Except the boarder areas on the left and right hand side the model is sufficient covered with rays. In order to fit the calculated to the measured data velocity gradients had to be introduced in the model for each layer (2000 s^{-1} for the EDZ and 500 - 1300 s^{-1} for the intact rock). Such steep P-wave velocity gradients were also observed in the results derived from interval velocity measurements in boreholes BEB-B09 and BEB-B19.

3.4.2.6 Final model

The final model can be seen in Fig. 3.4-11. Very pronounced is the topography. A thin layer with laterally varying P-wave velocities corresponds to the EDZ. P-wave velocities vary between 900 m/s and 1400 m/s. These velocities lie clear beneath the velocities one expect for the undamaged Opalinus Clay. Towards the end of the profile, what is also the end of the EB niche, the thickness of this layer become slightly thinner. A very sharp interface marks the transition to the intact rock. Velocities vary laterally between 2300 m/s and 3000 m/s. Areas marked with question marks are not covered with rays during the forward computation and should consequently not be taken into account.

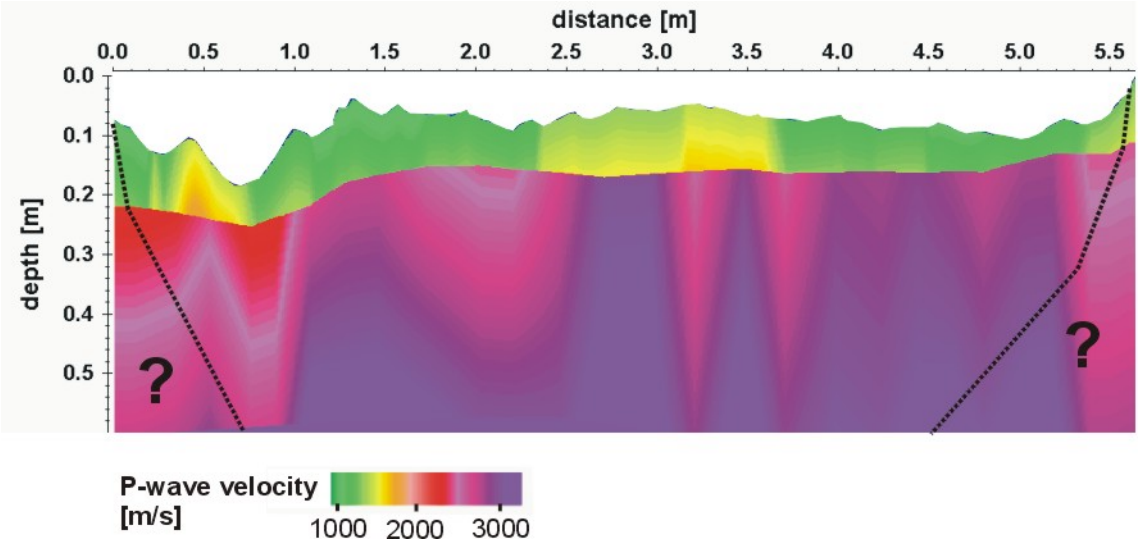

Fig. 3.4-11: Final model, derived from seismic refraction measurements along the NE sidewall in the EB niche (Profile Mt05). Areas with question marks are not covered by rays during the forward modelling. The thin layer with velocities between 900m/s and 1400m/s is the EDZ.

3.4.2.7 Fit of travel time data

Fig. 3.4-12a shows for shotpoint S05 the measured and the calculated travel times which result from the final model. The data fit can be regarded as very good except some points which deviate very clear. The total time difference for this example is 40.7 μs.

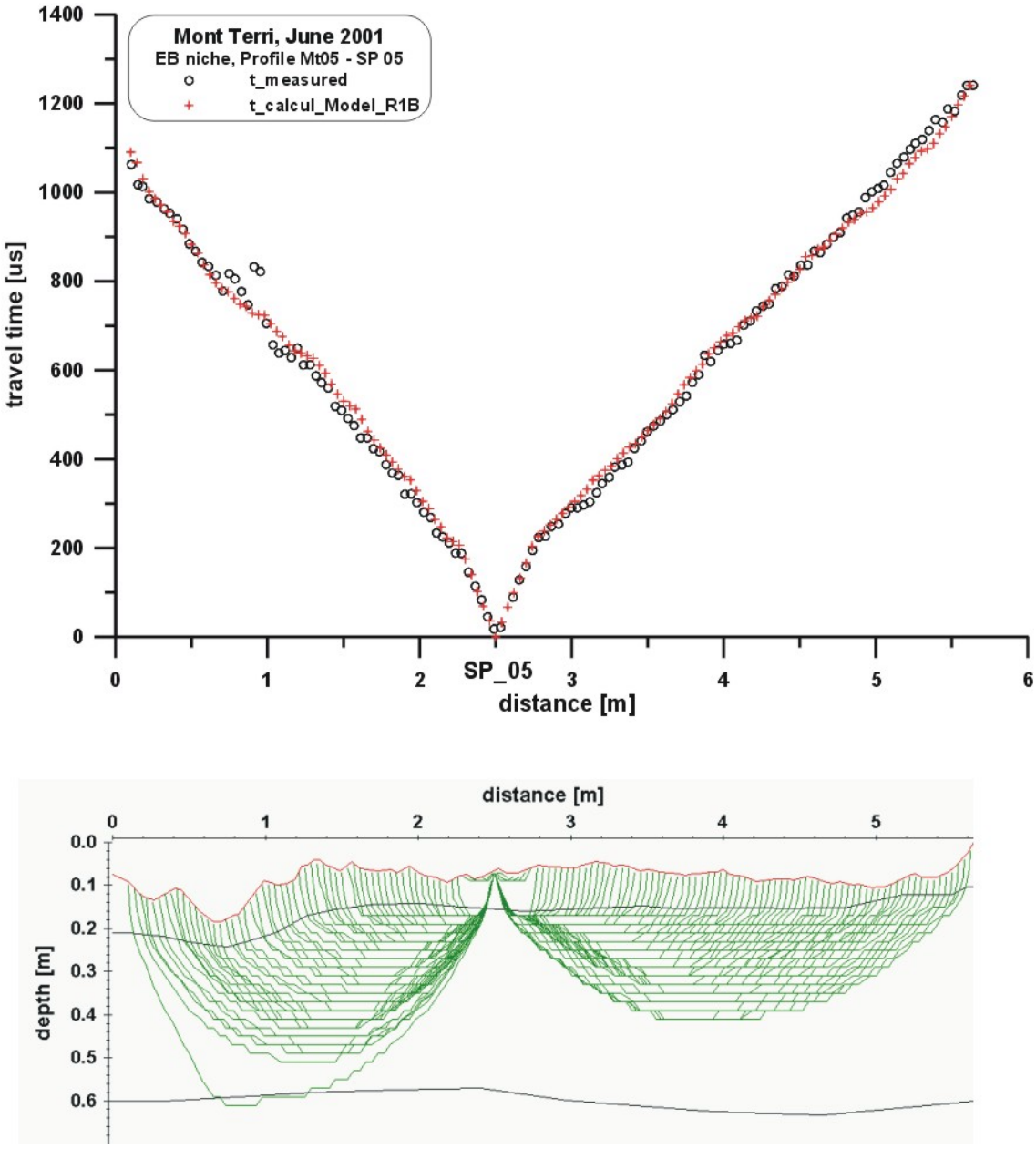

Fig. 3.4-12: Results from FD forward modelling. Top (a): Fit between calculated and measured travel times for SP_05. Bellow (b): Corresponding ray paths.

Deviations are visible for example around 1 m. This is a region where fault planes and open fractures were observed (Nussbaum et al. 2002) and the topography of the profile undulates very strong. The topography was considered for the modelling but up to now the structural elements have not been taken into consideration in the model. This will be done in a future step. Fig. 3.4-12b shows the corresponding ray paths used during the FD forward calculation. The quality of the data fit for the travel time data of the other ten shotpoints is comparable to the data presented in Fig. 3.4-12a.

3.4.2.8 Correlation between structural elements and travel time data

As mentioned before a structural mapping of artificial fractures and tectonic features of the EB niche was performed by Nussbaum et al. (2002). As an example Fig. 3.4-13 shows a detail of the refraction profile. On the right side of the photograph two lines in light yellow indicate mapped bedding traces and / or artificial discontinuities.

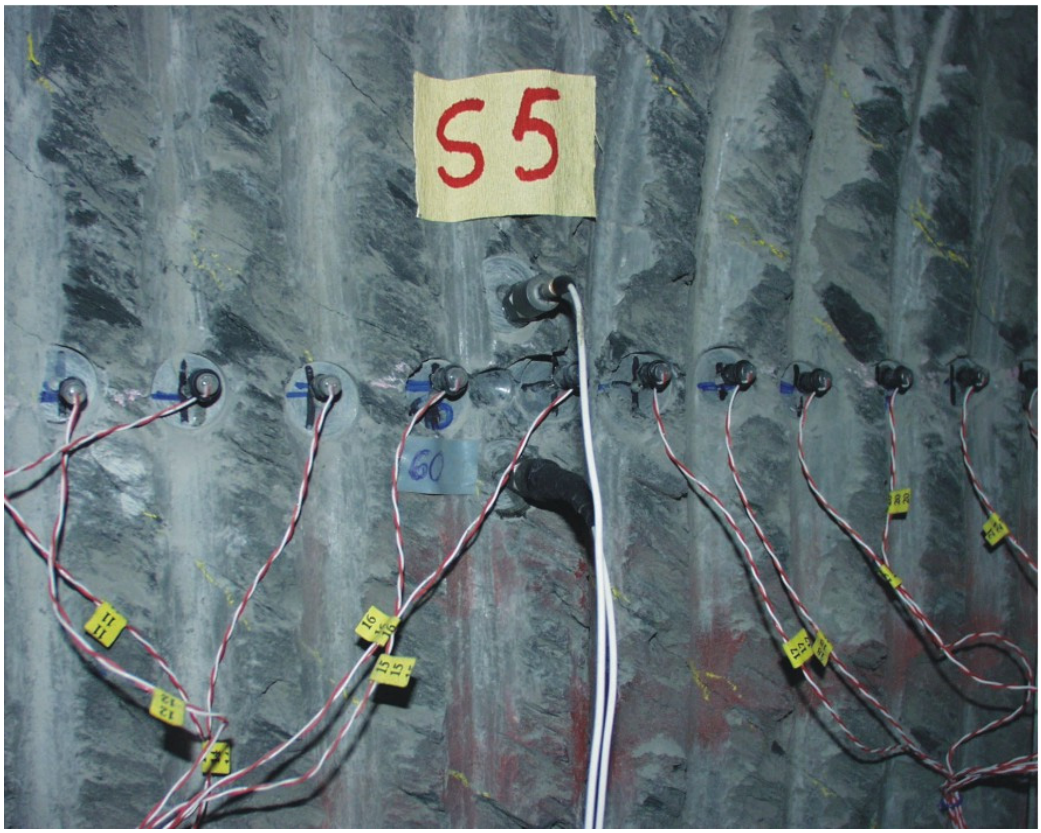

Fig. 3.4-13: Detail of seismic refraction Profile Mt05 around SP_05. In light yellow mapped bedding traces and artificial discontinuities are marked.

A part of the travel time curves from all shotpoints along profile Mt05 (only measured left from the shotpoints) are plotted in Fig. 3.4-14. Structural features were additionally plotted as crosses. They were taken from the structural mapping report (Nussbaum et al. 2002). No differentiation between different types of structural elements was done up to now. Some of the discontinuities in the travel time curves can be correlated with structural elements.

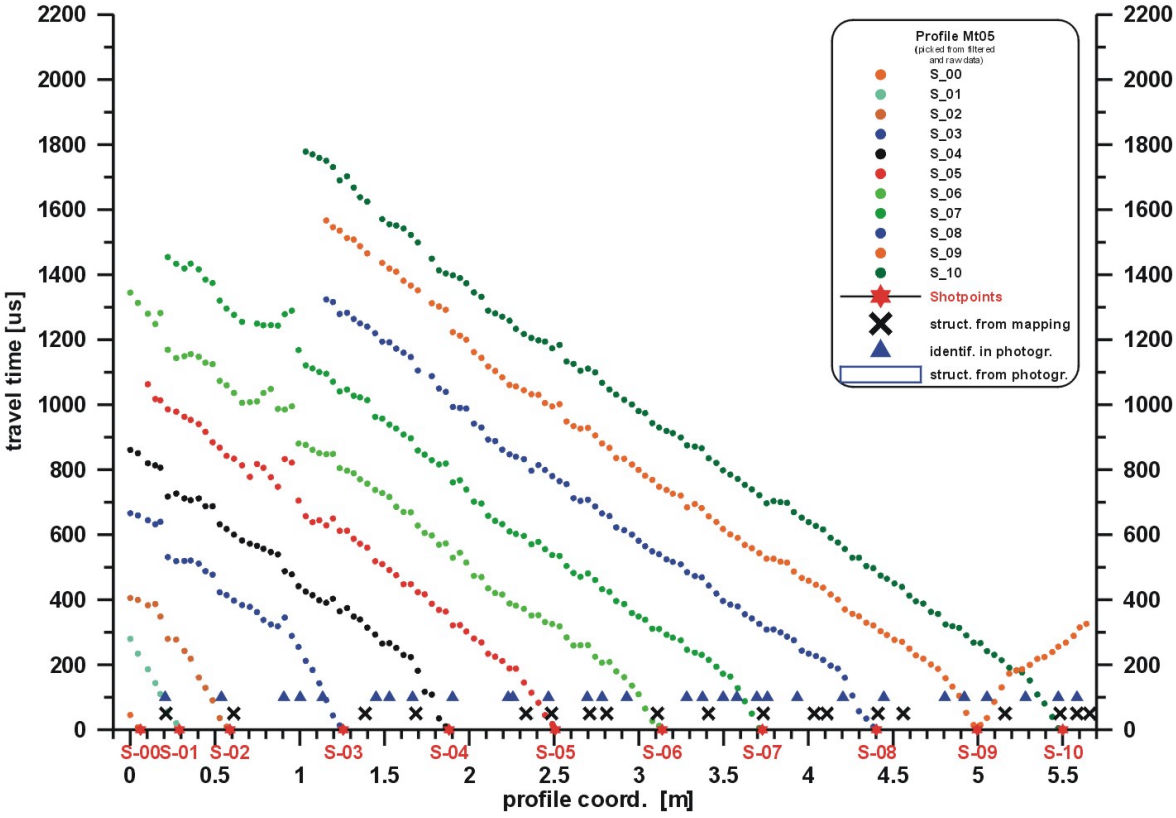

Fig. 3.4-14: Part of the travel time curves from all shotpoints along profile Mt05 (only measured left from the shotpoints). In addition the location of structural features are plotted as crosses, taken from structural mapping (Nussbaum et al. 2002) and as triangles, taken from own photographs. No differentiation between different types of structural elements was done up to now.

The locations of these structural elements on the refraction profile can contain some errors because the transfer from the map to the profile coordinates could not be done with the desired accuracy. We assume an uncertainty of about ± 10 cm. Therefore in addition all observations (structural elements) we found in our own photographs are plotted in the same figure. Again, no differentiation between the types of structural elements was done up to now. The assumed uncertainty in this

case should be better then ± 2 cm. It seems that some travel time discontinuities do not correspond to mapped structural elements. The question arises if there are not visible structural elements exist. This could be investigated in the future in more detail.

3.4.3 Results

The EDZ was resolved as an approx. 10 cm thick layer with laterally varying P-wave velocities between 900 m/s and 1400 m/s (see Fig. 3.4-11). A steep increase in P-wave velocities indicates undamaged rock for depth greater 10 cm. The velocities vary also laterally between 2300 m/s and 3000 m/s. Results are in good accordance with results from interval velocity measurements in two subhorizontal boreholes approx. 15 cm above the profile. Travel time discontinuities which correlate with mapped structural elements indicate the existence of fractures and / or joints.

Furthermore results are in good accordance with results from geoelectric measurements performed at the same location (Kruschwitz 2002).

3.4.4 Uncertainties and Errors

A variety of possible errors can influence the final result. First of all the phase correlation has to be mentioned in conjunction with the travel time picking of first arrival phases. Both influences the determination of a start model. But in the end the quality of the final model depends on the fit of the calculated data to the measured data.

Due to the knowledge of the P-wave velocity structure, derived from interval velocity measurements, this information was integrated into the start model. Without this information the parameters of the final model might be slightly different. But the differences would be of minor importance.

Several tests were done to determine the sensitivity of the deviation of calculated travel times from measured ones concerning small model changes. Three types of tests were performed. The model was modified each time in the following ways

(only one parameter, depth of interface, P-wave velocities or velocity gradients, was changed):

- The interface between the EDZ and the intact rock was shifted 4 cm towards a greater extent of the EDZ.
- The P-wave velocity for the intact rock was held constant (2200 m/s, 2500 m/s and 2800 m/s).
- The velocity gradient was held constant (10 s^{-1}, 1000 s^{-1}, 2000 s^{-1} , 3000 s^{-1}).

With this modified parameters it was found that the deviations of the calculated travel times form the measured ones are significant. They also deviate very clear from the travel times belonging to the best fit model (final model, see Fig. 3.4-11).
For areas where bedding traces, joints, faults and fractures exist the derived P-wave velocities are average velocities. A low velocity area includes most probably one or more of these structural elements (integrating effect).

3.4.5 Transmission Test

In order to test which distance can be penetrated with seismic waves generated by a hammer stroke a part of the installation of the seismic refraction profile Mt05 which was described previously was used. The piezoelectric transducers from subprofile C of the seismic refraction profile on the NE wall of the EB niche were used as a receiver array. This part of the profile covers the deepest part of the EB niche. A hammer stroke (0.5 k g) was used as a seismic source in the New Gallery in the window at profile coordinate NG 116 m. Fig. 3.4-15 (top) shows schematically the test arrangement. The distance between the window in the New Gallery and the end of subprofile C (5.64 m) was estimated roughly to 18 m (pers. com. Heinz Steiger).
In the middle part of Fig. 3.4-15 a processed data set is plotted. The quality of the data is very good. P-wave phases can be identified on all 45 receivers. For a homogeneous medium one would expect a straight line for the travel time curve as indicated in the lower graph in Fig. 3.4-15. The deviations of individual travel time values from this line are caused to a less degree by the topography along the receiver array and the uncertainty of the first arrival picks but mainly by the tectonic situation. The waves have to cross many structural elements like fault planes,

fractures and bedding planes under different angles. So the test gave proof of the feasibility of seismic investigations in a bigger scale and under difficult geological situations.

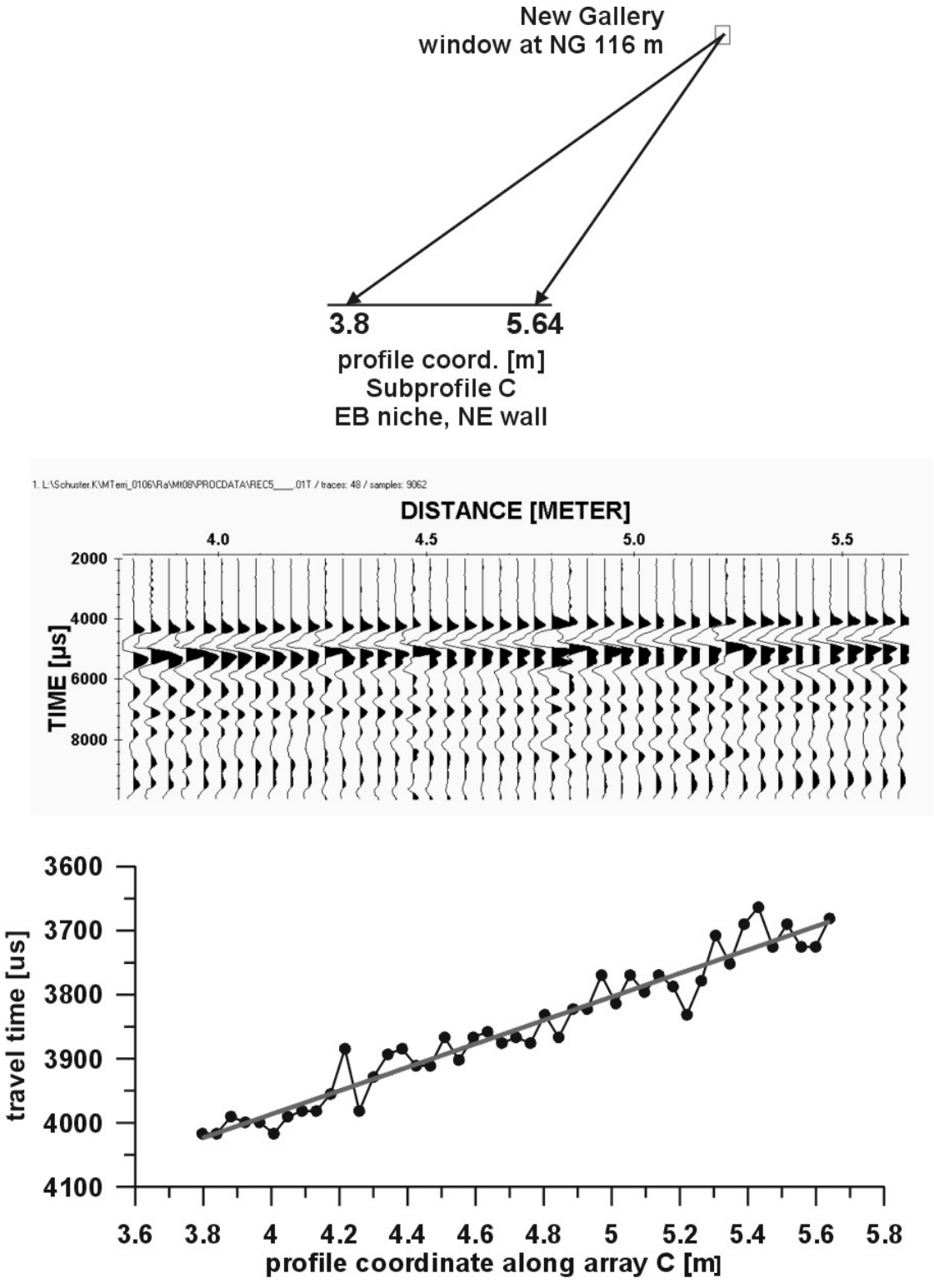

Fig. 3.4-15: "Long range" transmission test performed between the New Gallery (hammer stroke at window at NG 116 m as seismic source) and receivers in the EB niche. Distance is approx. 18 m .

4 Conclusions

For the characterisation of the excavation damaged zone (EDZ) **different seismic borehole methods** as well as the **seismic refraction method**, as non-destructive investigation method, were applied very successfully at several international rock laboratories. The EDZ can be characterised with the help of seismic parameters as for instance seismic P- and S-wave velocities, amplitude damping and the characteristics of seismogram sections. Knowledge of bulk density enables the calculation of additional elastic parameters like Poisson's ratio, Young's modulus and modulus of rigidity.

The following **seismic borehole methods** were applied: seismic interval velocity, cross hole and tomographic measurements. A mini-sonic borehole probe was used for the measurements. The minimum diameter of the boreholes can be 80 mm. All applied borehole methods are robust tools. They yield reliable data, as could be proved by repetition measurements, and they can be applied routinely, also under harsh conditions. With the help of these methods the EDZ was characterised very successfully in different potential host rock formations: Opalinus Clay, Boom Clay, granite and rock salt. The derived extents of the EDZ vary between approx. 0.1 m (Granite and Opalinus Clay) and 2.8 m (Boom Clay). Furthermore faults and joints were detected successfully with interval velocity methods. Seismic anisotropy was revealed through the application of cross hole measurements between two boreholes. The elastic parameters Poisson's ratio, Young's modulus and modulus of rigidity correlate well with derived velocity gradients perpendicular to the borehole wall. Repetition of measurements offers the opportunity to obtain hints for changes in local stress distributions around an underground opening. The observed changes in the derived P-wave velocities after four months gave such indications of changes in the local stress distribution. Comparison between results from seismic borehole measurements and results from other geophysical investigations at the same locations are in very good accordance.

The **non-destructive seismic refraction method** was modified and applied with success for the determination and characterisation of the EDZ. A 48 channel high

resolution recording system is now available which was tested successfully under harsh in situ conditions (salt rock and Opalinus Clay).

Because the EDZ is characterised by reduced velocities, which in general are connected with positive velocity gradients, the refraction method yields a very good image of the velocity distribution along a profile. The depth range covered by the measurements includes the transition zone between the EDZ and the undamaged rock. Low velocity zones beyond the undamaged rock can hardly be resolved. The maximum extent of the EDZ which can be determined, depends mainly on the degree of damage (attenuation of amplitudes), the velocity gradients in the EDZ, and the profile length which can be used along the wall.

Structural elements along the profile as for instance fractures and joints can be detected. The quality of resolution depends on their strike direction and their width. As wider a fracture and as greater angles between the strike direction of fractures and the profile orientation as better they can be resolved.

The EDZ can be scanned over a larger lateral distance range without any influence on the rock masses. But a prerequisite for the application is the direct access to the wall of the drift or cavity. The existence of a shotcreate layer is an almost insuperable obstacle.

Seismic anisotropy of rock masses is difficult to record from walls of underground openings. But it is not impossible. A possible solution is to make use of triaxial instead of uniaxial receivers and use the S-waves for further analyses.

The results achieved with the refraction seismic method in Opalinus Clay at the Mont Terri Rock Laboratory are in very good accordance with results from seismic borehole measurements, geological mapping of fractures and joints as well as geoelectrical measurements. Along a 5.6 m long horizontal profile the extent of the EDZ varies between 0.05 m and 0.15 m, and P-wave velocities vary between 900 m/s and 1400 m/s. P-wave velocities for the undamaged Opalinus Clay along the profile lie in the range between 2300 m/s and 3000 m/s.

For the determination and characterisation of the EDZ several **in situ seismic methods** proved to be reliable and robust tools. However, the appropriate selection of one of these introduced methods is dependent on scientific or geotechnical questions and of course site dependent. On the other hand labour force, expenses

and advantages have to be taken into account as well. The **combined application** of seismic borehole and refraction methods yield very high resolution data.
A further improvement can be achieved by applying supplementary geoelectrical measurements. Derived parameters from both methods complement one another for optimum results. With a combined application of seismic and geoelectric measurements at the Mont Terri Rock Laboratory very good results were achieved (Alheid et al. 2002).

BUNDESANSTALT FÜR GEOWISSENSCHAFTEN UND ROHSTOFFE
HANNOVER

In Charge

(Dr. H. Raschka)
- Dir. u. Prof. -
Abteilungsleiter B2

(Dr. M. Wallner)
- Dir. u. Prof. -
Projektleiter Endlagerung

(Dr. H.-J. Alheid)
- Wiss. Oberrat -
Arbeitspaketleiter

Author

(Dr. K. Schuster)
- Wiss. Angestellter -

5 References

Alheid, H.-J., Knecht, M. (1996): Distribution of Seismic Wave Velocities Around Underground Drifts. Proceedings of the Excavation Disturbed Zone Workshop, Ed. Martino, J.B., Martin, C.D., Canadian Nuclear Society, 47-56.

Alheid, H.-J., Kruschwitz, S., Schuster, K. and Yaramanci, U. (2002): Charakterisierung der Auflockerungszone um Strecken im Opalinuston mit seismischen und geoelektrischen Verfahren, Z. Angew. Geol., **2**, 48-55.

Bernier, F., M. Buyenes, D. Brosemer and D. De Bruyn, (2000): Extension of an Underground Laboratory in a Deep Clay Formation. GeoEng2000 - An International Conference on Geotechnical & Geological Engineering, Melbourne, 19-24 Nov. 2000, Volume 2.

Bock, H. (2001): RA Experiment. Rock Mechanics Analyses and Synthesis: Data Report on Rock Mechanics. Mont Terri Technical Report (TR 2000-02).

Dijkstra, E. W. (1959): A note on two problems in connexion with graphs, Numer. Math. **1**: 269-271.

Emsley S., Olsson O., Stenberg L., Alheid H.-J., Falls S. (1997): ZEDEX - A study of excavation disturbance for blasted and bored tunnels, Technical Report 97-30, SKB, Stockholm

Ewing, M., Wollard, G. P. and Vine, A. C. (1939): Geophysical investigations in the emerged and submerged Atlantic Coastal Plain, Part 3, Barnegat Bay, New Jersey section: GSA Bull. **50**: 257 – 296.

Fairhurst, C., Damjanac, B. (1996): The Excavation Damage Zone - An International Perspective. Proceedings of the Excavation Disturbed Zone Workshop, Ed. Martino, J.B., Martin, C.D., Canadian Nuclear Society, 3-14.

Kertz, W. (1969): Einführung in die Geophysik I, Bibliographisches Institut Mannheim, Bd. 275.

Kruschwitz, S. (2002): Detection and characterisation of the disturbed rock zone in claystone with complex valued geoelectrics. Diploma Thesis, Technical University of Berlin, Germany.

Liedtke, L., Engelhardt, I., Fiene, M., Kröhn, K.-P., Jakobs, H., Thorenz, C., (2001): Two-Phase Flow in Fractured Crystalline Rock.- Investigations in Niche 2175- SKB International Cooperation Report (2001).

Himmelsbach, Th., Shao, H, Schuster, K., Alheid, H.-J., Flach, D., Wieczorek, K. Liou, T.-S., Bartlakowski, J. & Krekeler, T. (2002): R + D - Nuclear Waste Disposal - Part I: Effective Field Parameters (EFP). – 124 p., in preparation. BGR Hannover, Germany.

Moser, T. J. (1991): Shortest path calculation of seismic rays, Geophysics **56**: 59-67.

Nussbaum, Ch., Inderbitzin, L., Steiger, H. and Bossart, P. (in preparation): Phase 7, Drilling Campaign. Drilling and Field Mapping of Drillcores. Geotechnical Institute Ltd., Switzerland. Mont Terri unpublished Technical Note (TN 2002-10).

Nussbaum, C., Bossart, P., Mayoraz, J., Niederhauser, B., Steiger, H. and Zingg, A. (2002): Engineered Barrier Experiment. Structural mapping of artificial fractures and tectonic features of the EB niche. Mont Terri unpublished Technical Note (TN 2002-05).

Schuster, K. and Alheid, H.-J. (2000): Seismic Measurements in lined and unlined sections of a drift in the Asse Research Mine, Proc. 6th Meeting - Environmental and Engineering Geophysics, Sept. 3-7, 2000, Bochum, Germany

Schuster, K., H.-J. Alheid, P. Eichhorn and W. Stille (2000a): In-situ-seismics at the Underground Research Facility Mol / Belgium - Feasibility test. BGR-Report, Archive-No.: 0119959, Tagebuch-No.: 10578/00.

Schuster, K., H.-J. Alheid, D. Böddener, P. Eichhorn and T. Spies, D. Heidrich (2000b): ED-C Experiment. Seismic Investigations of the EDZ and Acoustic Emission Measurements in the New Gallery. Mont Terri unpublished Technical Note (TN 2000-61).

Schuster, K., Alheid, H.-J., Böddener, D. (2001a): Seismic investigation of the Excavation damaged zone in Opalinus Clay, Engng. Geol. 61: 189-197.

Schuster, K., H.-J. Alheid, P. Eichhorn and D. Böddener (2001b): In-situ-seismic in the new shaft at the Underground Research Facility Mol / Belgium, BGR-Report, Tagebuch-No.: 10953/01.

Schuster, K. and Alheid, H.-J. (2002): ED-C Experiment. Seismic Investigation of the EDZ in the EB niche. Mont Terri unpublished Technical Note (TN 2002-04).

Sheriff, R. E. and Geldart, L. P. (1982): Explosion Seismology, Cambridge University Press, Cambridge.

Thury, M. and Bossart, P. (1999): Mont Terri Rock Laboratory - Results of the Hydrogeological, Geochemical and Geotechnical Experiments in 1996 and 1997 -; Geol. Ber. Landeshydrol. u. -geol. **23**, 171 - 182, Bern.

Vidale, J. E. (1988): Finite-difference calculation of travel times, Bull. Seism. Soc. Am., **78 No. 6**: 2062-2076.

Wieczorek, K. (2001): Untersuchungen zur hydraulisch wirksamen Auflockerungszone um Endlagerbereiche im Salinar (ALOHA2), 3. Fachgespräch zum Thema "Stoßnahe Auflockerungszonen: Detektion, Quantifizierung und Modellierung ihrer mechanischen und hydraulischen Eigenschaften", 24.Okt. 2001 in Clausthal-Zellerfeld.

6 List of Publications

Schuster, K., Alheid, H.-J. and Böddener, D. (1999): ED-C Experiment. Seismic Borehole Measurements for the Investigation of the EDZ of the New Tunnel. Mont Terri unpublished Technical Note (TN 1999-62).

Schuster, K. and Alheid, H.-J. (2000): Seismic Measurements in lined and unlined sections of a drift in the Asse Research Mine, Proc. 6th Meeting - Environmental and Engineering Geophysics, Sept. 3-7, 2000, Bochum, Germany

Schuster, K., H.-J. Alheid, P. Eichhorn and W. Stille (2000): In-situ-seismics at the Underground Research Facility Mol / Belgium - Feasibility test. BGR-Report, Archive-No.: 0119959, Tagebuch-No.: 10578/00.

Schuster, K., H.-J. Alheid, D. Böddener, P. Eichhorn and T. Spies, D. Heidrich (2000): ED-C Experiment. Seismic Investigations of the EDZ and Acoustic Emission Measurements in the New Gallery. Mont Terri unpublished Technical Note (TN 2000-61).

Schuster, K., Alheid, H.-J., Böddener, D. (2001): Seismic investigation of the Excavation damaged zone in Opalinus Clay, Engng. Geol. 61: 189-197.

Schuster, K., H.-J. Alheid, P. Eichhorn and D. Böddener (2001): In-situ-seismic in the new shaft at the Underground Research Facility Mol / Belgium, BGR-Report, Tagebuch-No.: 10953/01

Schuster, K. and Alheid, H.-J. (2002): Mesures microsismiques en forages formation du Kimmeridgien, Rapport d'operation (RO) - ANDRA D RP 0BGR 02-001/A, 79 pages (unpublished).

Schuster, K. and Alheid, H.-J. (2002): ED-C Experiment. Seismic Investigation of the EDZ in the EB niche. Mont Terri unpublished Technical Note (TN 2002-04).

Alheid, H.-J. und Schuster, K. (2001): Seismische Messungen zur Bestimmung der ALZ, 3. Fachgespräch zum Thema "Stoßnahe Auflockerungszonen: Detektion, Quantifizierung und Modellierung ihrer mechanischen und hydraulischen Eigenschaften", 24.Okt. 2001 in Clausthal-Zellerfeld.

Alheid, H.-J., Kruschwitz, S., Schuster, K. and Yaramanci, U. (2002): Charakterisierung der Auflockerungszone um Strecken im Opalinuston mit seismischen und geoelektrischen Verfahren, Z. Angew. Geol., **2**, 48-55.

Himmelsbach, Th., Shao, H, Schuster, K., Alheid, H.-J., Flach, D., Wieczorek, K. Liou, T.-S., Bartlakowski, J. & Krekeler, T. (2002): R + D - Nuclear Waste Disposal - Part I: Effective Field Parameters (EFP). – 124 p., in preparation. BGR Hannover, Germany.

Homand, F., S. Pepa, H.-J. Alheid & K. Schuster (1999): Perméabilité et vitesse des ondes in situ dans la zone endommagée des argilites du Mont Terri. Poster zur Tagung: Journées Scientifiques de l'ANDRA, december 7-9, 1999.

Lüdeling, R., Alheid, H.-J. und Schuster, K. (1999): Erforschung von Auflockerungszonen mit Hilfe seismischer Methoden, Wissenschaftliche Berichte - FZKA-PTE Nr. 6, 4. Statusgespräch zu FuE-Vorhaben auf dem Gebiet der Entsorgung gefährlicher Abfälle in tiefen geologischen Formationen, 14. u. 15. Sept. 1999 in Clausthal-Zellerfeld, 63-78.

Lüdeling, R., Alheid, H.-J. und Schuster, K. (2001): Einsatz verschiedener seismischer Methoden zur Charakterisierung von Auflockerungszonen, Wissenschaftliche Berichte - FZKA-PTE Nr. 7, 5. Statusgespräch zu FuE-Vorhaben auf dem Gebiet der Entsorgung gefährlicher Abfälle in tiefen geologischen Formationen, 15. u. 16. Mai 2001 in Leipzig, 27-44.

7 List of Figures

features from drillcore mapping plotted in the Vp-graph (rectangle: sandy layer, arrow: artificial discontinuity, cross: slickenside).

Fig. 2.1-13: Borehole BEB-B09, June 2001: Seismic parameters derived from analyses of S-waves from interval velocity measurements.

Fig. 2.1-14: Borehole BEB-B09, June 2001: Seismic and elastic parameters derived from analyses of P- and S-waves from interval velocity measurements.

Fig. 2.1-15: Data sets from interval velocity measurements for all boreholes in plane 1 and plane 2 measured in June 2001 in the EB niche of the Mont Terri Rock Laboratory. Channel 2 data (source receiver distance = 20 cm). Bandpass filtered 5 - 100 kHz, point mode display, amplitudes colour coded, ensemble normalised.

Fig. 2.1-16: Data sets from interval velocity measurements for all boreholes in plane 1 and plane 2 measured in October 2001 in the EB niche of the Mont Terri Rock Laboratory. Channel 2 data (source receiver distance = 20 cm). Bandpass filtered 5 - 100 kHz, point mode display, amplitudes colour coded, ensemble normalised.

Fig. 2.1-17: Extent of the EDZ according to different criteria. Top (a): June 2001, Below (b): October 2001.

Fig. 2.1-18: Illustration of the extent of the EDZ for boreholes BEB-B09 - BEB-B11 (plane 1) and BEB-B19 - BEB-B21 (plane 2). Top (a): drilled and measured in June 2001, Below (b): drilled and measured in October 2001.

Fig. 2.1-19: Comparison of interval velocities derived from measurements in June 2001 (top) and October 2001 (below) in borehole BEB-B09.

Fig. 2.1-20: Comparison of interval velocities derived from measurements in June 2001 (top) and October 2001 (below) in borehole BEB-B11.

Fig. 2.1-21: Differences in P-wave interval velocities measured in June and October 2001 along plane 1. Differences are expressed in percentage deviation relative to the results from June 2001.

Fig. 2.1-22: Differences in P-wave interval velocities measured in June and October 2001 along plane 2. Differences are expressed in percentage deviation relative to the results from June 2001.

Fig. 2.1-23: Mean P-wave velocity gradient for boreholes BEB-B09 - BEB-B11 (plane 1) and BEB-B19 - BEB-B21 (plane 2). Top (a): drilled and measured in June 2001, Below (b): drilled and measured in October 2001.

Fig. 2.1-24: Compilation of elastic parameters derived from interval velocity measurements along plane 1 in June 2001.

Fig. 2.1-25: Comparison between "mean P-wave velocity gradients" and elastic parameters derived from interval velocity measurements along plane 1 in June 2001.

Fig. 2.1-26: Data example from cross hole measurements between boreholes BEB-B09 (source) and BEB-B19 (receiver) (top) and the reverse direction (below). Ensemble normalised display with colour coded amplitudes. For colour code see Fig. 2.1-7.

Fig. 2.1-27: Comparison of P-wave velocities derived from interval velovity measurements (IVVM) in boreholes BEB-B09 and BEB-B19 and from cross hole measurements (CRX) between both boreholes (measured in June 2001).

Fig. 2.1-28: Ray coverage from seismic tomography measurements between boreholes BEB-B09 and BEB-B19 (measured in June 2001).

Fig. 2.1-29: Data example from seismic tomography measurements between boreholes BEB-B09 and BEB-B19 (measured in June 2001). Source at z=0 in borehole BEB-B09, receivers moved between 0 and 1.7 m in borehole BEB-B19.

Fig. 2.1-30: Ray coverage (top) and derived P-wave velocities (below) from seismic tomography measurements between boreholes BEB-B09 and BEB-B19 (measured in June 2001). Examples are shown for sources in borehole BEB-B09 at z = 0, 0.4 m, 1 m and 1.5 m and all receiver positions in borehole BEB-B09 (R01 – R18). Velocities vary remarkable. They are influenced mainly by the anisotropy structure (e.g. bedding planes).

Fig. 2.1-31: Ray coverage (top) and derived P-wave velocities from seismic tomography measurements between boreholes BEB-B19 and BEB-B09 (measured in June 2001). Examples are shown for sources in borehole BEB-B19 at z = 0, 0.4 m, 1 m and 1.5 m and all receiver positions in borehole BEB-B19 (R01 – R18). Velocities vary remarkable. They are influenced mainly by the anisotropy structure (e.g. bedding planes).

Fig. 2.1-32: Derived P-wave velocities from seismic tomography measurements between boreholes BEB-B09 and BEB-B19 (measured in June 2001). Data from two source positions in borehole BEB-B09 and two in borehole BEB-B19 are plotted over the ray angle. The 0° - 180° direction is approx. in parallel with the axis of the EB niche. A strong anisotropy of velocity is visible. The connection between the relative orientation of ray paths and the ray angle can be taken from the four small sketches.

Fig. 2.1-33: As Fig. 2.1-32 but here all 576 rays used for the calculation. The main strike directions of the bedding is marked in light green, the perpendicular direction in light yellow. An ellipse which could be a fit (not calculated) of the data emphasises the seismic anisotropy. The main axis of the ellipse is slightly deviated against the bedding parallel direction.

Fig. 2.1-34: Histograms with the frequencies of occurrence of derived P-wave velocities (top), ray angle (middle) and the used ray lengths (straight lines)

(below). Data belong to the seismic tomography measurements between boreholes BEB-B09 and BEB-B19.

Fig. 2.1-35: Seismic tomography measurements between borehole BEB-B09 and BEB-B19. 2-dimensional P-wave velocity distribution as a result of a tomography inversion with an inadequate data set. For details see text.

Fig. 2.2-1: Sketch of test site in the new shaft, URF Mol, Belgium.

Fig. 2.2-2: Photograph of test site in the new shaft, URF Mol, Belgium.

Fig. 2.2-3: Seismic section from interval velocity measurements in borehole 2000/04, channel 1 data. a: wiggle mode, trace normalised, b: point mode, ensemble normalised.

Fig. 2.2-4: Seismic section from cross hole measurements between borehole 2000/04 and borehole 2000/05, channel 1 data. a: wiggle mode, trace normalised, b: point mode, ensemble normalised.

Fig. 2.2-5: Seismic parameters derived from analyses of P-waves, interval velocity measurements in borehole 2000/04.

Fig. 2.2-6: Seismic parameters derived from analyses of S- and P-waves, interval velocity measurements in borehole 2000/04.

Fig. 2.2-7: Parameters derived from analyses of P-waves, cross hole measurements between borehole 2000/04 and 2000/05. (e: orientation: top is 0°, then counted clockwise).

Fig. 2.2-8: Comparison of derived velocity distributions from interval velocity and cross hole measurements in and between boreholes 2000/04 and 2000/05. In addition a result from interval velocity measurements in the test drift from March 2000 is plotted (borehole 77-78-TD).

Fig. 2.2-9: Compilation of main results which describe the extent of the EDZ and the occurrence of anomalous regions. Different signatures are used.

Fig. 2.3-1: Seismic section along borehole KXP24BGR for channel 1 data set. Source-receiver distance: 10 cm, measurement interval: 10 cm, point mode display, ensemble normalised, amplitudes colour coded. For colour code see Fig. 2.1-7.

Fig. 2.3-2: Seismic parameters derived from analyses of interval velocity measurements in borehole KXP24BGR. Analyses of first arrival phases (P-waves) and S-wave onsets.
Top (a): P-wave-velocity, S-wave velocity and the ratio Vp/Vs is shown. Below (b): normalised amplitude.

Fig. 2.3-3: Compilation of detected fractures in borehole KXP24 derived from Borehole Imaging Processing System (BIPS) and seismic interval velocity measurements.

Fig. 2.3-4: Seismic section from a detailed investigation in borehole KXP25BGR. Source-receiver distance: 10 cm, measurement interval: 2 cm, real amplitudes. a: wiggle mode, b: point mode (colour code: violet/red: positive amplitudes, blue/green: negative amplitudes, amber: zero level).

Fig. 2.4-1: Borehole EFP98020 : P-wave (top) and S-wave interval velocities (below) derived from channel 3 data (source – receiver distance of 30 cm).

Fig. 2.4-2: Borehole EFP98019 : P-wave (top) and S-wave interval velocities (below) derived from channel 3 data (source – receiver distance of 30 cm).

Fig. 2.4-3: Borehole EFP98020 : Ensemble normalised representation of seismic data from interval velocity measurements. Amplitudes are colour coded. Disturbances in the wave field are related to fractures and / or joints.

Fig. 2.4-4: Borehole EFP98019 : Ensemble normalised representation of seismic data from interval velocity measurements. Amplitudes are colour coded. Disturbances in the wave field are related to fractures and / or joints.

Fig. 2.5-1: Asse Research Mine, 700 m level. Seismic interval velocity measurements inside the lining (Tübbing-Strecke).

Fig. 2.5-2: Asse Research Mine, 700 m level. Seismic interval velocity measurements in the unlined section.

Fig. 2.5-3: Seismic sections (0 - 2.1 m) for channel 2 data (distance source - receiver 20 cm) from interval velocity measurements in vertical boreholes at the Asse Research Mine (700 m level). Wiggle mode data (trace normalised) superimposed with colour coded amplitudes (ensemble normalised). Colour code: violet/red: positive amplitudes, blue/green: negative amplitudes, amber: zero level. Top (a): data from lined section. Below (b): data from unlined section. (st: steel, con: concrete).

Fig. 2.5-4: Comparison between results from seismic interval velocity measurements and measurements of permeability (Project ALOHA 2, GRS, Wieczorek 2001) at the Asse Research Mine (700 m level). Results from lined section: red colours (bars and graphs). Results from unlined section: blue colours (bars and graphs).
P-wave velocities: left ordinate, permeability: right ordinate. Depths are corrected to the beginning of rock salt. Permeability lies outside the seismically identified EDZ (>0.25 m in the lined section and >1.2 m outside) below 10^{-18} m^2.

Fig. 3.1-1: First results of a seismic refraction test measurement at the Rock Laboratory Grimsel. a: all received signals at receiver position RE-7 at 5.9 m, trace normalised display. b: first arrival travel time curves for all nine receiver positions.

Fig. 3.1-2: Result of a 1-dimensional inversion of travel time curves in the profile range 4 - 8 m. At eight locations the depth-P-wave velocity distribution (V_p = 3800 - 5500 m/s and z = 0 - 0.6 m) are plotted. Light yellow marks the depth range with P-wave velocities < 5000 m/s.

Fig. 3.2-1: Test measurements at the laboratory with the new 48 channel equipment. Rear view of the three digital storage oscilloscopes (without casing). 48 piezoelectric transducers are deployed on a salt block.

Fig. 3.3-1: Seismic refraction measurements at the Asse Research Mine (490 m level) with the new 48 channel equipment. The three digital storage oscilloscopes are protected by cases. Piezoelectric transducers are deployed along a horizontal profile at the sidewall.

Fig. 3.3-2: Data set from seismic refraction measurements at the Asse Research Mine (490 m level). Shot position x = 5.5 m. Left: 48 traces, trace normalised display, S-waves are dominant. Right: Enlargement of the left rectangle, P-waves as first arrivals are visible.

Fig. 3.4-1: Principle of high resolution seismic refraction measurements. 48 channels supported. S: Impact source, 1 - 45: receiver positions.

Fig. 3.4-2: Topography along the seismic refraction profile Mt05 in the EB niche (NE sidewall). Shotpoints marked with S-00 to S-10, some receiver points marked with their numbers.

Fig. 3.4-3: Data example from seismic refraction measurements along the NE sidewall in the EB niche for shotpoint S-02 (profile Mt05). All 135 traces are distributed nearly equidistantly (spacing of approx. 4.2 cm) over the 5.64 m long horizontal profile. Top (a): raw data, below (b): filtered data (DC-shift subtracted and mean filter applied). Both data sets are trace normalised.

Fig. 3.4-4: Compilation of seismic shotpoint sections with reduced travel times for shotpoints S-00 - S03 in a time window between -200 μs - 1400 μs (profile Mt05). Travel times are reduced distance dependent with a velocity of 2700 m/s. P-wave first arrivals appear at about 100 μs. Data are filtered for this display (Bandpass, Butterworth 0.3 kHz - 16 kHz).

Fig. 3.4-5: Compilation of seismic shotpoint sections with reduced travel times for shotpoints S-04 - S07 in a time window between -200 μs - 1400 μs (profile Mt05). Travel times are reduced distance dependent with a velocity of 2700 m/s. P-wave first arrivals appear at about 100 μs. Data are filtered for this display (Bandpass, Butterworth 0.3 kHz - 16 kHz).

Fig. 3.4-6: Compilation of seismic shotpoint sections with reduced travel times for shotpoints S-08 - S10 in a time window between -200 μs - 1400 μs (profile Mt05). Travel times are reduced distance dependent with a velocity of 2700 m/s. P-wave first arrivals appear at about 100 μs. Data are filtered for this display (Bandpass, Butterworth 0.3 kHz - 16 kHz).

Fig. 3.4-7: First arrival travel time curves from all shotpoints along seismic refraction profile Mt05. Travel times were picked from first arrival phases (P-waves).

Fig. 3.4-8: Superimposition of travel time curves from all shotpoints along seismic refraction profile Mt05. For comparison apparent velocity graphs are plotted (V_{app} = 1250 m/s for the first layer [EDZ] and V_{app} = 2700 m/s for the undamaged rock).

Fig. 3.4-9: Derived apparent velocities from travel time curves from shotpoint S-05 (profile Mt05). For both travel time branches a 1 dimensional model (top left and right) was calculated with the help of the Intercept time method.

Fig. 3.4-10: Ray paths used in the 2 dimensional FD forward modelling for the determination of the final model (best fit).

Fig. 3.4-11: Final model, derived from seismic refraction measurements along the NE sidewall in the EB niche (Profile Mt05). Areas with question marks are not covered by rays during the forward modelling. The thin layer with velocities between 900m/s and 1400m/s is the EDZ.

Fig. 3.4-12: Results from FD forward modelling. Top (a): Fit between calculated and measured travel times for SP_05. Bellow (b): Corresponding ray paths.

Fig. 3.4-13: Detail of seismic refraction Profile Mt05 around SP_05. In light yellow mapped bedding traces and artificial discontinuities are marked.

Fig. 3.4-14: Part of the travel time curves from all shotpoints along profile Mt05 (only measured left from the shotpoints). In addition the location of structural features are plotted as crosses, taken from structural mapping (Nussbaum et al. 2002) and as triangles, taken from own photographs. No differentiation between different types of structural elements was done up to now.

Fig. 3.4-15: Long range" transmission test performed between the New Gallery (hammer stroke at window at NG 116 m as seismic source) and receivers in the EB niche.

Figures in Appendix:

Fig. A-1: Borehole BEB-B11, June 2001: Seismic parameters derived from analyses of P-waves from interval velocity measurements. In addition structural features from drillcore mapping plotted in the Vp-graph (arrow: artificial discontinuity).

Fig. A-2: Borehole BEB-B11, June 2001: Seismic parameters derived from analyses of S-waves from interval velocity measurements.

Fig. A-3: Borehole BEB-B11, June 2001: Seismic and elastic parameters derived from analyses of P- and S-waves from interval velocity measurements.

8 List of Tables

9 Appendix

Figures A-1 to A12 are compiled on the following pages.

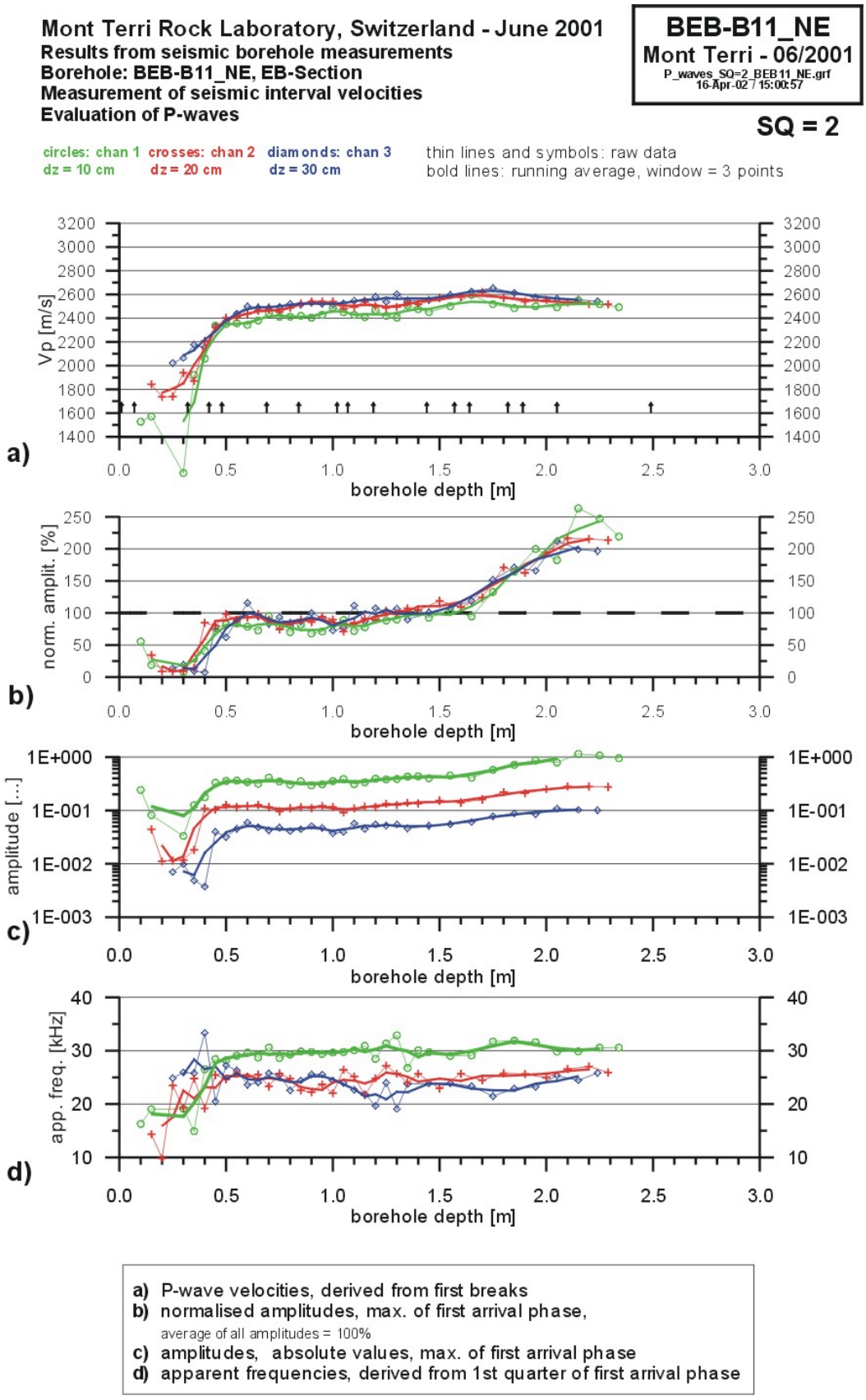

Fig. A-1: Borehole BEB-B11, June 2001: Seismic parameters derived from analyses of P-waves from interval velocity measurements. In addition structural features from drillcore mapping plotted in the Vp-graph (arrow: artificial discontinuity).

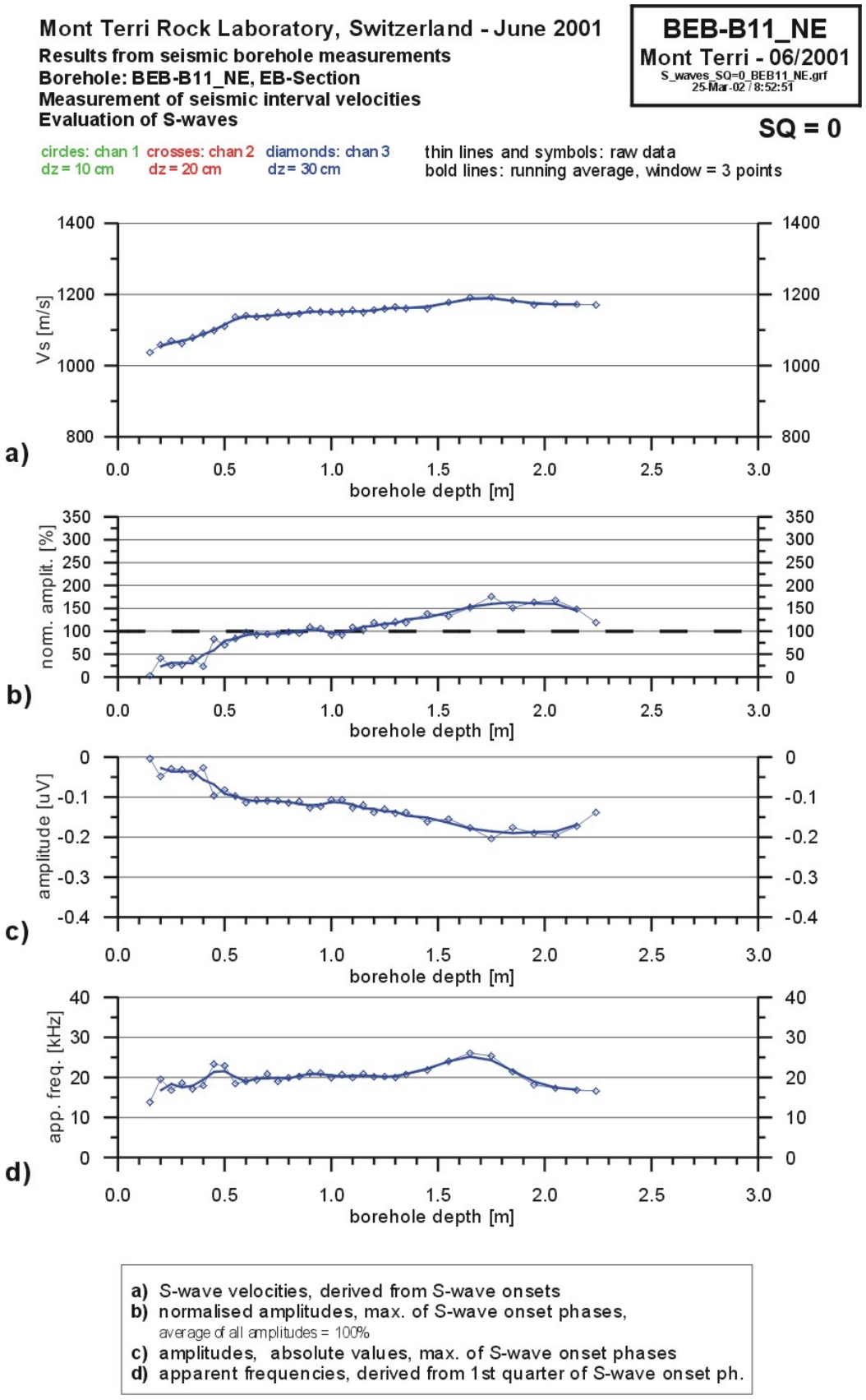

Fig. A-2: Borehole BEB-B11, June 2001: Seismic parameters derived from analyses of S-waves from interval velocity measurements.

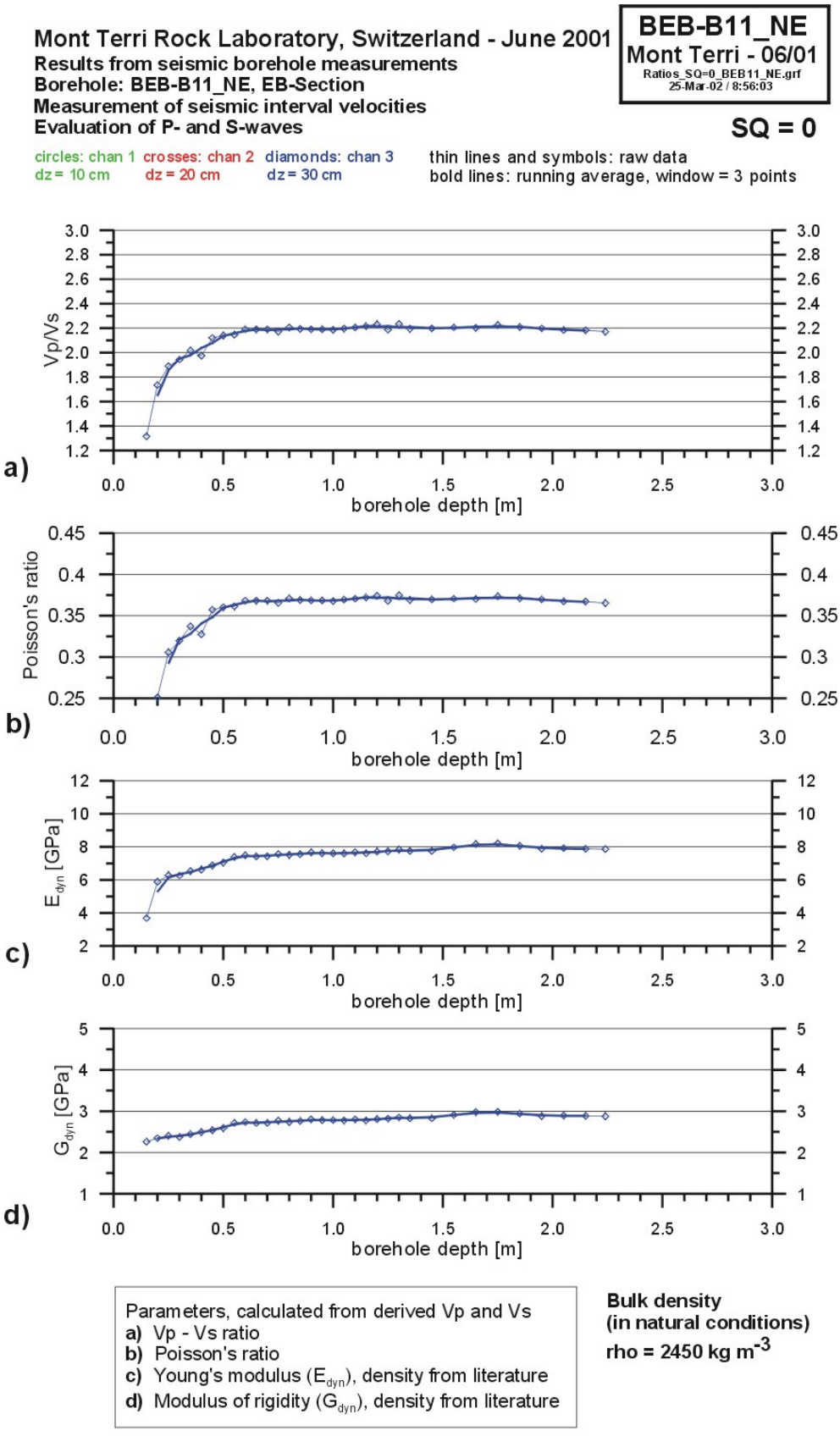

Fig. A-3: Borehole BEB-B11, June 2001: Seismic and elastic parameters derived from analyses of P- and S-waves from interval velocity measurements.

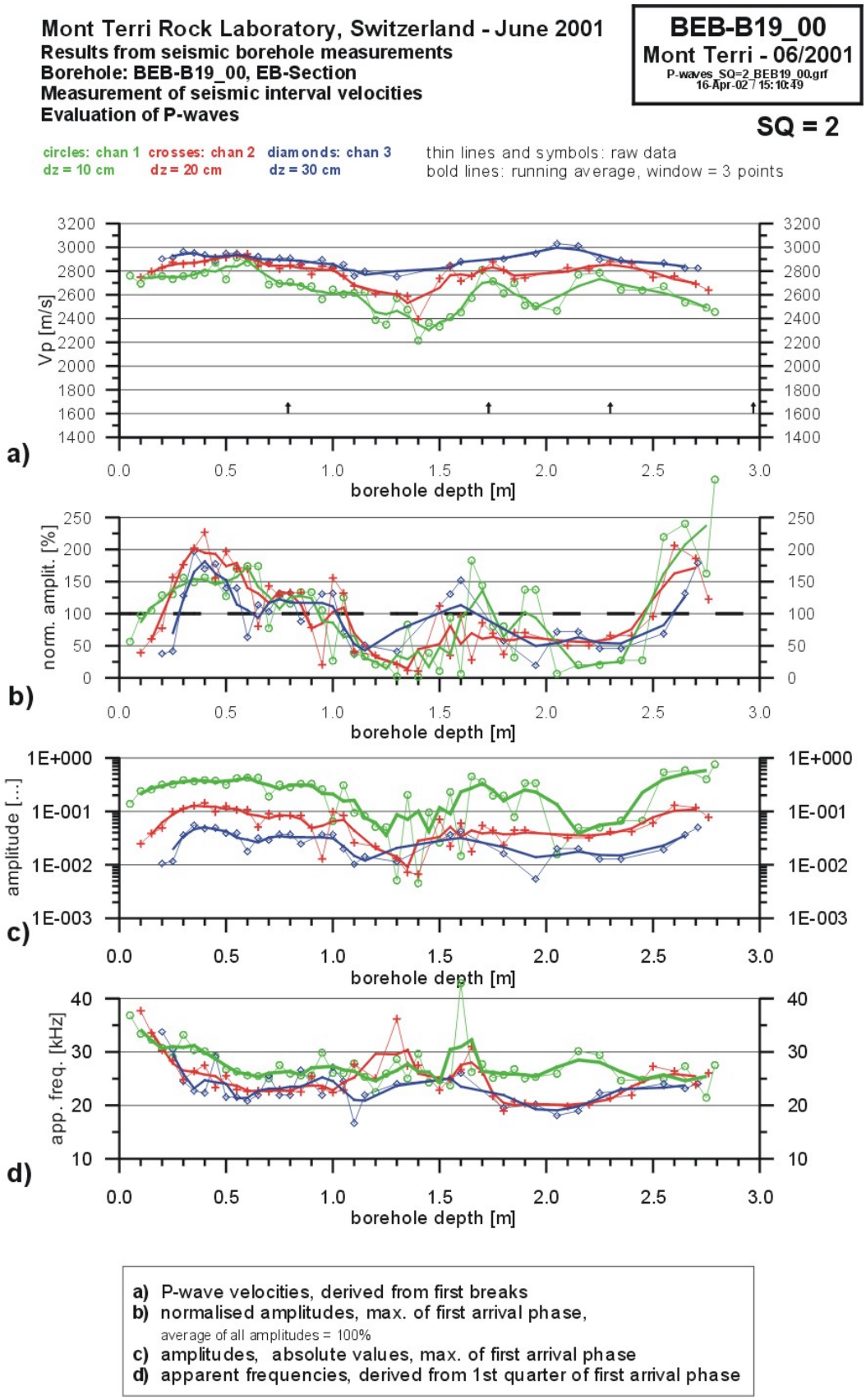

Fig. A-4: Borehole BEB-B19, June 2001: Seismic parameters derived from analyses of P-waves from interval velocity measurements. In addition structural features from drillcore mapping plotted in the Vp-graph (arrow: artificial discontinuity).

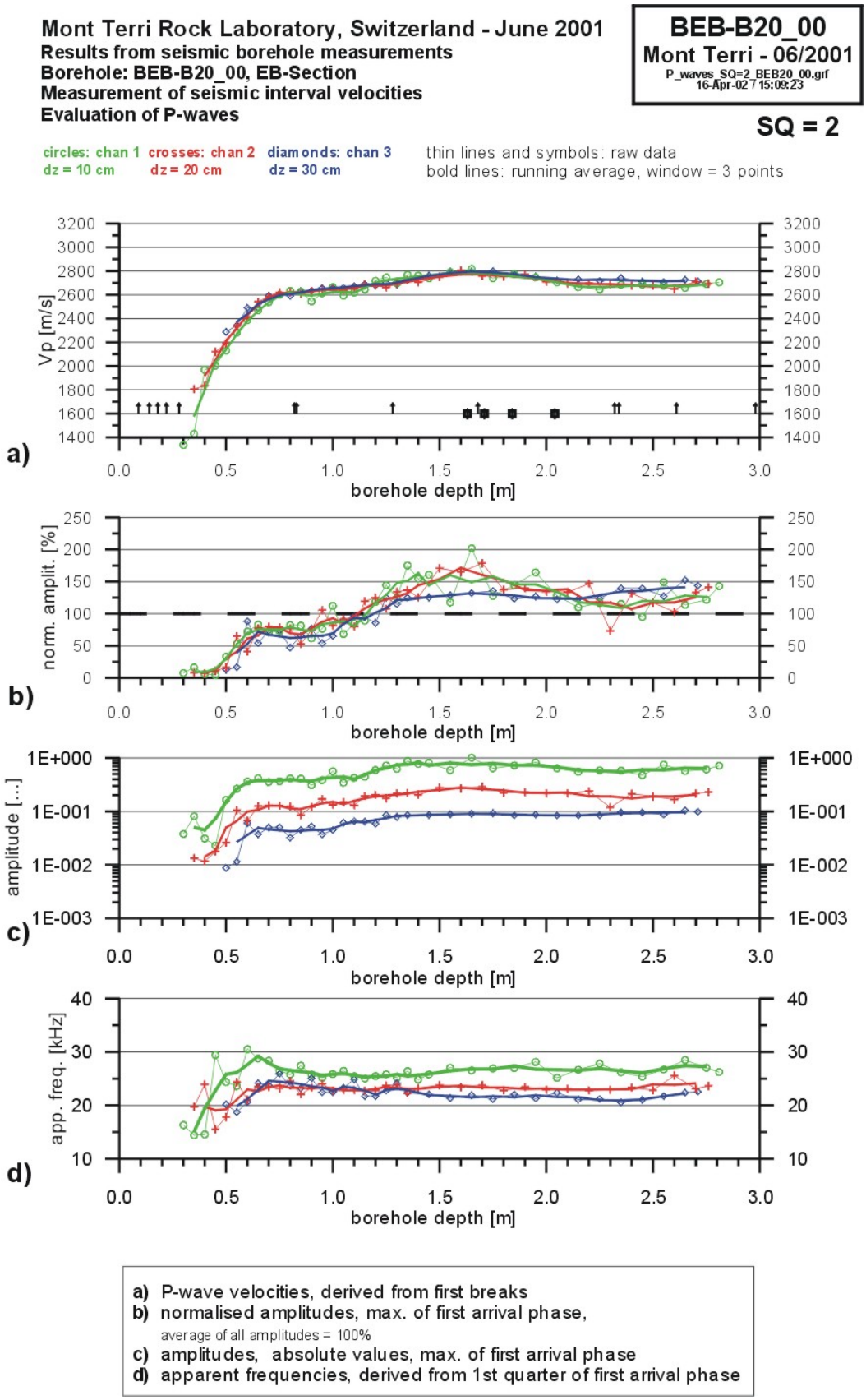

Fig. A-5: Borehole BEB-B20, June 2001: Seismic parameters derived from analyses of P-waves from interval velocity measurements. In addition structural features from drillcore mapping plotted in the Vp-graph (rectangle: sandy layer, arrow: artificial discontinuity).

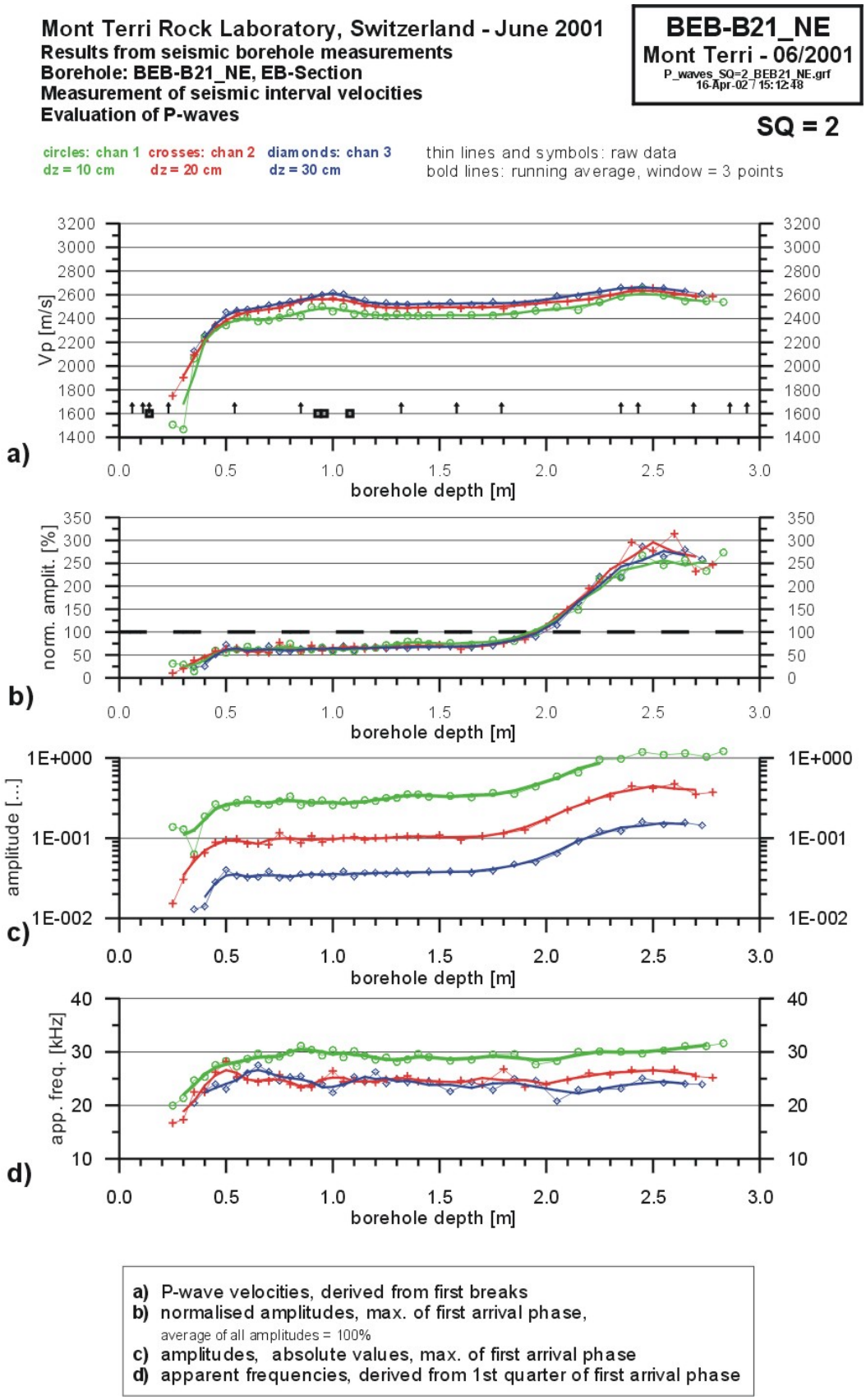

Fig. A-6: Borehole BEB-B21, June 2001: Seismic parameters derived from analyses of P-waves from interval velocity measurements. In addition structural features from drillcore mapping plotted in the Vp-graph (rectangle: sandy layer, arrow: artificial discontinuity).

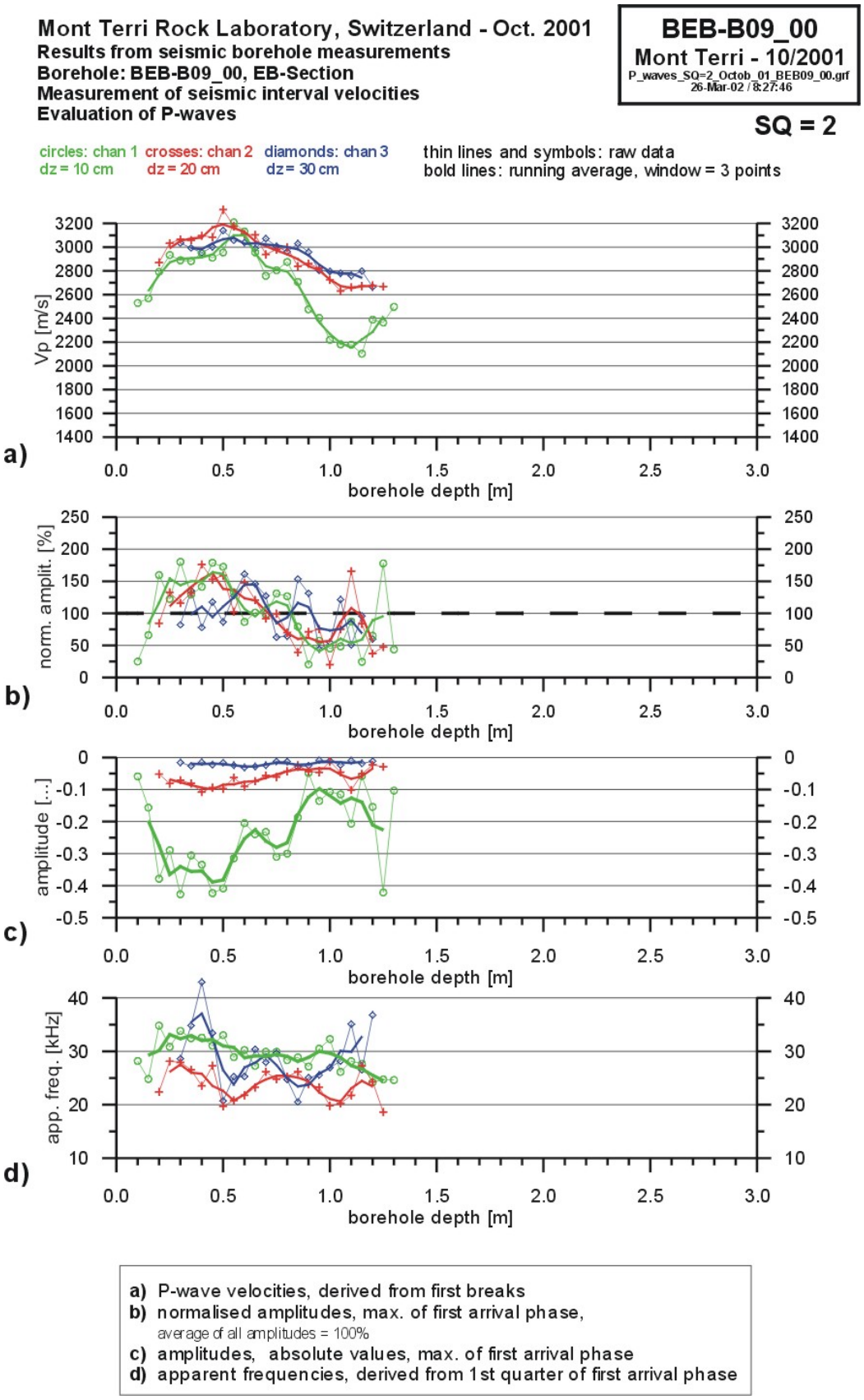

Fig. A-7: Borehole BEB-B09, October 2001: Seismic parameters derived from analyses of P-waves from interval velocity measurements.

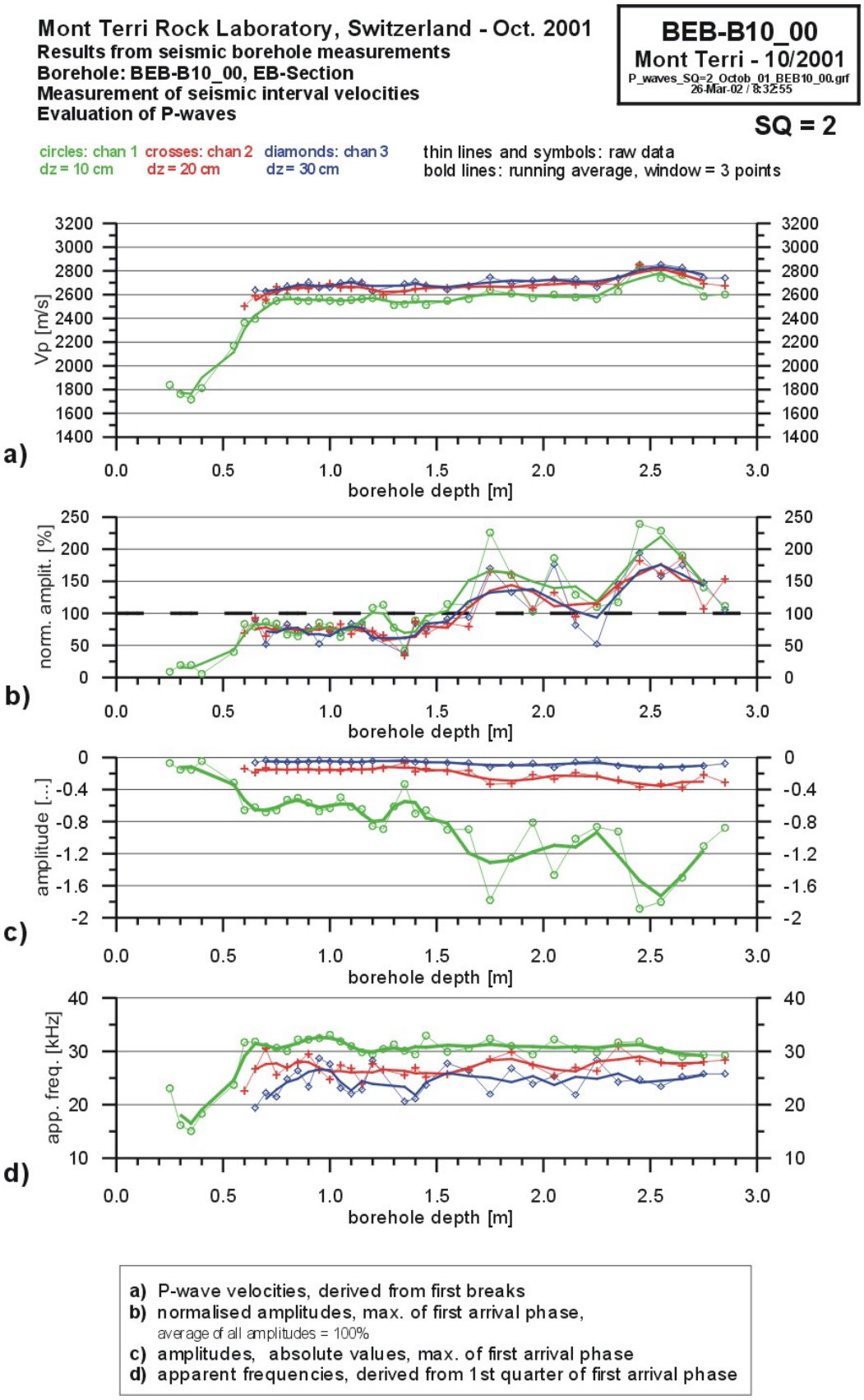

Fig. A-8: Borehole BEB-B10, October 2001: Seismic parameters derived from analyses of P-waves from interval velocity measurements.

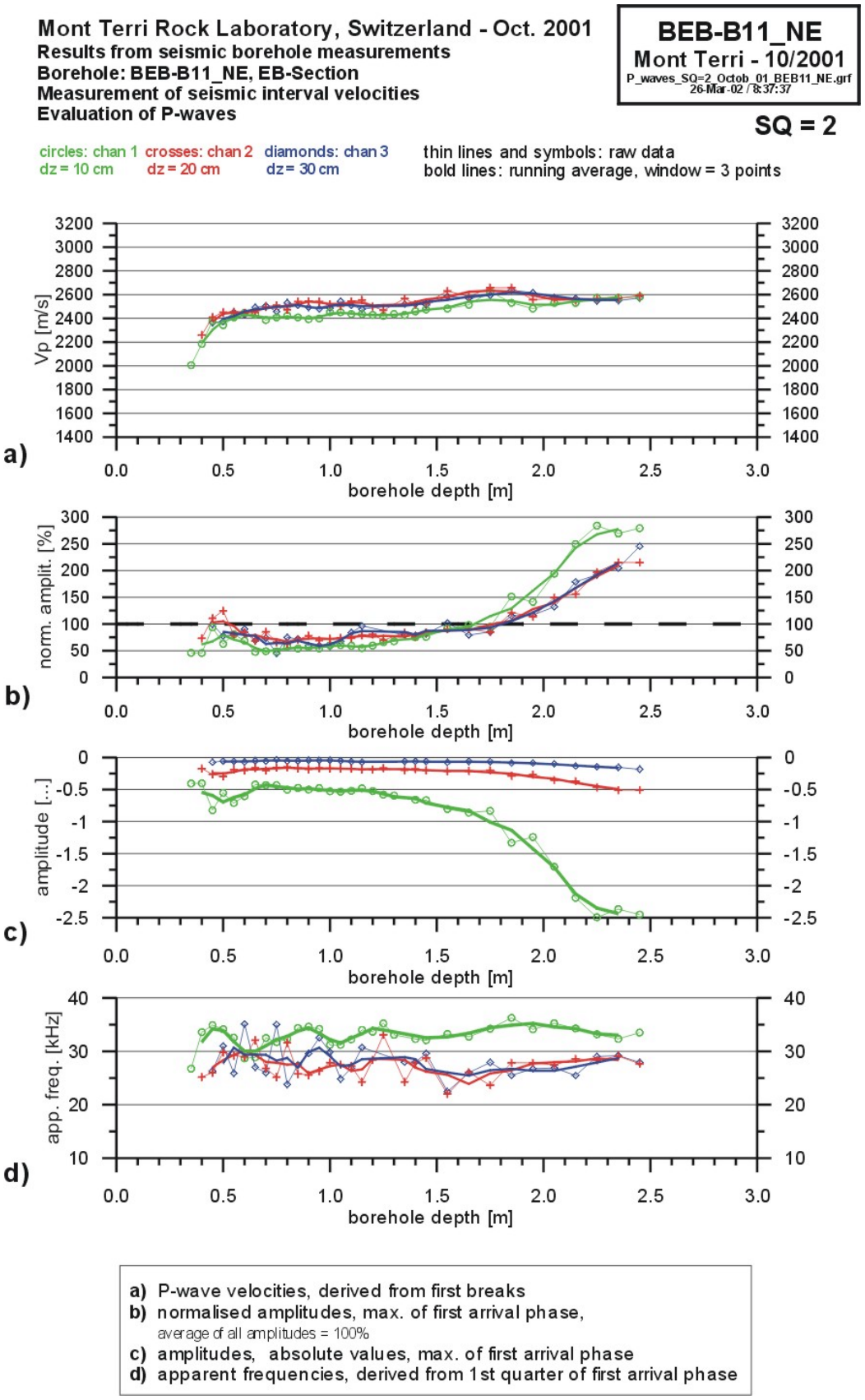

Fig. A-9: Borehole BEB-B11, October 2001: Seismic parameters derived from analyses of P-waves from interval velocity measurements.

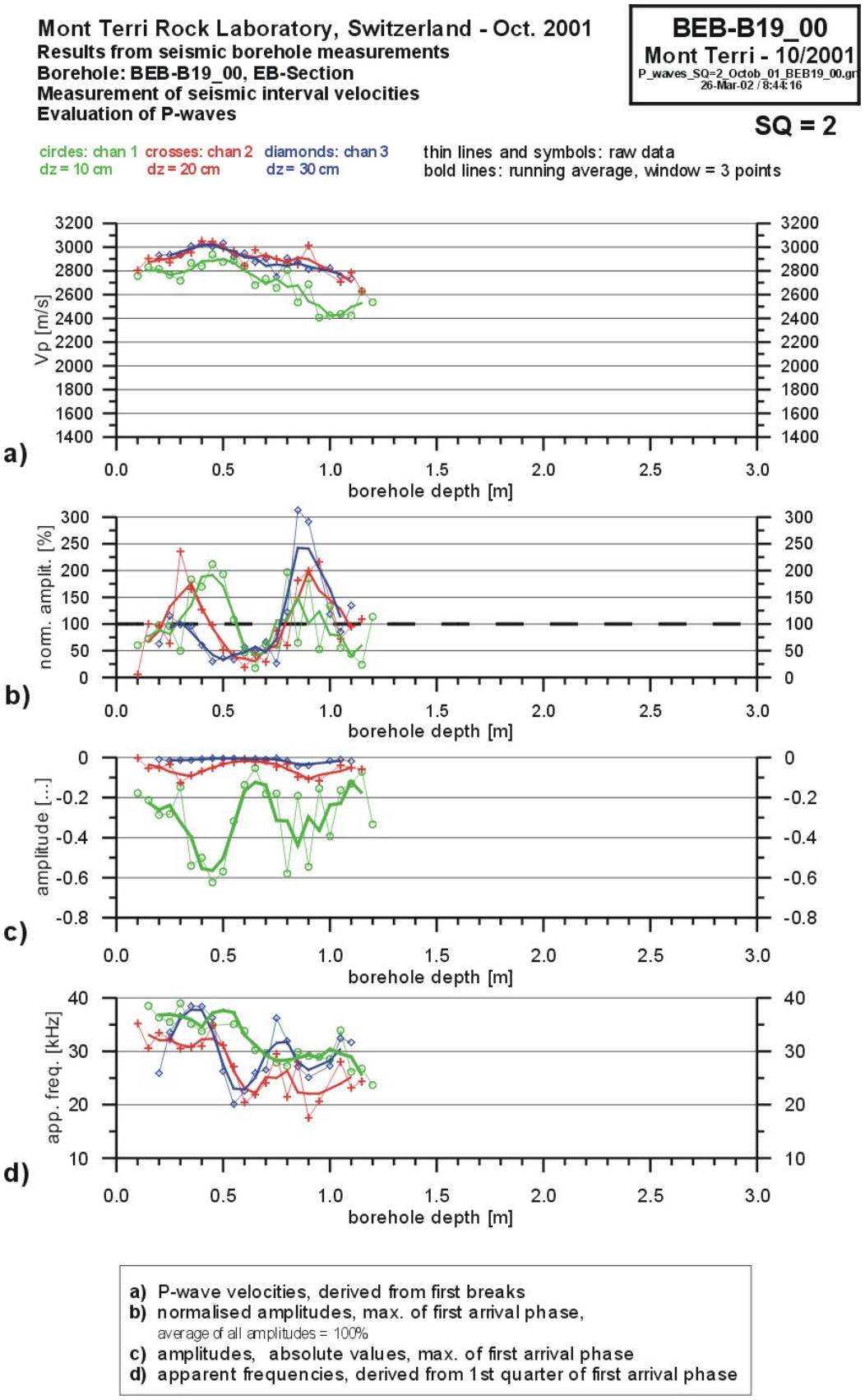

Fig. A-10: Borehole BEB-B19, October 2001: Seismic parameters derived from analyses of P-waves from interval velocity measurements.

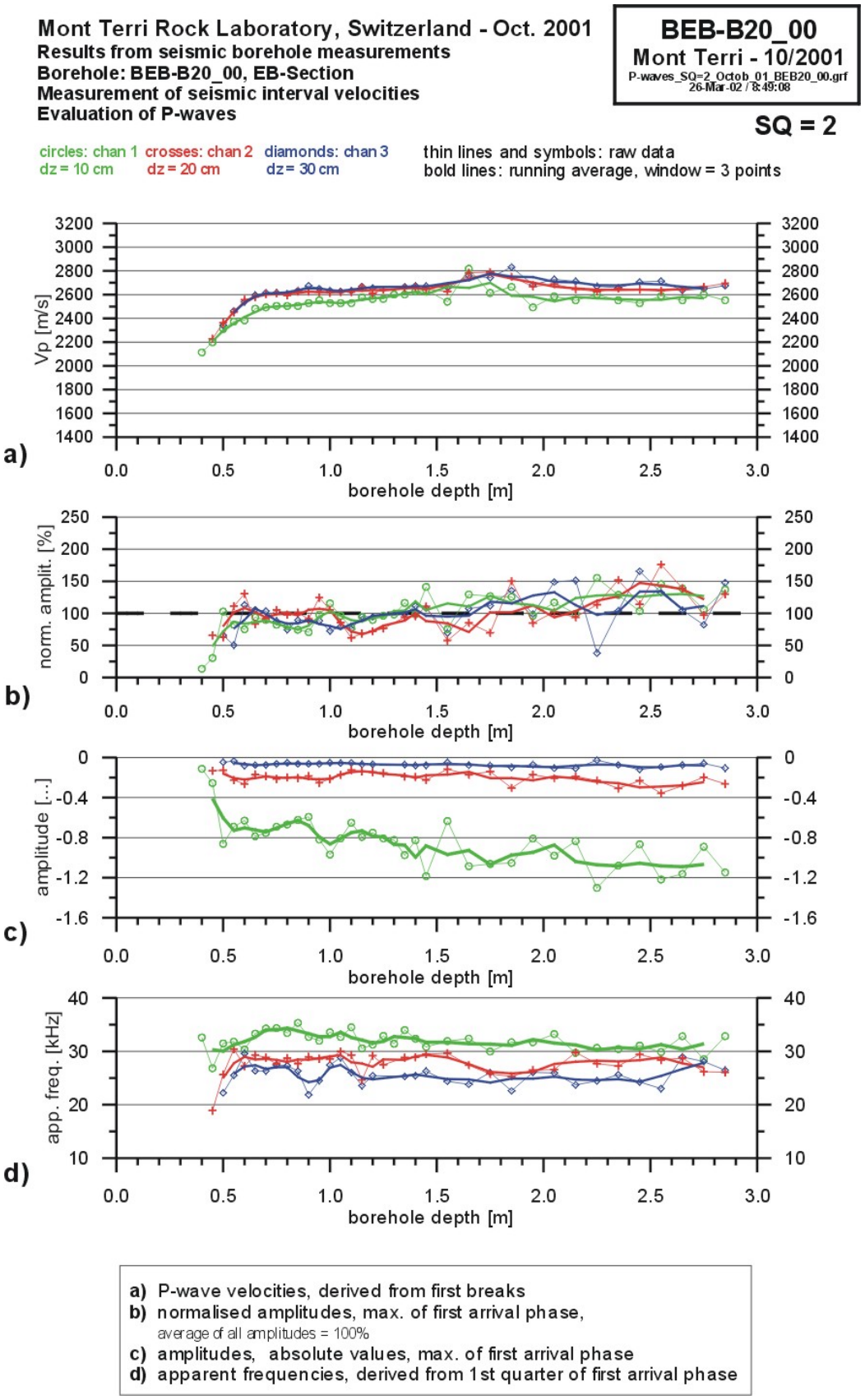

Fig. A-11: Borehole BEB-B20, October 2001: Seismic parameters derived from analyses of P-waves from interval velocity measurements.

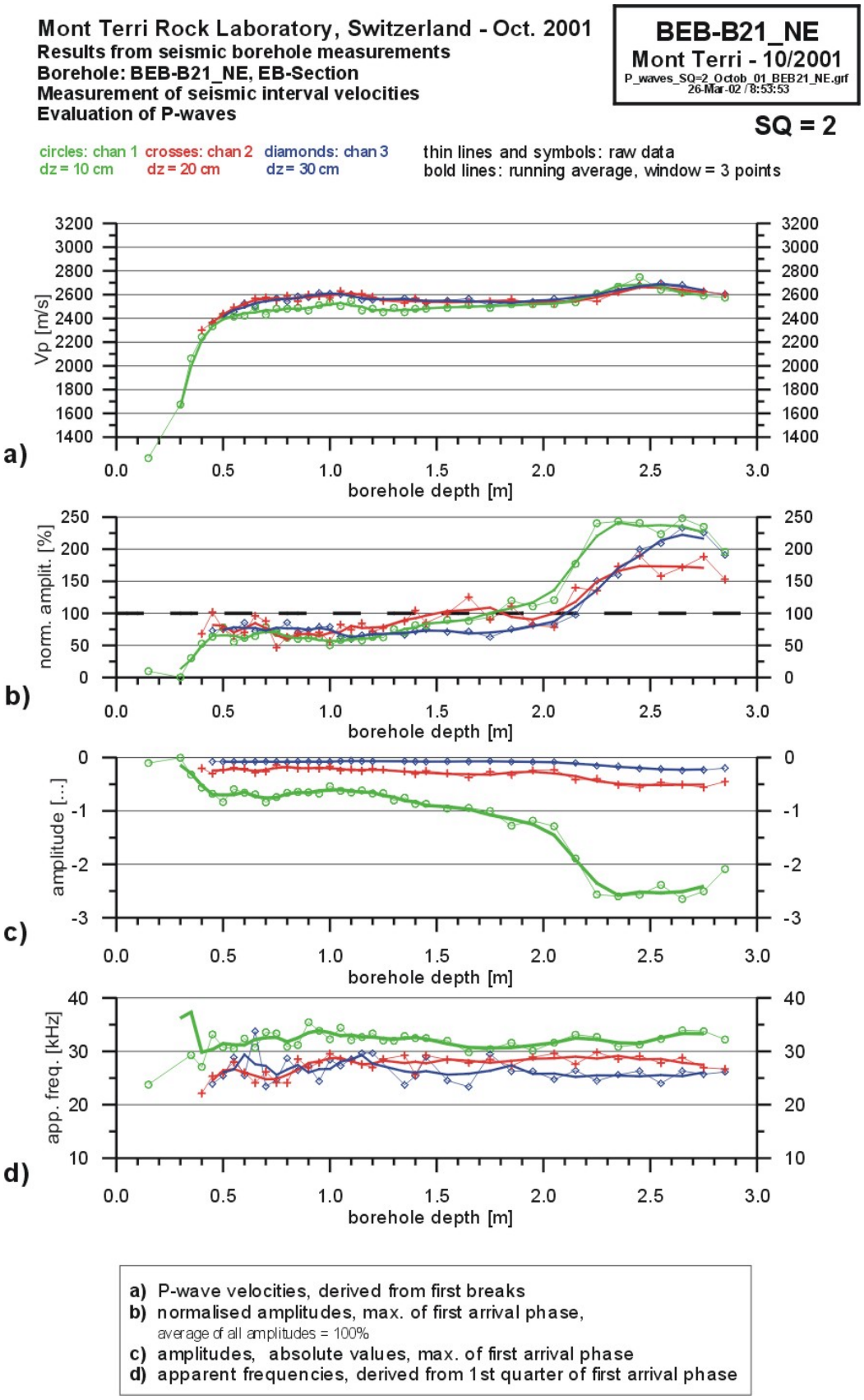

Fig. A-12: Borehole BEB-B21, October 2001: Seismic parameters derived from analyses of P-waves from interval velocity measurements.